INFORMATION TO USERS

This manuscript has been reproduced from the microfilm master. UMI films the text directly from the original or copy submitted. Thus, some thesis and dissertation copies are in typewriter face, while others may be from any type of computer printer.

The quality of this reproduction is dependent upon the quality of the copy submitted. Broken or indistinct print, colored or poor quality illustrations and photographs, print bleedthrough, substandard margins, and improper alignment can adversely affect reproduction.

In the unlikely event that the author did not send UMI a complete manuscript and there are missing pages, these will be noted. Also, if unauthorized copyright material had to be removed, a note will indicate the deletion.

Oversize materials (e.g., maps, drawings, charts) are reproduced by sectioning the original, beginning at the upper left-hand corner and continuing from left to right in equal sections with small overlaps. Each original is also photographed in one exposure and is included in reduced form at the back of the book.

Photographs included in the original manuscript have been reproduced xerographically in this copy. Higher quality 6" x 9" black and white photographic prints are available for any photographs or illustrations appearing in this copy for an additional charge. Contact UMI directly to order.

UMI

A Bell & Howell Information Company
300 North Zeeb Road, Ann Arbor MI 48106-1346 USA
313/761-4700 800/521-0600

CRYSTALLOGRAPHIC STUDIES OF SELECTED PEROVSKITE-GROUP COMPOUNDS

by Shannon Farrell ©

A thesis submitted in partial fulfilment of the requirements for the degree of

Master of Science

Supervisor: Dr. R.H. Mitchell

Lakehead University

Thunder Bay, Ontario

Canada

November 1997

CRYSTALLOGRAPHIC STUDIES OF SELECTED PEROVSKITE-GROUP COMPOUNDS

Abstract

This study investigates the tausonite-loparite solid solution series. Members of this series are important in some alkaline complexes, thus making studies of their crystallography essential. Rietveld refinement of the crystal structures of the tausonite-loparite solid solution series, using *X*-ray diffraction powder patterns, indicates that there is a reduction in symmetry from cubic ($Pm\bar{3}m$) to orthorhombic (*Pnma*), by way of an intermediate tetragonal (*P4/mbm*) modification. The symmetry changes appear to occur at about ~66.6 and ~33.3 wt% tausonite, which are consistent with formulae of approximately $Sr_2(NaLa)Ti_3O_9$ and $Sr(NaLa)_2Ti_3O_9$, respectively. The pseudo-cubic cell parameter a_p decreases with increasing loparite content, while the [*111*] tilt angle Φ (Φ=0 in $Pm\bar{3}m$) on inception at 50 wt% loparite achieves a maximum and decreases thereafter with increasing loparite content. Rietveld refinements indicate that no ordering at the *A*-site exists throughout the solid solution series.

This study also investigates a titanium perovskite ($Na_{2/3}Th_{1/3}TiO_3$), which is unusual in that it contains a tetravalent cation at the *A*-site. This thorium titanium perovskite was synthesised in an attempt to determine its structure. Although powder diffractometry suggests an $Fm\bar{3}m$ space-group, attempts at Rietveld refinement of the structure show the actual space-group must be of reduced symmetry.

This study also provides data on the pseudo-binary system between hollandite ($K_2Cr_2Ti_6O_{16}$) and the n=3 member of the homologous series $K_2La_2Ti_{3+n}O_{10+2n}$, *i.e.*, $K_2La_2Ti_6O_{16}$. This series is important in understanding the location and environment of the rare-earth cations in natural hollandite specimens and the capability of hollandite (*i.e.*, SynRoc) to immobilize large elements of varying charge and size. This pseudo-binary system is characterized by the presence of the following phases: hollandite $[K_{1.54}(Cr_{1.43}Ti_{6.52})_{7.95}O_{16}]$; perovskite-1 $[(K_{0.28}La_{0.55})_{0.81}(Cr_{0.05}Ti_{0.98})_{1.03}O_3]$; potassium hexatitanate ($K_{1.99}Ti_{6.01}O_{13}$); perovskite-2 ($LaCrO_3$); and perovskite-3 ($La_2Ti_2O_7$). Complete solid-solution between the end-members of this system does not occur. The hollandites (space-group *I4/m*) have an *A*-site occupancy of approximately 75-82%, and exhibit no significant substitution of La^{3+} at any of the cation sites. Perovskite-1 is considered to be a non-stoichiometric *A*-site deficient perovskite. Potassium hexatitanate is the only main phase that is stoichiometric and contains no substitution of Cr^{3+} in any of the cation sites. All the Cr^{3+} excluded from the potassium hexatitanate structure is incorporated into perovskite-2.

Acknowledgements

I am grateful to Dr. Roger H. Mitchell who supervised this research project and whose support and guidance throughout the study made this thesis possible. His patience and many valuable suggestions on earlier drafts of this thesis are appreciated.

Special thanks to Alan MacKenzie and Keith Pringnitz of the Lakehead University Instrumentation Laboratory for their instruction, advice, and assistance with *X*-Ray Diffractometry and Scanning Electron Microscopy techniques.

I am also indebted to Dr. Anton Chakhmouradian of St. Petersburg State University, Russia for his generous help concerning structure refinements, and to Dr. Mati Raudsepp of the University of British Columbia and Neil Ball of the University of Manitoba for their advice regarding Rietveld refinement.

To the faculty, staff, and students of the Geology department I extend my appreciation for their freely given counsel when requested.

I thank my family for their sustained support and trust in me, especially when far from my home in Nova Scotia. I am especially grateful to my wife Michelle, who providing relief from the tension and anxiety and her continued expression of faith in me.

Table of Contents

List of Figures

Chapter 5

Chapter 6

List of Tables

Chapter 5

Chapter 6

Chapter 1

PEROVSKITE -AN INTRODUCTION

1.1 Perovskite -Scientific and Economic Importance

Perovskites are a very large family of crystalline compounds, named after the mineral known as perovskite (*i.e.*, $CaTiO_3$). This mineral was first described from the Ural Mountains, Russia, by the geologist Gustav Rose and was named in the 1830's after the famous Russian mineralogist Count Aleksevich von Perovski. Perovskite-group minerals are those with a similar structure to that of $CaTiO_3$ (Kay and Bailey 1957). These minerals are of great importance geologically, as well as both scientifically and economically.

Perovskite structured phases [$(Mg,Fe,Ca)SiO_3$] are the most abundant minerals in the earth and comprise the bulk of the lower mantle (Hazen 1988). Perovskites are important minerals in undersaturated alkaline rocks, as they are major hosts of Rare Earth Elements (*REE*) and are a common economic or accessory mineral (Mitchell 1996). Some perovskite deposits are of great economic value due to the effectiveness of perovskite in extracting the light *REE* (*LREE*), niobium, titanium, tantalum and strontium from magmas. Of all the *REE*-rich perovskite-group minerals, only loparite-(Ce) ($CeTiO_3$) may be considered as a distinct rare earth mineral. Loparite may form complex solid-solutions with other *REE*-free perovskite-group minerals (Mitchell 1996), *e.g.*, the solid solution between loparite and tausonite (*REE*-free) which is discussed in this thesis.

Perovskites are important from a technological point of view due to their electrical properties as semiconductors and catalysts and their ability to sequester radioactive

elements. The scientific and industrial applications of perovskite comprises more than a fifty-billion dollar per year industry (Bourdillon and Bourdillon 1994).

Semiconductors

Natural and synthetic perovskites exhibit a vast array of electrical properties from insulators (nonconductors) to semiconductors, superionic conductors, metal-like conductors and high-temperature superconductors (Hazen 1988). Presently the most intensely studied perovskites are those which are high-temperature superconductors. This diversity of properties is derived from the fact that almost all of the natural metallic elements can be incorporated into the perovskite structure. The superconducting property of many perovskites is a function of structural distortions (Hazen 1988). In reality, most perovskites are not ideal (usually distorted) due to the occurrence of defects and random faults, which may include tilting of polyhedra, layering disorder, cation disorder, or point defects. Any slight modification of the ideal perovskite structure may result in the manifestation of new features, electrical or other; although, the exhibited new properties do not appear to show any simple correlation with the associated distortions (Hazen 1988).

Ceramics

Perovskites are ceramics (solid materials combining metallic elements with nonmetals, usually oxygen) which have a particular structure (Hazen 1988). These compounds were first employed as catalysts in the early 1950's, and their use became common in the early 1970's (Tejuca *et al.* 1989).

Radioactive Waste Containment

SynRoc (synthetic rock) is a solid titanate ceramic wasteform made specifically for the disposal of high-level radioactive waste which is to be buried within the earth. It consists essentially of rutile (TiO_2), hollandite [$Ba(AlTi)Ti_6O_{16}$], zirconolite ($CaZrTi_2O_7$) and perovskite ($CaTiO_3$), with the latter three compounds having the ability to incorporate the majority of radioactive elements into their crystal structures (Ringwood 1985). SynRoc is postulated to have a capacity to persist for millions of years in a wide range of geologic environments. This is due to its high resistance to leaching by ground waters, especially above 100°C, and since high levels of radiation damage does not obviously impair immobilization of elements (Ringwood 1985).

1.2 Perovskite

1.2.1 Ideal Perovskite-type Structure

Compounds which adopt the perovskite structure have been studied since the 1940's. Perovskite has the general formula ABX_3, and may be considered as a derivative of the ReO_3 structure (Loeb 1962). The *A* or *B* position can be occupied by diverse elements due to the ability of the structure to tolerate significant deformation within its framework. Figure 1-1 is a survey of the elements known to be stable in the perovskite structure (Tejuca *et al.* 1989).

Typically, relatively large elements occupy the *A*-sites, whereas smaller elements occupy the *B*-site. Usually *REE*, Ca, or Ba occupy the *A* position, but more than 30 other elements may occupy this site. The *B* position can be filled by any one of more than 50%

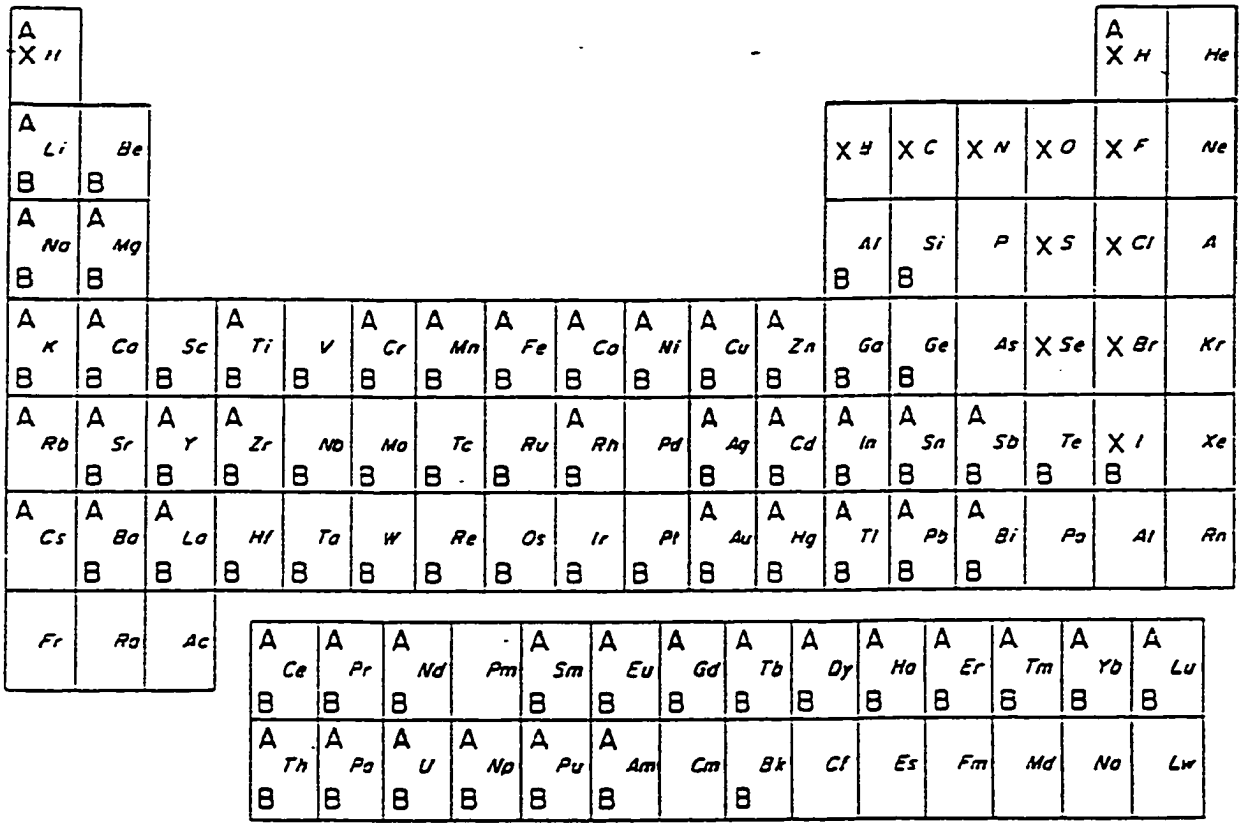

Figure 1-1 Elements that are known to be stable in the *A*, *B*, and/or *X* positions of perovskite structure (Tejuca *et al.* 1989).

of the known stable elements, but in natural systems Ti or Si typically occupy the *B*-site. The *X* position is usually occupied by O in naturally-occurring perovskites and the majority of ceramics; however, halogens may occupy this site as in synthetic $KMgF_3$.

The perovskite (ABX_3) structure is based on a cubic closest-packed array of anions (Figure 1-2A) and may be viewed in several ways. The ideal structure of perovskite (Náray-Szabó 1943) has a cubic unit cell, and can be viewed differently depending on whether the *B* cations (Figure 1-2B), the *A* cations (Figure 1-2C) or the *X* anions (Figure 1-2D) are placed at the corners of a cubic unit cell. Figure 1-2B, is the common representation of the perovskite structure. The *A* cation lies in the centre of a cube with corners defined by eight *B* cations, along with twelve oxygens found at the midpoints of each of the cube edges. In Figure 1-2C, the *B* cation lies in the centre of a cube with corners defined by eight *A* cations, along with six oxygens found at the centre of each of the cube faces. Figure 1-2D is a cube with corners defined by eight *X* anions. The ideal (cubic) perovskite structure is found only in some minerals, such as $SrTiO_3$ (tausonite). In Figures 1-2C and 1-2D, the structure is visualized as layers of atoms and are views frequently used by material scientists (Mitchell 1996). These representations are useful when describing layered derivatives of the perovskite structure: complex perovskites of the type $Ca_2BB'O_6$ (Figure 1-3A) (Mitchell 1996; Filip'ev and Fesenko 1965); Ruddlesden-Popper phases, $Sr_3Ti_2O_7$, (Figure 1-3B) (Ruddlesden and Popper 1957, 1958) or $K_2La_2Ti_3O_{10}$ (Gopalakrishnan and Bhat 1987); and high-temperature superconductors La_2CuO_4 (Figure 1-3C) (Bourdillon and Bourdillon 1994).

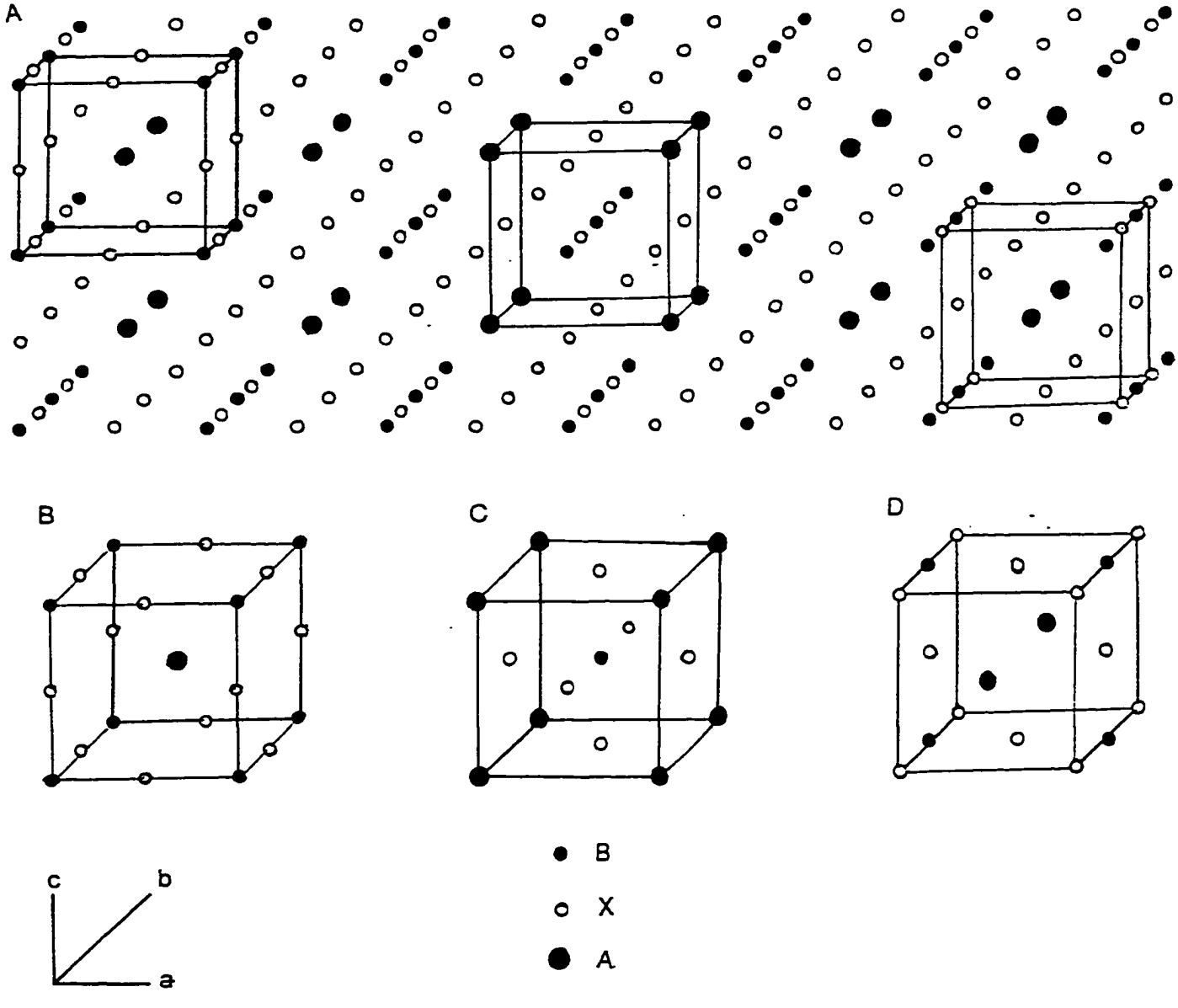

Figure 1-2 The perovskite structure based on a cubic closest-packed array of anions (A). B, C and D are different views of the perovskite structure.

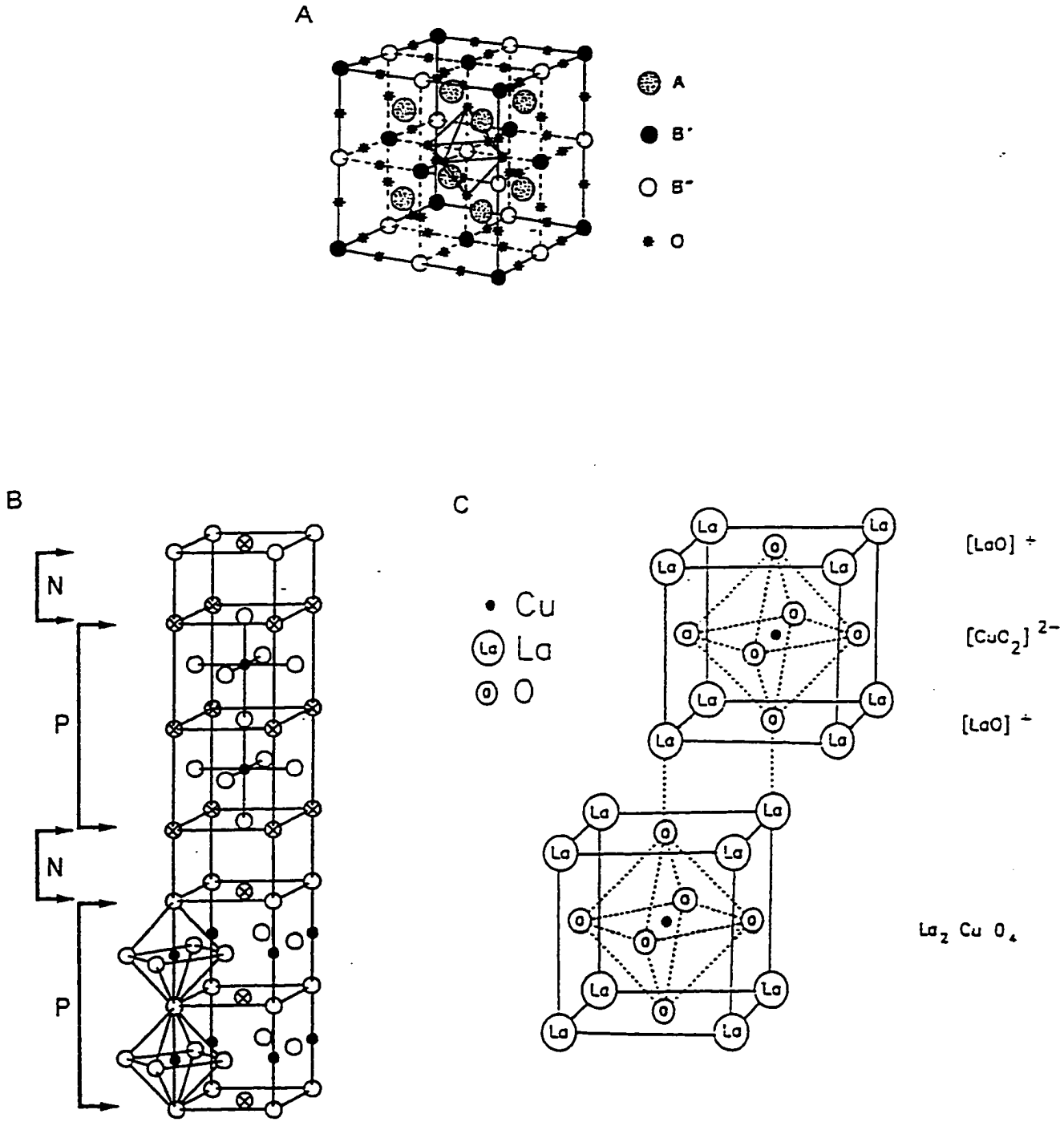

Figure 1-3 Structure of layered perovskites.
A A complex perovskite (Goldschmidt 1926).
B The Ruddlesden-Popper compound $Sr_3Ti_2O_7$ (Ruddlesden and Popper 1957).
C A high temperature superconductor (Bourdillon and Bourdillon 1994).

The structure of cubic perovskite consists of a single cube (Figure 1-2), but is commonly depicted as an array of polyhedrons (Figure 1-4). This polyhedron model is favoured by mineralogists. The structure (Hazen 1988) has each *B* cation (placed at each corner of a cube) surrounded by and closely bonded to six *X* anions forming the points of an octahedron. The *A* cation is surrounded by eight of the corner-linked octahedra, each with the *B* cation in the center. The *A* cation lies at the center of a cubo-octahedron, which is a coordination polyhedron defined by the twelve oxygens. The polyhedral model consists of both octahedra and cubo-octahedra (Figure 1-5).

1.2.2 ReO_3-type Structure

The ReO_3-type (or AlF_3) structure is closely related to that of perovskite, and has been described by Loeb (1962) as having the same structure, but with the removal of the *A* cation and substitution of Re for Ti (Figure 1-6). Both ABO_3 (perovskite) and ReO_3 have a network of corner-sharing XO_6 polyhedra, but the absence of the large *A* cation in the cuboctahedral cavities of the ReO_3 structure permits the formation of a tunnel structure. When the *A*-site is completely occupied, the perovskite structure results; when only partially occupied, the structure is known as a tungsten bronze. Tungsten bronzes are named for structures similar to M_xWO_3, where $0<x<1$ and *M* is K, Na, Ba, Pb, Tl or *REE* (Mitchell 1996). This non-stoichiometry is tolerated due to the structural similarities between the perovskite structure and the ReO_3 structure. Naturally occuring non-stoichiometric perovskites may be possible, but have not yet been recognized (Mitchell 1996).

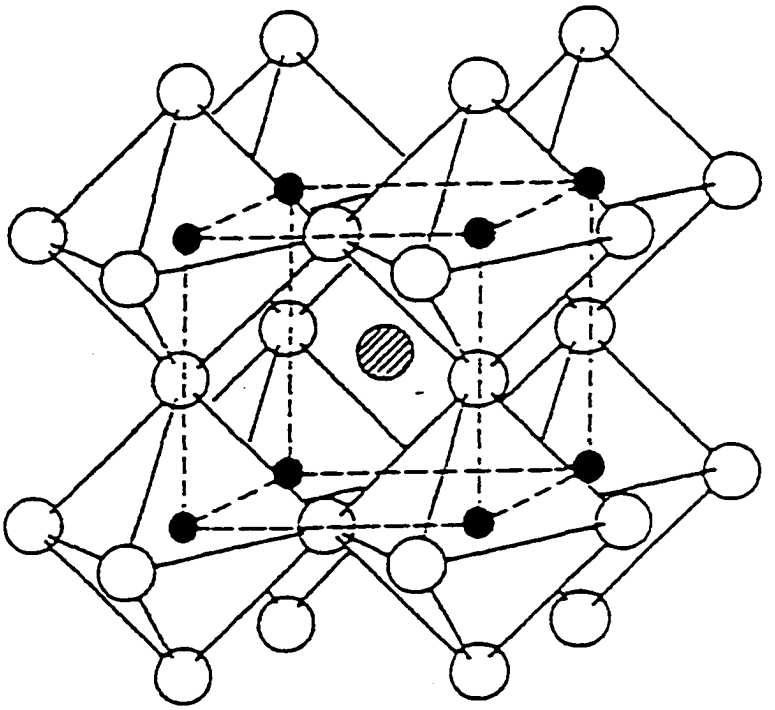

Figure 1-4 Ideal perovskite structure depicted as an array of polyhedra (Tejuca *et al.* 1989).

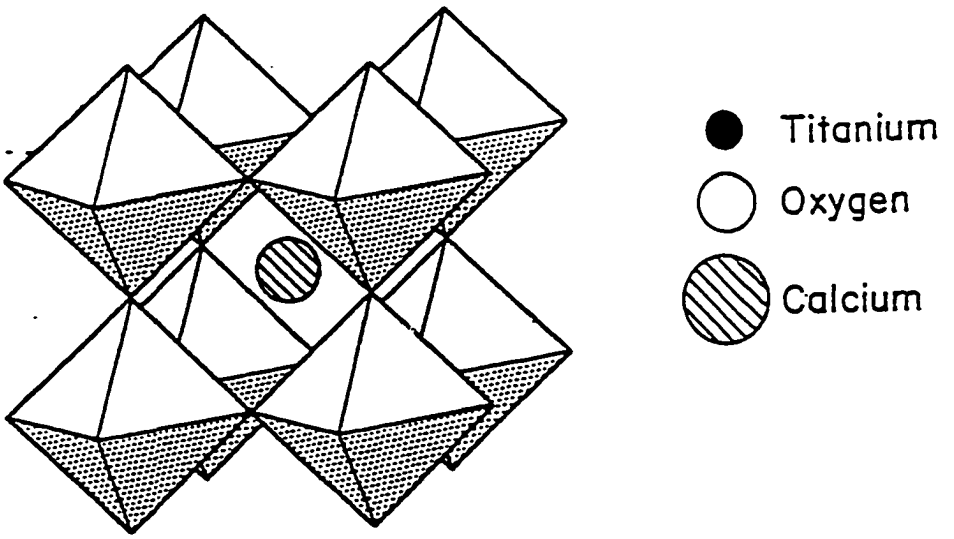

Figure 1-5 Polyhedral model of perovskite consisting of both octahedra and cubo-octahedra (Hazen 1988).

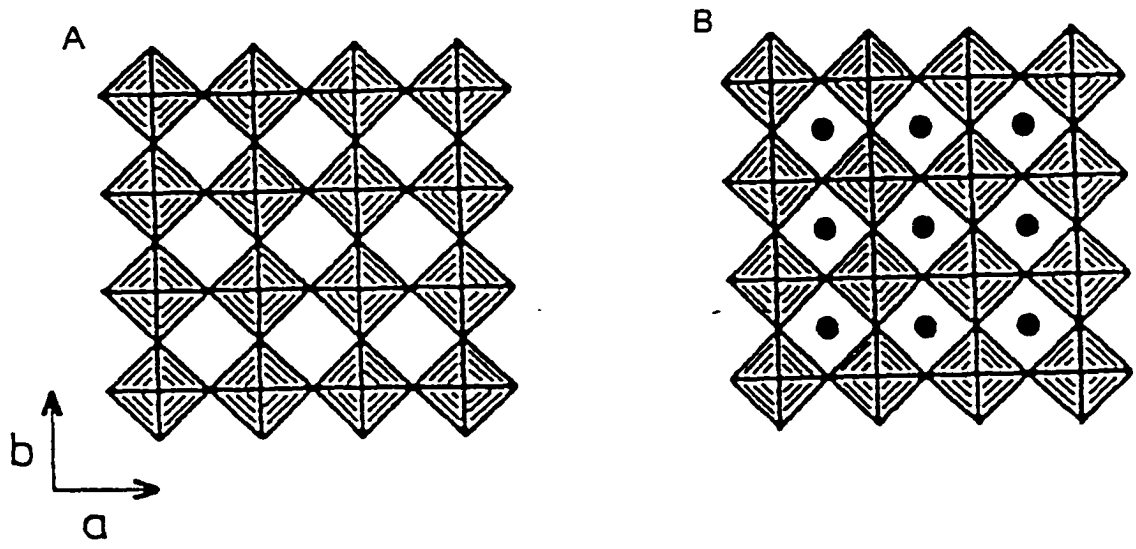

Figure 1-6 ReO_3 (A) and perovskite (B) structure-types represented as (XO_6) octahedra projected along [*001*] (Hyde and O'Keeffe 1973).

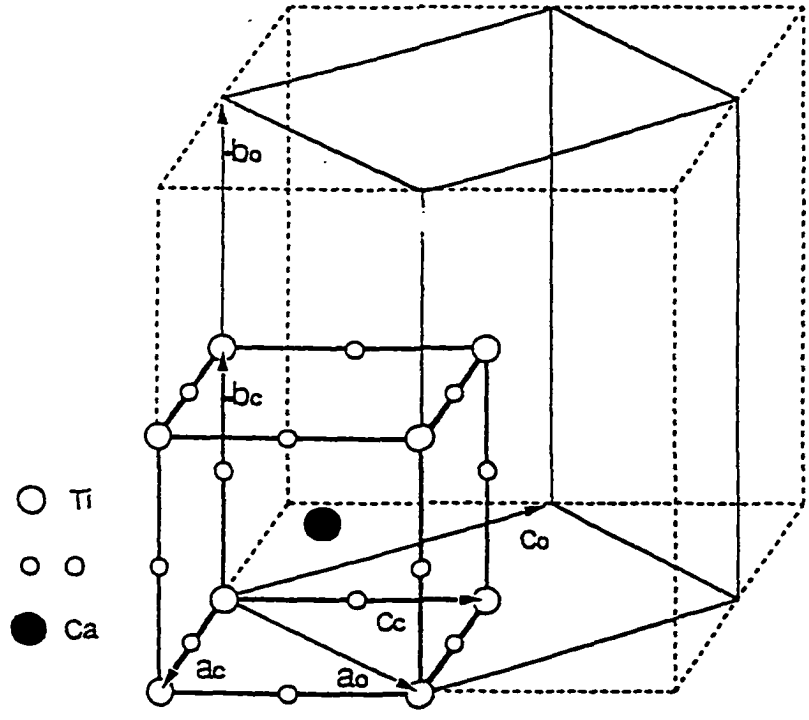

Figure 1-7 Geometrical relationship between the cubic unit cell ($Pm\bar{3}m$) and the orthorhombic unit cell (*Pnma*) of perovskite (Hu *et al* 1992).

1.2.3 Distorted Perovskite Structures

Some perovskite compounds conform strictly to the standard cubic ABX_3 structure, but many perovskite compounds have a structure that is slightly distorted from the ideal cubic configuration. To understand the behaviour of perovskites near phase transition boundaries it is necessary to have the most complete understanding possible concerning the location of the atoms in the structure. The ideal structure found in some materials ($SrTiO_3$), may be modified by *B* cation displacements ($BaTiO_3$), by tilting of octahedra ($CaTiO_3$), or by a combination of both as in $NaNbO_3$ (Glazer 1972). Cation displacements, unlike tilting, do not directly affect the lattice parameters, except by a relatively small distortion of the octahedra (Glazer 1972). Since overall symmetry typically follows that of the tilt, the polyhedral tilts are considered to be the most important parameter in reducing the overall symmetry.

$CaTiO_3$-perovskite is an example of where the ideal structure of perovskite has undergone tilting of polyhedra due to the *A* cation being too small for the ideal structure. The reduction of symmetry from cubic to orthorhombic results in a larger unit cell ($\mathbf{a}\approx\mathbf{c}\approx\sqrt{2}/2\mathbf{b}$) which contains more formula units (Z=4) (Figure 1-7). The structure of natural perovskite ($CaTiO_3$) is orthorhombic (Figure 1-8), with space-group *Pnma* (**a**=5.44Å; **b**=7.62Å; **c**=5.37Å; Hu *et al.* 1992), or *Pbnm* (Beran *et al.* 1996). Space-group *Pbnm* is a different setting for the same unit cell (**cab**) instead of the standard (**abc**) for *Pnma* (International Tables for *X*-Ray Crystallography 1965).

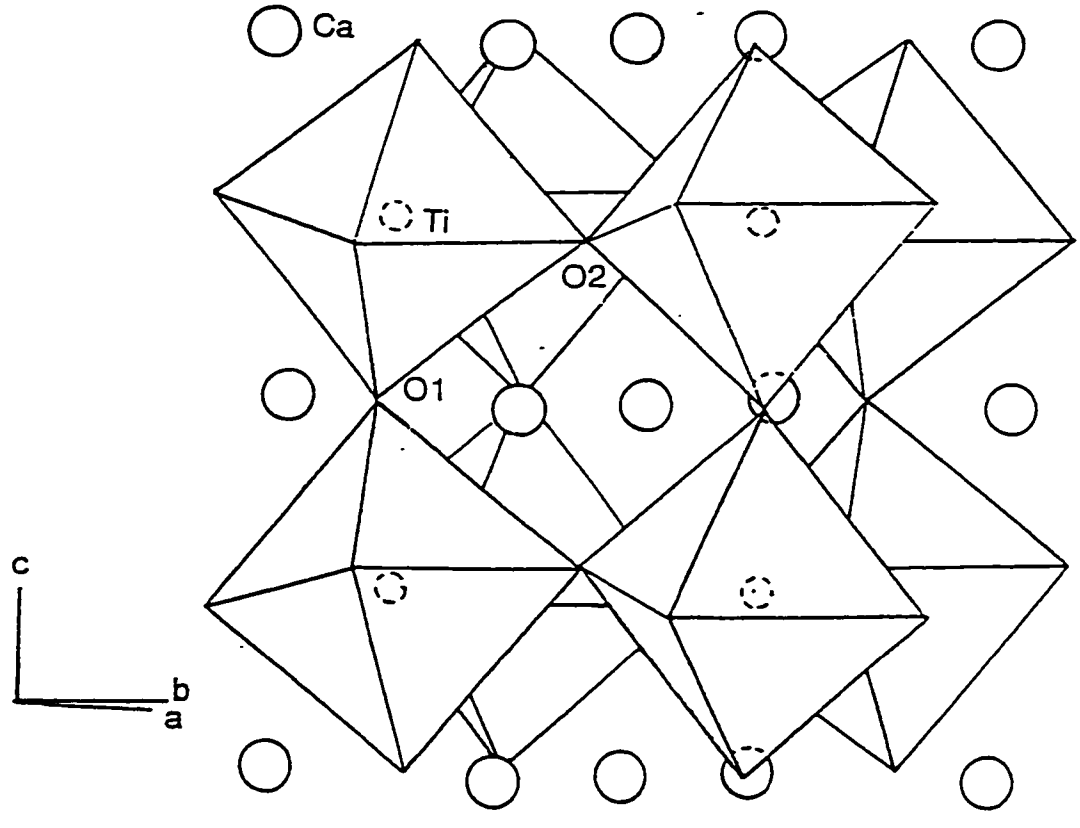

Figure 1-8 Corner-linked (TiO_6) octahedra in synthetic $CaTiO_3$ (Liu and Liebermann 1993).

1.2.4 Naturally-Occurring Perovskites

Naturally-occurring perovskite-group minerals (Mitchell 1996) are generally complex perovskites and embody complex solid-solutions expressed in terms of seven end-member compositions (Figure 1-9). The majority of these are cubic and orthorhombic in symmetry and have compositions which fall into the quaternary system, perovskite ($CaTiO_3$)-lueshite ($NaNbO_3$)-loparite ($Na_{0.5}REE_{0.5}TiO_3$)-tausonite ($SrTiO_3$). Tausonite is the only natural perovskite mineral with the ideal structure. Commonly, natural perovskites have *A*-site cations such as Na^+, K^+, Ca^{2+}, Sr^{2+}, $(REE)^{3+}$, Pb^{2+}, Th^{4+} and Ba^{2+}, while *B*-site cations include Ti^{4+}, Nb^{5+}, Fe^{3+}, Fe^{2+}, Ta^{5+}, Th^{4+}, and Z^{4+} (Mitchell 1996). Very little is known about the actual structures of the naturally-occurring perovskite-group minerals, as opposed to the synthetic variants (Mitchell 1996).

Perovskite minerals are significant components of the following rock types:

(1) Perovskite pyroxenites and perovskite dunites of some ultramafic alkaline rocks. These perovskites have compositions close to that of pure calcium titanate, *e.g.*, the Kola-Karelian area in the eastern part of the Baltic Shield (Chakhmouradian and Mitchell 1997).

(2) Layered intrusions of agpaitic nepheline syenite, *e.g.*, the Lovozero massif, Kola Peninsula, Russia. The minerals typically form cumulate layers of loparite and niobian loparite (Mitchell and Chakhmouradian 1996; Veksler and Teptelev 1990).

(3) Silica-poor rocks such as carbonatites, kimberlites and melilitites. In these rocks perovskite occurs as discrete crystals of niobian perovskite (Mitchell 1986).

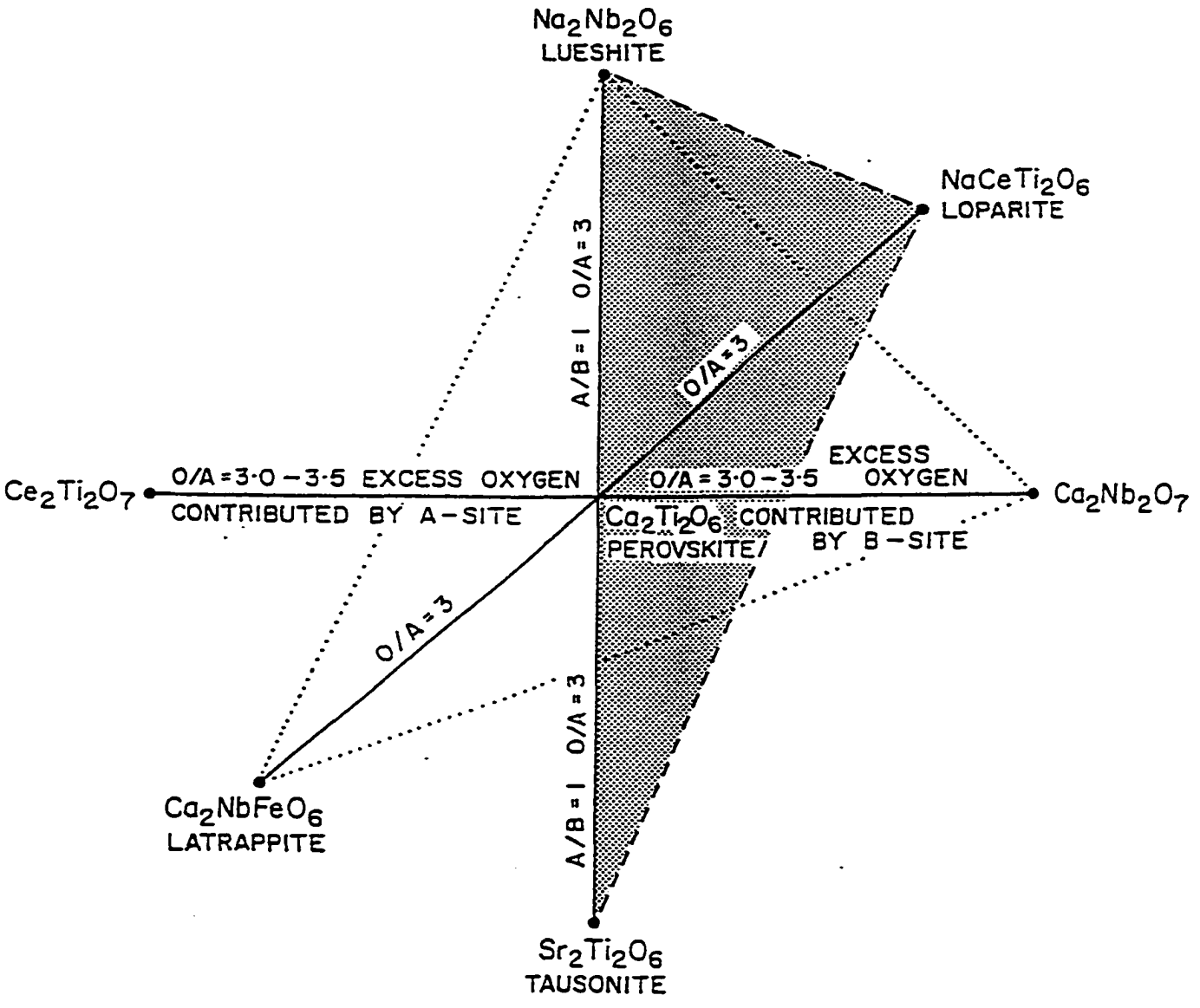

Figure 1-9 Perovskite solid-solutions expressed in terms of seven end-member compositions (Mitchell 1996).

(4) Areas of contact metamorphism, *e.g.*, the Nazamsky Mountains of the Urals, or metasomatism, *e.g.*, along the southern contact of the San Benito serpentinite massif, California (Beran *et al.* 1996; Hu *et al.* 1992).

1.3 Objectives

The objectives of this thesis are:

(1) To investigate solid-solutions occurring between some perovskite-group compounds of relevance to natural systems, specifically those that contain significant quantities of $(REE)^{3+}$ and Sr^{2+}, Cr^{3+}, and Th^{4+}.

(2) To apply Rietveld Analysis to the study of members of the tausonite-loparite solid solution series, the compound $Na_{2/3}Th_{1/3}Ti_2O_6$ and the K-Cr-hollandite-group compounds.

Chapter 2

EXPERIMENTAL PROCEDURES

2.1 Sample Preparation

2.1.1 Introduction

Several methods are available for the synthesis of perovskites, the choice being dependent on the nature of the investigation. The techniques are based on liquid-solid reactions, or solid-solid reactions (Tejuca *et al.* 1989). Liquid-solid reactions are of two types: physical reactions as in dry evaporation, explosion, spray-drying, or freeze-drying and chemical reactions, which involve crystallization, complexation, or co-precipitation of single compounds or mixtures (Tejuca *et al.* 1989). Solid-solid reactions are carried out by the ceramic method, named for its most frequent use in the preparation of ceramic materials (Tejuca *et al.* 1989).

A limited comparison of the advantages and disadvantages of the diverse synthesis methods is discussed by Tejuca *et al.* (1989, pp. 249-251). For the synthesis of perovskites, simplicity and a low surface to volume ratio, as well as the production of a homogenous product is essential. These criteria are maximized in the solid-solid technique, or ceramic method, which is ideal for the preparation of perovskites with special morphologies, such as minuscule monocrystals or thin layers (Tejuca *et al.* 1989).

2.1.2 Synthesis Techniques

Critical conditions for the synthesis and the subsequent *XRD* investigation are determined by several features: homogeneous and dry reactants; product particle size; heating temperature and time. The reactants used in this work and some of their relevant properties are listed in Table 2-1. Reactants are dried by storing the individual reactants within porcelain crucibles in a furnace at a temperature greater than 100°C for a minimum of 24 hours. This is done to eliminate any absorbed water, which if not removed would lead to an incorrect composition of mixes. The exclusion of water will also prevent the production of unwanted hydrated perovskites.

The amount of each reactant required for the production of each compound was calculated to four decimal places. These reactants are weighed out into aluminum weighing dishes. After weighing, the components are washed with acetone in an agate mortar, mixed and ground under acetone for approximately half an hour using extreme care to eliminate loss or contamination of this mixture. This mixture is then left to allow the complete evaporation of acetone. This is very important, as the acetone is extremely flammable and any remaining will ignite when placed in the furnace. This dry cake is then broken-up and placed into a platinum crucible for insertion into a furnace at a constant predetermined temperature. Very high temperatures (usually 1100°C) are required for complete reaction to occur. Intermittent grinding and firing steps every 24 hours for three days is typically required to achieve the homogeneity associated with complete reaction. Removal of the product from the furnace is done rapidly, this immediate decrease in temperature resulting in rapid quenching. Rapid quenching allows for the preservation of

Table 2-1 Properties of reactants used in the synthesis of the perovskite compounds.
* calculated from periodic table of elements
** suppliers information
*** Merck Index

Reactant	Molecular Weight *	Purity (%) **	Melting Pt. (°K) ***	Properties **	Reactions ***
TiO_2	79.8788	99.99	1855	white	
$SrCO_3$	147.6292	99.995	2430	white	$SrO + CO_2$ (1100 °C)
La_2O_3	325.8092	99.95	>2000	white	absorbs CO_2
Na_2CO_3	105.98874	99.95	851	white, crystalline	$Na_2O + CO_2$ (400 °C)
K_2CO_3	137.2058	99.99	891	white	
Cr_2O_3	151.9904	99.997	2435	green	
$CaCO_3$	100.0892	99.9965	1339	white	$CaO + CO_2$ (825 °C) absorbs CO_2
Nb_2O_5	265.8098	99.9	1520	greyish	
ThO_2	264.0369	99.99	3390	white, radioactive	

very small crystals, and for the retention of the high temperature equilibrium phase assemblage.

2.1.3 Specific Procedures

2.1.3.1 Tausonite-Loparite Solid Solution Series

The tausonite-loparite ($SrTiO_3$ - $NaLaTi_2O_6$) solid solution series was prepared on the basis of the following reactions at a temperature of 1100°C:

$$SrO_{(s)} + TiO_{2\,(s)} \Rightarrow SrTiO_{3\,(s)}$$

$$Na_2O_{(s)} + La_2O_{3\,(s)} + 4\ TiO_{2\,(s)} \Rightarrow 2\ NaLaTi_2O_{6\,(s)}$$

$$(x)\ Sr_2Ti_2O_{6\,(s)} + (1\text{-}x)\ NaLaTi_2O_{6\,(s)} \rightarrow (Sr_x(NaLa)_{1-x})Ti_2O_{6\,(s)}$$

For the first two equations, the weight percentage of each reactant required to produce the specific end-member product was calculated. For the creation of the solid-solution series it was then necessary to calculate the relative percentages of the end-members, (x) or (1-x), required for linear mixing. The members of this series were chosen at intervals of 10 wt. %, (x = 0.0-1.0, in increments of 0.1) between end-members. The solid-solution series members, and the reactants and weights required, to produce 1.2 grams of product are given in Table 2-2. The reactants SrO and Na_2O were substituted for by, and thus, weighed as, their carbonates $SrCO_3$ and Na_2CO_3. The results of this investigation appear in Chapter 4.

2.1.3.2 Thorium Perovskite

A thorium perovskite ($Na_2ThTi_3O_9$) was synthesized from the following chemical reaction (the results of which appear in Chapter 5):

$$Na_2O_{(s)} + ThO_{2\,(s)} + 3TiO_{2\,(s)} \rightarrow Na_2ThTi_3O_{9\,(s)}$$

The required amounts of reactant are 0.3747g, 0.9336g and 0.8473g, respectively.

2.1.3.3 The Pseudo-Binary System $K_2Cr_2Ti_6O_{16}$ -$K_2La_2Ti_6O_{16}$

The amounts of reactants required to form the perovskite-hollandite pseudo-binary system $K_2La_2Ti_6O_{16}$ - $K_2Cr_2Ti_6O_{16}$ were determined from the following equations:

$$K_2O_{(s)} + La_2O_{3\,(s)} + 6\ TiO_{2\,(s)} \rightarrow K_2La_2Ti_6O_{16\,(s)}$$

$$K_2O_{(s)} + Cr_2O_{3\,(s)} + 6\ TiO_{2\,(s)} \rightarrow K_2Cr_2Ti_6O_{16\,(s)}$$

$$(x)\ K_2La_2Ti_6O_{16\,(s)} + (1\text{-}x)\ K_2Cr_2Ti_6O_{16\,(s)} \rightarrow K_2La_{2x}Cr_{(2\text{-}2x)}Ti_6O_{16\,(s)}$$

The chosen compositions correspond to 0, 10, 20, 30, 50, 75, and 100 wt% $K_2La_2Ti_6O_{16}$ (x = 0.00, 0.10, 0.20, 0.30, 0.50, 0.75, 1.00). These were equilibrated at 1100°C, 1200°C and 1300°C in order to determine the phase assemblages in the perovskite-hollandite system. The solid-solution series members, the reactants and weights required to produce 2.0 grams of product appear in Table 2-3. The reactant K_2CO_3 was substituted for K_2O and the final weights were adjusted to compensate for the additional mass. Results of this investigation appear in Chapter 6.

Table 2-2 Tausonite-loparite solid solution series reactant weights.

Composition (x)	TiO_2 (grams)	$SrCO_3$ (grams)	La_2O_3 (grams)	Na_2CO_3 (grams)
1.0	0.5224	0.9653	0.0000	0.0000
0.9	0.5244	0.8688	0.0553	0.0180
0.8	0.5264	0.7723	0.1106	0.0360
0.7	0.5283	0.6757	0.1658	0.0539
0.6	0.5303	0.5792	0.2211	0.0719
0.5	0.5323	0.4827	0.2764	0.0899
0.4	0.5342	0.3861	0.3317	0.1079
0.3	0.5362	0.2896	0.3869	0.1259
0.2	0.5382	0.1931	0.4422	0.1439
0.1	0.5401	0.0965	0.4975	0.1618
0.0	0.5421	0.0000	0.5528	0.1798

Table 2-3 Reactant weights of the pseudo-binary system between hollandite ($K_2Cr_2Ti_6O_{16}$) and $K_2La_2Ti_6O_{16}$, a member of the homologous series $K_2La_2Ti_{3+n}O_{10+2n}$ (n=3).

Compostion(x)	TiO_2 (grams)	K_2CO_3 (grams)	Cr_2O_3 (grams)	La_2O_3 (grams)
0.00	1.3213	0.3810	0.4190	0.0000
0.10	1.2958	0.3736	0.3771	0.0725
0.20	1.2702	0.3663	0.3352	0.1449
0.30	1.2447	0.3589	0.2933	0.2174
0.50	1.1936	0.3442	0.2095	0.3623
0.75	1.1298	0.3258	0.1048	0.5435
1.00	1.0659	0.3073	0.0000	0.7246

2.1.4 Remarks

The simplicity of the solid state method is its best attribute, as synthesis can be obtained without the requirement of highly specialized instruments or highly complex reactions. The very high temperature of synthesis permits complete reaction of the individual reactants, and the rapid quenching effectively keeps surface areas to a minimum. Homogeneity is successfully achieved initially by grinding in the liquid medium and ultimately by the repeated mixing and firing. As a further check of the product purity and homogeneity, a detailed microstructural and compositional analysis of reaction products was carried out by SEM/EDS.

2.2 Analytical Methods

Microstructural and compositional analysis were undertaken at Lakehead University using a Philips *X*-Ray Diffractometer (*XRD*) with Ni-filtered Cu K_{α} radiation and a Link Energy Dispersive *X*-Ray Spectrometer (EDS) attached to a Hitachi 570 Scanning Electron Microscope (SEM).

2.2.1 *X*-Ray Diffraction

Powder *X*-ray diffraction patterns were captured by a Philips Goniometer (PW1820) linked to a Philips PW3710 microprocessor diffractometer control unit required to transfer information for use with Automated Powder Diffraction (APD) software. This analysis made use of a Philips proportional detector (PW17-10), which incorporated a primary Soller slit, a 0.5Å divergence slit and a 0.2Å receiving slit. The copper tube had a generator voltage

of 40 kV, and a generator current of 30 mA, operating at 1200 Watts. The Cu $K_{\alpha 1}$ wavelength is 1.540562 Å and Cu $K_{\alpha 2}$ wavelength is 1.544390 Å with an intensity ratio ($K_{\alpha 1}/K_{\alpha 2}$) of 0.50. Employment of a curved graphite monochromator and Ni filter were required for the elimination of all but Cu $K_{\alpha 1}$ and Cu $K_{\alpha 2}$ radiation (reduces 98% of K_{β} and 48% of $K_{\alpha 2}$). Most patterns were collected throughout an angular range of 10° to 140° (2θ), with a step size of 0.020°, and a 2 second count time per step. The angular range was chosen as to maximize the pattern size, while avoiding the lower angles where absorption, secondary extinction, valency effects, and backglass reflections were more pronounced. The step size and count time were selected as to provide the lowest error for least-squares refinement (Section 2.2.2). The precision and accuracy were calculated (Table 2-4) from successive runs of the same sample, and were found to be limited only by the step size. The Total Access Diffraction Database (TADD), which is a search and reference CD-ROM database, based on data from the International Centre for Diffraction Data (ICDD), was used to identify the synthesised compounds.

An aluminum sample holder was used in the *XRD* study, and the sample cell had a depth of 2 mm with a glass backing which allows for the reduction of background interferences. The cell holds approximately 800 milligrams of sample. To avoid errors each sample must have the same relative particle size, as well as having a reproducible emplacement and packing within the cell. This is carried out by sifting the sample with a razor blade, while overfilling the cell by a uniform thickness of approximately the same as the depth of the cell. When compressed into the cell by a glass slide, a portion of the sample will extrude onto the holder. Removal of this excess from around the edges results

Table 2-4 Precision and Accuracy of *XRD* for tausonite. Data records are for three of the more intense peaks which are representative of the entire spectrum. The peaks are auto-picked, and showing no deviation from a manual pick. * Expected *d*-values from Hanawalt file (05-634) refer only to the K_{α} or $K_{\alpha 1}$ peak, together with the associated relative intensity.

Measurement and Data	Reflection Angle (2θ)		Reflection *d*-value			Relative Intensity	
	$K_{\alpha 1}$	$K_{\alpha 2}$	$K_{\alpha 1}$	$K_{\alpha 2}$	K_{α}	$K_{\alpha 1}$	$K_{\alpha 2}$
Range 31-34(2θ)							
Expected*					2.759	1.000000	
1	32.375	32.475	2.763027	2.761592	2.762549	1.000000	0.418627
2	32.395	32.495	2.761367	2.759938	2.760891	1.000000	0.426040
3	32.395	32.495	2.761367	2.759938	2.760891	1.000000	0.410994
4	32.400	32.500	2.760952	2.759524	2.760476	1.000000	0.466657
Average	32.391	32.491	2.761678	2.760248	2.761202	1.000000	0.430580
Standard Deviation	0.010	0.010	0.000797	0.000794	0.000796	0.000000	0.021498
Precision (2σ)	0.020	0.020	0.001594	0.001588	0.001592	0.000000	0.042996
Accuracy					0.002202	0.000000	
Range 75-79 (2θ)							
Expected*			1.235			0.15	
1	77.165	77.390	1.235136	1.235167	1.235146	0.146620	0.066700
2	77.185	77.410	1.234865	1.234898	1.234882	0.142178	0.067426
3	77.180	77.405	1.234933	1.234965	1.234944	0.135545	0.062376
4	77.185	77.405	1.234865	1.234965	1.234898	0.140278	0.073969
Average	77.179	77.403	1.234950	1.234999	1.234966	0.141497	0.067178
Standard Deviation	0.008	0.008	0.000111	0.000109	0.000107	0.004651	0.004144
Precision (2σ)	0.016	0.016	0.000333	0.000327	0.000321	0.009302	0.008288
Accuracy			0.000050			0.008503	
Range 133-138(2θ)							
Expected*			0.8325			0.06	
1	135.375	136.065	0.832622	0.832648	0.832631	0.050795	0.022664
2	135.380	136.075	0.832607	0.832619	0.832611	0.051485	0.020000
3	135.375	136.075	0.832622	0.832619	0.832621	0.054654	0.020495
4	135.380	136.095	0.832607	1.832561	0.832592	0.051975	0.024291
Average	135.378	136.078	0.832615	0.832612	0.832614	0.052227	0.021863
Standard Deviation	0.003	0.011	0.000008	0.000032	0.000015	0.001462	0.001723
Precision (2σ)	0.006	0.022	0.000016	0.000064	0.000030	0.002924	0.003446
Accuracy			0.000115			0.007773	

in the packed sample being higher than the holder. A razor blade is now used to further sift and compress the sample. All particles on the holder are carefully brushed off to prepare for the final compaction. A final visual inspection should reveal a flat and level surface, or the procedure must be repeated. The sample holder is now ready to be placed within the *XRD* sample compartment.

2.2.2 Least-Squares Refinement Methods

A microcomputer package for indexing and least-squares refinement of powder diffraction data (Appleman and Evans 1973) was used to determine precise unit cell parameters of the perovskite compounds. This method operates best if only reflections with relative intensities greater than 1.00 are used. Fortunately, the contribution of the omitted peaks is insignificant when compared to all the data available from a single *XRD* spectrum. Unit cell parameters were calculated in two steps. Initially, only the main (>10 relative intensity) $K_{\alpha 1}$ peaks were employed to calculate trial parameters and the subsequent trial powder pattern. Utilizing the remaining reflections, which could now be properly indexed, the cell parameters were refined. The operating principle of least-squares is that the best-fit parameters are those that minimize the sum of the squares of the errors.

The XPOW interactive software (Downs *et al.* 1993) was used for calculating theoretical *X*-ray diffraction patterns. The XPOW program requires only the input of radiation wavelength, space-group (symbol or number), cell dimensions, lattice parameters (**a**, **b**, **c**, α, β, γ) and atomic coordinates (*x*, *y*, *z*) for each atom. The program calculates

the *d*-spacings and 2θ values associated with all Bragg indices, as well as the relative intensities, within a specified interval. If atomic parameters are unknown, the program is still effective for calculating the *d*-spacings and 2θ values, although the relative intensities will not be available.

2.2.3 Scanning Electron Microscopy

As a further check on product purity, a detailed study by *X*-ray energy dispersive spectrometry (EDS) using a Hitachi 570 scanning electron microscope (SEM) was undertaken. The SEM is equipped with a LINK ISIS analytical system incorporating a Super ATW Light Element Detector (133 eV FwHm Mn_k). The operating conditions are as follows: a take off angle of 30^0; accelerating voltage of 20 kV; a beam current of about 0.87 nA and a working distance of 28 mm. The EDS spectra of standards and unknowns were collected and processed with the LINK ISIS-SEMQUANT software package. They were acquired for 100 seconds (live time) to reduce random errors due to counting statistics. The standards that were selected, together with estimates of accuracy and precision of the method, are given in Table 2-5. Back-Scattered Electron (BSE) images were captured using the Link Tera autobeam program.

2.2.4 Rietveld Refinement

Rietveld refinement (Post and Bish 1989; Young 1995) makes use of the entire *XRD* spectrum for the derivation of very precise and accurate crystal structure determinations

Table 2-5 Precision and accuracy of the loparite-(Ce) standard as determined for SEM/EDS. Analysis is in wt%.

Analysis #	La	Ce	Pr	Nd	Σ REE	Sr	Ta	Th	Ca	Nb	Ti
1	13.02	18.67	1.12	1.92	34.73	1.69	0.24	1.40	36.51	8.18	43.57
2	13.15	18.93	1.00	1.92	35.00	1.71	0.16	1.42	36.31	8.87	42.51
3	12.68	18.10	0.11	2.16	33.05	1.70	0.13	1.29	36.50	9.05	42.41
4	12.56	18.04	0.67	1.97	33.24	1.70	0.20	1.24	36.59	8.17	42.50
5	13.01	18.40	0.73	1.15	33.29	1.89	0.16	1.30	36.48	8.35	42.91
6	12.64	18.10	0.00	1.49	32.23	1.84	0.19	1.23	36.79	8.27	42.75
7	13.49	19.16	1.20	1.61	35.46	1.91	0.17	1.19	36.40	8.22	42.65
8	13.05	18.32	1.65	2.02	35.04	1.88	0.31	1.28	36.33	8.76	42.72
9	12.79	18.16	1.14	1.98	34.07	1.93	0.37	1.02	37.00	8.82	43.05
10	12.59	18.11	1.27	1.76	33.73	1.93	0.37	1.04	36.99	8.43	43.03
11	12.89	18.75	1.98	2.32	35.94	1.80	0.39	1.34	36.75	8.35	42.71
12	12.74	18.90	1.88	2.41	35.93	1.73	0.28	1.33	36.42	8.34	42.55
13	12.90	19.05	1.79	2.35	36.09	1.69	0.30	1.32	36.52	7.79	42.55
14	12.01	18.24	1.98	3.01	35.24	1.86	0.26	1.11	36.29	7.95	42.92
15	12.49	18.16	1.34	2.83	34.82	1.88	0.19	1.31	36.30	9.05	42.89
Expected	13.03	18.66	1.12	1.88	34.69	1.67	0.28	1.39	36.40	8.28	43.00
Average	12.80	18.47	1.19	2.06	34.52	1.81	0.25	1.25	36.55	8.44	42.78
Standard dev.	0.33	0.38	0.60	0.47	1.15	0.09	0.08	0.12	0.23	0.37	0.29
Accuracy	-0.23	-0.19	0.07	0.18	-0.17	0.14	-0.03	-0.14	0.15	0.16	-0.22
Precision (2σ)	0.66	0.76	1.20	0.94	2.30	0.18	0.16	0.24	0.46	0.74	0.58

(Chapter 3). The method permits the refinement of the unit cell dimensions and atomic positions in the crystal structure simultaneously. The Rietveld method requires a proper starting model, which can be established by comparison with similar structures. An initial model is refined using background coefficients, scale factors, error correction factors, peak-shape parameters, and lattice parameters. At each cycle in the refinement a comparison of observed and calculated diffraction patterns, as indicated by the weighted profile residual (*Rwp*), are necessary to determine the degree to which parameters are refined. The fitting of the diffraction pattern is achieved by a least-squares method of minimizing the differences between the observed pattern and the synthetic pattern.

The program 'Atoms for Windows' (version 3.0; Dowty 1995) was used to calculate bond lengths and angles for each member of the tausonite-loparite solid solution series. This program used cell parameters as refined by the Rietveld refinement program (DBWS-9411).

Chapter 3

RIETVELD REFINEMENT

3.1 Rietveld Refinement

3.1.1 Introduction and Key Features

This crystal structure refinement technique is named for H.M. Rietveld, who was the first to devise computer-based analytical procedures which make use of the entire information content of an *XRD* powder pattern (Rietveld 1969, 1967). The Rietveld refinement technique (Post and Bish 1989) is useful in the derivation of crystal structure information from powder *XRD* data. This method provides an alternative to structural studies where single-crystal methods are not available. In the Rietveld method, each data point (2 θ step) in a powder diffraction pattern is an observation, and during the refinement procedure, crystal structure parameters and instrumental parameters are varied in a least-squares technique until the entire calculated powder profile, based on a structure model, best parallels the entire observed pattern. The refinement can yield very precise and accurate unit cell parameters, and quantitative analysis of mixtures of phases. On the negative side, this is merely a refinement technique and is inaccurate for determination of atomic structural parameters, especially temperature factors. This commonly results in poor or incorrect refinements, due to inaccuracies in Bragg intensities, for samples which exhibit systematic structure disorder (preferred orientation, surface roughness, *etc.*,).

3.1.2 Requirements and Conditions

Powder *XRD* has been an important tool for decades for identification and characterization of minerals and other crystalline materials (Post and Bish 1989). It was considered, until recently, as being unsuitable for application to serious crystal structural analysis, due to peak overlap, and difficulties in accurately measuring Bragg intensities. Many (not all) of these problems have been overcome with the advent of computer-automated diffractometers, making it possible to acquire data using a step-scan technique, and the application of the Rietveld refinement method to powder *XRD* studies. The Rietveld method overcomes the problems of peak overlap by utilizing the entire powder diffraction pattern, thus allowing for the extraction of the maximum amount of information from any pattern. Although patterns collected from powder *XRD* techniques are complex and are consequently difficult to model, this is countered by the advantages of easy accessibility and smaller sample requirements, together with improvements in peak shape functions. Powder *XRD* data is also advantageous over other methods due to the rapid acquisition time, making it applicable to phase transformation studies, heating or cooling experiments, pressure change studies, *etc.*

Since the publication of Rietveld's original program, there has been a proliferation of versions of computer programs for local and general use on personal computers. A large number of available programs, including more than a dozen for Rietveld refinement, are listed in a report to the International Union of Crystallography (IUCr) Commission on Powder Diffraction by Smith and Gorter (1991). These include GSAS (Generalized Structure Analysis System), RIETAN (Japanese standard), XRS-82 (*X*-ray Rietveld

System), LHPM (Lucas Heights Research Laboratories), and DBWS (current version is 9411). The newest version, DBWS-9411, is the latest in a long chain of versions and is differentiated from the previous version (DBWS-9006) by the incorporation of a more user friendly input control file, the addition of four surface-roughness models, a Split-Pearson VII asymmetry profile function, and a quantitative phase analysis routine, as well as various other corrections and features (Young *et al.* 1995). Rietveld refinements undertaken in this work employed DBWS-9411.

3.1.3 Sample Considerations

Sample preparation is one of the most important stages of any crystal structure refinement which is based on powder *XRD* data (Post and Bish 1989). Most materials, especially those exhibiting cleavage, invariably yield powder samples exhibiting preferred orientation due to non-randomly oriented crystallites. This results in discrepancies within observed peak intensities leading to an inaccurately refined structure. If possible, preferred orientation effects must be reduced or eliminated. In the case of the tausonite-loparite solid solution series, investigated in this work (chapter 4), the grain size is sufficiently small (<10μm) such that preferred orientation problems are minimized. Several methods of preparing random *XRD* powder mounts are possible, but these offer no guarantees that the orientation is random, making it important to compare data from several sample mounts to determine the extent of preferred orientation effects.

Quenching to room temperature may be a possible sample related mechanism for producing line broadening due to the resulting stresses and/or fracture of particles (Tien

and Hummel 1967). Stresses may be primary and are often attributed to the thermal expansion of the surface relative to the interior of the sample as quenching progresses; and to the crystallite transformation to a lower symmetry system (*e.g.*, tetragonal) on cooling. This transition may be beyond the resolution of the equipment.

Another consideration is the amount of the sample to be used within the mount (Post and Bish 1989). A suitable thickness, depending on the radiation used and absorption properties of the sample, is required for the reduction of background and transparency effects to the resulting pattern. These effects, when not properly modelled in the refinement, can result in significant errors, particularly in temperature factors. The surface area has to be sufficiently large enough to contain fully the *X*-ray beam throughout its angular range.

3.1.4 *XRD* Requirements

The use of automated powder diffractometers, for the quick and accurate collection of digitized step-scan (2θ intervals) intensity information, has facilitated numerous successful Rietveld studies (Post and Bish 1989). Previous refinements have used a wide range of step intervals, which seem to depend mainly on personal preference. Data precision (Table 2-4) can be improved by decreasing the step width and/or increasing the counting time, resulting in a longer collection time, until the counting variance becomes negligible compared to other sources of error. The choice of operating conditions is problematic. As the step size is decreased, although there is an increase in the number of observations, there is a decrease in the Bragg intensities that are fundamental to the

structure analysis. Post and Bish (1989) summarize diverse experiments regarding optimum operating conditions and recommend counting times which result in no more than a few thousand counts for the strongest peak and step intervals that are one-fifth to one-half of the minimum full-width at half maximum of resolved peaks in any pattern. Rietveld refinement of the tausonite-loparite solid solution series has necessitated the reduction of the step size from .040° to .020° (2θ) for better resolution and more accurate peak profiles.

Another notable operating condition to consider is the data collection range (Post and Bish 1989). Data should be collected to the highest possible angle, especially for successful refinement of temperature factors. Peak intensities, unfortunately, tend to decrease significantly with increasing angle, primarily due to the decrease in atomic scattering factors (Klug and Alexander 1974), making it necessary to use longer counting times at higher angles. Additional complexity arises from both $K_{\alpha 1}$ and $K_{\alpha 2}$ radiation and subsequently the appearance of reflection doublets at high angles. Use of monochromatic radiation or $K_{\alpha 2}$ stripping may eliminate the problem, but significantly reduces the total amount of information available.

Klug and Alexander (1974) have identified six major diffraction functions that modify the pure Bragg peaks: geometry of the *X*-ray source, flat specimen error, axial divergence of the *X*-ray beam, specimen transparency, effects of receiving slits, and misalignment of the diffractometer. An understanding and correction of these factors is essential for a proper refinement.

3.2 Observed Data Input File

The observed data input file (ODIF) contains the raw data from the *X*-ray diffractometer. The *XRD* data collected in this study has to be modified to fit the format required for the DBWS refinement programs. Modification of the data may require use of a simple Fortran program (CONVUDF.EXE) to convert an *XRD* UDF data file format (ASCII format; *e.g.*, TAUSONIT.UDF) into another file format (ASCII x-y format; *e.g.*, TAUSONIT.DAT) recognized by the Wyriet conversion program (CONV).

This new format (ASCII x-y) can now be transformed by the Wyriet CONV program to the FORT 4 format, and vice versa, for use in DBWS-9411. As an important note, any desired data range can easily be chosen by setting the start and stop angles in the data input file to that range, and by declaring an excluded region (NEXCRG, *line 2* 5-I4) and its bounds (*line 6*).

3.3 Input Control File

The input control file (ICF) (Young 1995) contains various options concerning refinement control variables, instrumental and crystal structure models, and other refinable parameters. The ICF is usually referred to as FORT 5 or TAPE 5 in most programs, but for simplicity the term INPUT will be used. The following sections are a line-by-line description of the layout of the ICF, accredited to the User's Guide by Young *et al.* (1995).

Refinement Controls

The first part of any Rietveld refinement, and perhaps most important part, is the set-up of choices concerning options such as output desired and model functions (Young 1995). These controls generally lie within the first three lines of the input control file and have an interval of space (Fortran notation) for their location. It is very important to ensure that the proper parameters are 'turned on' or 'turned off' for the selection of the various refinement control variables.

3.3.1 The Starting Model

Rietveld refinement requires initial estimates of various crystallographic and instrumental parameters. The ideal starting model for a proper refinement is, therefore, a pre-existing ICF that is a reasonable approximation to the actual crystal structure for use as a template. A number of sample ICFs are provided with any of the available programs. The clearest choice for a starting model is one in which, firstly, the instrumental model (section 3.3.1.1) best approximates the type of instrument used, and secondly, the crystal structure model (section 3.3.1.3) best approximates the compound to be refined. After a template is chosen, the ICF is ready to be 'customized' by input of all known parameters into their proper locations.

Proper codewords (see Appendix A.1) are now entered for any parameter which is required to be refined. It is important to note that if *N* parameters are to be refined (MAXS= *N*, *line 9*, I8), then no codewords with *DDD* in the range from 1 through to *N* can be absent, otherwise an error message "hole in matrix" will result. It is possible to have

more than *N* parameters present in the ICF, but they will not be refined. The use of zero for *C.CC* in the codewords, results in that parameter not being refined. This presents a problem, as even though the parameter is turned off, the applied shifts being set to zero will give unrealistic correlation-matrix elements.

3.3.1.1 Instrumental Model

The instrumental model consists of those particular measurements associated with the instrument, and are not refinable, but are adjusted if necessary. These include *X*-ray wavelengths, starting angle, ending angle, step size, scattering lines if necessary, *etc.*

3.3.1.2 Background Model

When doing refinements, it is essential to account for the background radiation which is included with every instrumental analysis. Background radiation can be accounted for by an *XRD* observed data file for background (FORT 3) and setting NBCKGD= 1 (*line* 2). When FORT 3 is not required, setting NBCKGD= 0 (*line* 2) allows the background to be refined in *line 11.* When NBCKGD= *N* (*N*≥ 2), then background is to be determined by interpolation between *N* points given in *line 6.*

3.3.1.3 Crystal Structure Model

An ideal crystal structure model is proposed by analogy with similar structures, *e.g.*, other members of a solid-solution series or isostructural materials of known structure (Post and Bish 1989). Post and Bish (1989) suggest that high-resolution electron microscope

images may be of use to provide sufficient information from which to assemble a structure model, when nothing else is available. Essentially, no refinement can start without some minimum vital parameters that must be obtained before the refinement commences: space-group; ideal site occupancies (International Tables of *X*-Ray Crystallography 1965); atomic positions of each atom (easier to use previous data for non-fixed positions, rather than to estimate); temperature coefficient, B; and cell parameters.

The Bragg peaks (Post and Bish 1989) of any powder diffraction pattern are the integrated intensities as distributed by a peak-shape function. Peak-shape in any *X*-ray diffraction pattern is a complex convolution of several instrumental and sample effects. The profile of pure diffraction maxima are determined largely by the crystallite-size distribution, crystal structure distortions, and the spectral distribution in the incident radiation (Klug and Alexander 1974). *Lines 17*, and *19-22*, in DBWS relate to the peak-shape of a given *XRD* pattern.

3.3.1.4 Modifications of the Overall Model

The first step in a proper refinement is to do a refinement with no parameters varied, and manually adjust the input control file to reduce any mismatches within the plot. This manual refinement should follow the order of the parameter turn-on sequence (section 3.3.2) up to step four. This should be repeated until one of two conclusions are reached: 1) a radically different starting model is required; or 2) a match is developing, where the *R*-value (section 3.3.2) should drop quickly to eventually settle into a slow steady decline. If the former is the case, check the scale factor, space-group, or determine if another

phase exists. It may be necessary to refine peak parameters initially while estimating an accurate scale factor; to begin a difficult refinement. If the latter is the case the actual refinement should now be ready to commence, and this primary input control file should be saved separately to prevent starting over from scratch if the updating of the input control file at each cycle (see below) is turned on and scrambles some data. It is advantageous to save input files under different names (input1, input2, *etc.*,) as the refinement progresses to provide a number of reference points from which the refinement can continue.

3.3.2 Refinement Strategies

The refinement program must be run within the set-up data subdirectory (*e.g.*, TAUSONIT.LU), using the execute command DBWS DATA INPUT OUTPUT, where DATA refers to the converted (by CONV) ODIF, INPUT refers to the ICF, and OUTPUT refers to the main output file. Following is a typical refinement strategy used for tausonite.

3.3.2.1 Parameter Turn-on Sequence

Many strategies exist for the proper parameter turn-on sequence, nearly as many as there are refinements. The appropriate method for any one refinement is determined by trial and error variations on some predetermined order in a similar refinement or taken from the QTEST or FTEST subdirectories. This general order of refinement will apply when the composition is not known precisely. Grouping of the steps is possible when the starting model is known to be accurate, and will prove more time effective. Each

successive step in the following general sequence includes the parameters refined in the previous steps, unless indicated. It is of the upmost importance to make constant use of plots and the criteria-of-fit (section 3.4.3) to recognize gross misfits so as to understand and correct for them as the refinement develops.

1) Overall Zeropoint -which must originally be set to zero.

2) Scale Factor -for major phase first, if multi-phased.

-pre-determined from the manual refinement.

3) Background Coefficient (Bo).

4) Background Parameters remaining -up to a maximum of three.

5) Unit Cell Dimensions -for major phase first if multi phased.

-initial estimates required, and way be varied separately when necessary.

6) Peak Parameter W -cannot start at zero, initial estimates required.

7) Peak Parameter U -can start at zero, initial estimates not required.

8) Peak Parameter V -can start at zero, initial estimates not required.

9) Peak Shape Function -(Y1) cannot start at zero.

10) Asymmetry parameter -cannot start at zero.

At this point, steps 6-10 should have their values set (flags removed), and steps 1-5 will continue to be varied. These parameters (6-10) may be rejected while attempts are made to refine the following parameters:

11) Atomic Coordinates -for non-fixed positions.

-if non-cubic, they should be varied in order *x*, *y*, and then z.

12) Site occupancies -only when disorder exists; and atoms with similar atomic coordinates should have their site occupancies varied relative to each other (using positive and negative flags).

-if no disorder exists, these may be varied last as a check on whether a gross error is present.

13) Overall Isotropic Temperature Factor (B overall), or the individual anisotropic temperature parameters. Refining of anisotropic factors is probably futile if the data are not precise.

14) Preferred Orientation Parameter.

15) Peak Shape Function -(Y2) cannot start at zero.

-most sensitive, and should usually be done last.

The previously fixed parameters are now refined collectively and are followed by any remaining unrefined parameters refined in a step-wise fashion. From this point there exist no further refinement strategies, and the continuation of the refinement depends on the user, through careful observation of the plots and criteria-of-fit.

3.3.2.2 Following the Refinement

At any point within the refinement certain misfits may occur which must be dealt with by manually adjusting specific parameters. This may require going back a few steps, changing a value, and going forward once again. This is where it is extremely helpful to run several input files with a trial-and-error strategy to discover the best course of action.

Following is a list of some possible hints to overcome some errors or common misfits between observed and calculated plots during the refinement (Young 1995).

1) If the error message 'scattering data missing' is displayed, then there is a error with the programs reading of the atoms names, valence or scattering data.

2) If the error message 'invalid integer' is displayed, then there is an error in the format of the ICF.

3) If the error message 'hole in matrix' is displayed, then there is a number missing in the sequence of codewords refined.

4) It is important to ensure that no parameters have the same codeword.

5) If the refinement stops and the message 'Square of FWHM is negative' appears, alter, dampen, or refine the profile parameters.

6) If the *R-wp* increases with each cycle then check the parameter values for the one which is misbehaving and determine if it is redundant (should be fixed) or should be dampened.

7) If the plot of observed versus calculated pattern has no resemblance, check the scale factor, the space-group, or the number of phases present. Examine the two plots to see if any order exists.

A) If no order exists, than it may be a fundamental error with the model, *e.g.*, an error in the space-group determined.

B) If the difference plot is an almost duplicate of the observed plot, then there is a scale factor problem, which can be overcome by manually varying the scale

factor while fixing all else, otherwise the scale factor will continue to cause significant misfit.

C) If there are peaks occurring where there are no Bragg-reflection markers, then this indicates the presence of an additional phase or a different space-group.

8) If the two plots have a resemblance, but differ slightly in intensities and approximate positioning of peaks, then this is likely a lattice parameter, specimen displacement, zero point offset, or peak shape problems.

9) If the two plots differ only in intensities, the problem is associated with atomic coordinates, peak widths and angle-dependent parameters (*e.g.*, surface roughness, absorption, and temperature factors).

10) When more background parameters are turned on then required, this will lead to a false minimum in misfit early in the refinement and will eventually result in improper refinement with high criteria-of-fit at the refinements conclusion. It is generally necessary to refine at most 3 terms of the background polynomial.

11) If the calculated profile is truncated too much, then the WDT parameter (*line 4*, 5-F8) is likely the problem and the standard value of 3 is too small.

3.3.2.3 When to Stop

The perfect time to stop any refinement is a matter of individual choice. It is essential that the refined model make both physical and chemical sense (*e.g.*, no absurd numerical values such as negative site occupancies). Termination of the refinement may depend upon the following criteria (Young 1995):

1) Numerical criteria-of-fit (section 3.4.3, especially *R-wp* and *S*) have achieved the desired value.

2) Shifts are less than the estimated standard deviation divided by ϵ (arbitrary value chosen by user in the ICF), where ϵ is generally much smaller than one (usually 0.30 - 0.05).

3) Output parameter values are simply oscillating.

4) Poor fit indicates a different model should be tried.

5) Computer and user time for refinement exceeds the value of the problem.

6) Graphics (section 3.4.2) are invaluable as 'numbers are blind'.

3.4 Output Data Files

3.4.1 Updated Input Control File

If output of a new input control file is selected in NXT (*line* 3, 5-I1), the current ICF will be updated at the end of the last cycle. This is done to ensure that any step in the refinement process can proceed from the previous one without needless keyboarding. To reiterate, it is very important to save the ICF under a different file name occasionally to provide a back-up in the event that a refinement step presents a problem, for which the only solution would be re-writing the ICF in use.

3.4.2 Plot Files

One type of plot file can be generated, PLOTINFO (unit 9), within the PC version. This is an alpha-numeric file consisting of: the title information from line 1 of the ICF; a

separate labelled listing of the geometrically possible Bragg reflection positions, with Miller indices (*h k l*) for each phase involved in the refinement (IPC= 1 or 2, *line 3*, 3-I1); a listing of the calculated and observed intensities at each step (IOT= 1, *line 3*, 1-I1); and/or any other output control formats. PLOTINFO allows both the SPLOT and the DMPLOT programs (included as Shareware items) to produce a plot of calculated and observed patterns, which can be manipulated to allow almost any desired on-screen or plotter output. Several other available software packages are compatible with PLOTINFO to make other Rietveld refinement plots.

3.4.3 Terminal Output

The terminal output displays the program name (DBWS) and version; the sizes declared for the five most frequently redimensioned arrays; the title information for the run; the number of cycles called for; the number of parameters refined; the START angle, STEP size, and STOP angle; and a dynamic series of dots following the progress of the program through the current cycle. At the conclusion of each refinement cycle, there is a report of *R-p*, *R-wp*, and *R-exp*. *R-wp* is the most meaningful of the *R*-values because it best reflects the progress of the refinement, because its numerator is the quantity being minimized. The 'goodness of fit' (*S*) functions well as a warning, indicating more serious problems such as the need for changing the starting model (Young 1995). All of these criteria-of-fit are essential for discovering the true structure refinement of a compound. The graphical display of criteria-of-fit is of the utmost importance because it is visual and not numerical.

Following are the definitions of some criteria-of-fit.

E.S.D = $\sigma_{jj} = M^{-1}_{jj} \{(y_{oi} - y_{ci})^2 / (N-P+C) \}^{½}$ -the estimated standard deviation.

Where: -M^{-1}_{jj} is the corresponding diagonal element in an inverted normal matrix.

-N is the number of observations.

-P is the number of parameters that are refined.

-C is the total number of constraints.

R-p = $100 \sum | y_{oi} - y_{ci} | / \sum | y_{oi} |$ -the pattern *R*-factor.

R-wp = $100 \{ \sum w_i (y_{oi} - y_{ci})^2 / \sum w_i (y_{oi})^2 \}^{½}$ -the weighted pattern *R*-factor.

R-exp = $100 \{ (N-P+C) / \sum w_i \ y_{oi} \}^{½}$ -the expected *R*-factor.

S = The ratio of *R-wp / R-exp* -the goodness of fit.

*R-Bragg*and *R-F* will be printed out at the end of the final cycle when the reflection list is called for (IPC, *line 3*, 3-I1).

R-Bragg = $100 \sum | I_o - I_c | / \sum I_o$ -the *R*-value for the Bragg intensities.

R-F = $100 \sum | | F_o | - | F_c | | / \sum | F_o |$ -the *R*-value based on the deduced observed and calculated structure amplitudes (useful in *ab initio* structure determinations).

The Durbin-Watson statistic (*D*) is included in the output from each cycle as a possible indicator of the progress of the refinement, because it is considered to be the most sensitive to misfit. This is sensitive to misfit, in areas, positions and most importantly shape, of the calculated and observed reflection profiles. Ideally *D* should be equal to 2.00, and any difference usually indicates a fundamental problem.

$$D = \sum_{I=2}^{N} (\Delta y_i - \Delta y_{i-1})^2 / \sum_{I=2}^{N} \Delta y_i^2$$

where: $\Delta y_i = w_i (y_{oi} - y_{ci})$

A refinement with an acceptable fit should have *R-p* <10, *R-wp* <10, *S* <1.5, *R-Bragg* <5, and *D* ≈2.00. However, *R-p* <11, *R-wp* <16, *S* <2, and *R-Bragg* <8 may be acceptable for many purposes. It should be noted that *R-p* and *R-wp* are very sensitive to the background level through the relation of the factor y_{oi}. Thus, an experienced user now knows not to expect to judge the relative quality of a refinement made for different data sets by these two factors. The importance of these factors are essentially to judge the progress of a particular refinement only. For comparison of differing structure refinements *S* and *R-Bragg* are essential.

3.4.4 Main Output File

The main output file (MOF) consists of both standard parts and optional parts (Young 1995). The standard output consists of all the control variables and structure parameters, which will allow a given run to be reconstructed unambiguously. As each cycle is completed, the parameters with their relative applied shifts, the quantitative phase analysis result, various numerical criteria-of-fit and related values are listed in the MOF. The optional outputs are those selected (1 or 2) or suppressed (0) by the settings of flags in line 3 of the ICF (section 3.3 refinement controls).

Chapter 4

Tausonite-Loparite Solid Solution Series

4.1 Introduction

The structure and properties of the perovskite group compounds can be varied through chemical substitution of the *A*- and *B*-site cations. Of all the *REE*-rich perovskites, only loparite-(Ce) may be considered as a distinct rare earth mineral. Loparite-(Ce) forms complex solid-solutions with other *REE*-free perovskite-group minerals. This study investigates such a complex solid-solution, between synthetic loparite ($NaLaTi_2O_6$) and the *REE*-free perovskite tausonite ($Sr_2Ti_2O_6$). The solid-solution was synthesized over the following compositional range; $Sr_{(2x)}(NaLa)_{(2-2x)}Ti_2O_6$ (where x represents linear mixing between the two end-members, in steps of x=0.1) at a temperature of 1100°C (see Chapter 2).

Structure refinements were conducted to provide essential information concerning the symmetry as well as the location and environment of all cations in this series. This study examines the following three questions: Does the substitution of Na^+ and La^{3+} for Sr^{2+} at the *A*-site result in an orthorhombic solid-solution series, due to a symmetry reduction? Will the pseudo-cubic cell parameter a_p decrease, while the [*111*] tilt angle Φ (Φ=0 in $SrTiO_3$) increases with increasing loparite content (Mitchell 1996)? Of great importance, with respect to the symmetry of the solid-solution series, is whether the *A*-cations are distributed randomly or are ordered in the structures. If the conclusions of Galasso (1969) for *B*-cation ordering also apply to the *A*-site, it would be expected that

ordering may occur due to the very different size in proportion to valence of Na^{+}, La^{3+} and Sr^{2+}.

4.2 Perovskite -Structure and Space-Group

4.2.1 Mineralogy

Tausonite

The mineral tausonite was named in honour of the Soviet geochemist, Academician L.V. Tauson. Synthetic $SrTiO_3$, has been widely-studied and produced as a substitute for gem-quality diamond for many years. The natural equivalent (Vorob'yev *et al.* 1984) was not discovered until 1980, in alkaline rocks of the Little Murun potassic syenite massif, in the western part of the Aldan Shield, Russia. This mineral is actually strongly zoned with respect to strontium and *REE* and no useful average composition may be calculated as its composition ranges from tausonite to strontian cerian loparite on a microscale (Mitchell and Vladykin 1993). Thus, this mineral cannot be viewed as a true strontium end-member due to the significant content (~5-61%) of other components.

The name tausonite, as used in this work, represents the synthetic variety of $SrTiO_3$. Tausonite crystallizes with the ideal cubic perovskite structure at ambient temperatures (space-group $Pm\bar{3}m$; **a**= 3.9054Å; *t*=1.0016, from this synthesis; to be defined on page 77). In the tausonite structure (illustrated in Figure 1-4 and 1-5), the TiO_6 octahedra are corner-linked, with Sr^{2+} cations in twelve-fold coordination occupying the interstices within the framework. Unit cell parameters for tausonite are comparable to those given by Galasso (**a**=3.9050Å; *t*=1.002; 1969). A single crystal *XRD* study by Buttner and Maslen

(1992) gave **a**=3.9092Å. These differing results may be attributed to associated Fe impurities within the crystals, crystal face imperfections, and to the procedures employed. Atomic coordinates of tausonite appear in Table 4-1.

Loparite-(Ce)

The mineral loparite-(Ce) is the *REE* rich end-member [$(Na_{.50}REE_{.50})TiO_3$] of the perovskite group of minerals, where *REE* represents the total content of rare earth elements, typically with La^{3+} or Ce^{3+} dominant. Loparite-(Ce) has been found in agpaitic nepheline syenites, urtites, juvites and alkali pegmatites of the Kola Peninsula (Chakhmouradian and Mitchell 1997).

The synthetic counterpart of loparite-(Ce) used in this study is $(NaLa)Ti_2O_6$, and henceforth, will be referred to as loparite. Mitchell (1996) indicates loparite-(Ce) has a centrosymmetric structure (Figure 1-8) which is orthorhombic (space-group *Pnma*; **a**=5.4817Å; **b**=7.7467Å; **c**=5.4771Å; $\mathbf{a}_p$=3.8741Å; t=0.9787; Φ=2.50°; Z=4, from this synthesis). This space-group is equivalent with *Pbnm*, which has been used as an alternative setting (Beran *et al.* 1996). Space-group *Pbnm* is a different setting for the same unit cell (**cab**) instead of the standard (**abc**) for *Pnma* (International Tables for *X*-Ray Crystallography 1965). Loparite is considered to have disordered *A*-site cations and a distorted perovskite structure. Woodward (1997b) describes the possible octahedral tilts of the perovskite structure. The atomic coordinates expected for loparite, assuming no ordering of Na^+ and La^{3+} appear in Table 4-1.

Table 4-1 Table of crystallographic properties of the tausonite-loparite solid solution series. Data derived from specific references and from the International Tables for *X*-Ray Crystallography (1965).

End-member Composition	$Sr_x(NaLa)_{(1-x)}Ti_2O_6$										
	x=1.0-0.7			x=0.6-0.3				x=0.2-0.0			
Coordination #	6	12	2	6	12	2	2	6	12	2	2
Occupant	Ti^{4+}	Sr^{2+}	O^{2-}	Ti^{4+}	$Sr^{2+}/La^{3+}/Na^{+}$	O^{2-}	O^{2-}	Ti^{4+}	La^{3+}/Na^{+}	O^{2-}	O^{2-}
Point Symmetry	*m3̄m*	*m3̄m*	*4/mmm*	*4/m*	*4/m*	*4/m*	*m*	*1*	*m*	*m*	*1*
Wyckoff Notation	*1a*	*1b*	*3c*	*2a*	*2b*	*2b*	*8i*	*4a*	*4c*	*4c*	*d*
Atomic Coordinates:											
x	0	1/2	1/2	0	0	0	0.2600	0	-0.0068	0.0714	0.7108
y	0	1/2	1/2	0	1/2	0	0.7600	1/2	0.0360	0.4838	0.2888
z	0	1/2	0	0	1/2	1/2	0	0	1/4	1/4	.0371
Site Occupancy (*n*)	1/48	1/48	3/48	2/16	2/16	2/16	8/16	4/8	4/8	4/8	8/8
Z	1			1				4			
Crystal Symmetry	Cubic			Tetragonal				Orthorhombic			
Point Group	*m3̄m*			*4/mmm*				*mmm*			
Space Group	*Pm3̄m* (#221)			*P4/mbm* (#127)				*Pbnm* -standard for *Pnma* (#62)			
Limiting Conditions For Reflections	no limits			*0kl: k=2n; hkl: h+k=2n*				*hkl: k+l=2n, h=2n; h0l: h+l=2n; h00: h=2n; hk0: h+k=2n*			
a_p (Å)	3.9050 Å			3.8923 Å				3.879 Å			
a (Å)				5.5079 Å				5.476 Å			
b (Å)				5.5079 Å				7.777 Å			
c (Å)				3.8876 Å				5.481 Å			
volume ($Å^3$)	59.5474 $Å^3$			117.938 $Å^3$				233.419 $Å^3$			
Tilt Angles											
Tetrad axis [*001*] (ϕ)	0.0°			3.5°				0.9°			
Diad axis [*010*] (Θ)	0.0°			0.0°				2.4°			
Triad axis [*111*] (Φ)	0.0°			0.0°				2.5°			
References	Galasso 1969			Woodward 1997a				Mitchell 1996			

Tausonite-Loparite

Minerals exhibiting complex solid solution between tausonite and loparite are common, as in the Little Murun potassic alkaline complex of Yakutia, Russia (Mitchell and Vladykin 1993) and Sr-poor, Nb-bearing loparite from the Kola region, Russia (Vlasov 1966). Principal *A*-site substitutions are represented by $0.5\ Na^{+} + 0.5\ La^{3+} \rightleftharpoons Sr^{2+}$ and suggest a complete solid-solution between tausonite and loparite.

Structural distortions and phase transitions of the centrosymmetric $ATiO_3$ perovskite from the cubic aristotype are typically the result of cooperative tilting and rotation of the TiO_6 octahedral framework (Glazer 1975, 1972). In loparite, the ideal structure of perovskite may have undergone tilting of polyhedra due to a decrease in the average atomic radius of the substituting *A*-site cation. Reduction of symmetry from cubic to tetragonal results in a new, larger unit cell ($\mathbf{a=b\approx\sqrt{2}a_p}$, $\mathbf{c\approx a_p}$, $Z=1$); and from tetragonal to orthorhombic in an even larger unit cell ($\mathbf{a\approx c\approx\sqrt{2}a_p}$, $\mathbf{b\approx 2a_p}$, $Z=4$) (see Figure 1-7).

Studies of the perovskite-tausonite ($CaTiO_3$ - $SrTiO_3$) binary system at high temperature (1800-2100°C), indicate a structural transition from orthorhombic to cubic symmetry at ~60% $SrTiO_3$ (Čeh *et al.* 1987); where $CaTiO_3$ is orthorhombic (**a**=5.383Å, **b**=7.642Å, and **c**=5.439Å) and $SrTiO_3$ is cubic (**a**=3.9075Å). McQuarrie (1955), in an earlier investigation of the same system, determined a structural transition from orthorhombic to tetragonal symmetry at ~60% $SrTiO_3$, and another transition from tetragonal to cubic symmetry at ~80% $SrTiO_3$. On the basis of these data, similar transitions might be expected in the tausonite-loparite solid solution series.

The tausonite-loparite ($SrTiO_3$ - $NaLaTi_2O_6$) solid solution series was prepared on the basis of the following reactions at a temperature of 1100°C (see section 2.1.3.1):

$$SrO_{(s)} + TiO_{2(s)} \Rightarrow SrTiO_{3(s)}$$

$$Na_2O_{(s)} + La_2O_{3(s)} + 4\ TiO_{2(s)} \Rightarrow 2\ NaLaTi_2O_{6(s)}$$

$$(x)\ Sr_2Ti_2O_{6(s)} + (1\text{-}x)\ NaLaTi_2O_{6(s)} \rightarrow (Sr_x(NaLa)_{1-x})Ti_2O_{6(s)}$$

4.2.2 Crystal Structure

Megaw (1973), suggests that the amount of distortion in perovskite-type compounds increases as the average ionic radii of the central cation decreases relative to that of the octahedral cations. This would suggest a reduction in symmetry would be expected with the replacement of the divalent Sr^{2+} ions in $SrTiO_3$ by equal amounts of monovalent (Na^+) and trivalent (La^{3+}) cations, of lesser average ionic radius.

Various tilt systems as well as predicted atomic positions and unit cell descriptions for all space-groups generated from simple tilting of the perovskite octahedra are described by Woodward (1997a). These predicted positions (for cubic, tetragonal and orthorhombic symmetry) were used as starting parameters for Rietveld refinement of the various compositions. Although, ordering of the *A*-site cations may be expected in this series as a large difference in size and charge of the *A*-site cation favours such structures (Hazen and Navrotsky 1996), none was recognized in this study. The replacement of the divalent Sr^{2+} cations occurs in a disordered manner; as indicated by the symmetry transitions (accepted space-groups) encountered.

Distortions in perovskite are attributed mainly to octahedral tilting, where the TiO_6 octahedra tilt while the corner-sharing connectivity is preserved. This is most often the lowest energy distortion mode, since the *A*-O distances can be shortened while maintaining the first coordination sphere about the Ti cation (the flexible Ti-O-Ti bond angle is disturbed).

The tetragonal space-group *P4/mbm* is distorted from the ideal cubic structure by a single octahedral tilt ϕ about the tetrad [*001*] axis (Zhao *et al.* 1993). The orthorhombic space-group *Pnma* is distorted from the ideal cubic structure by two independent octahedral tilts, one about the diad [*010*] axis (Θ) and another about the tetrad [*001*] axis (ϕ) (Zhao *et al.* 1993). The magnitude of the tilt is determined from the pseudo-cubic ($\mathbf{a_p}$, $\mathbf{b_p}$ or $\mathbf{c_p}$) unit cell dimensions; and is a necessary and sufficient description of all symmetry losses for the distorted perovskite structure with respect to the ideal cubic ($Pm\bar{3}m$) (Zhao *et al.* 1993). The Θ tilting causes distortion of the Ti-O-Ti bond angle and the subsequent shortening of the **b** and **c** axes, relative to the **a** axis; as expressed in the equation $\Theta=\cos^{-1}(\mathbf{c/a})$. The ϕ tilting causes shortening of the **a** and **c** axes relative to the **b** axis; as expressed in the equation $\phi=\cos^{-1}(\sqrt{2}\mathbf{c/b})$ (for tetragonal [*P4/mbm*], the equation $\Theta=\cos^{-1}(\sqrt{2}\mathbf{a/c})$ applies). O'Keefe and Hyde (1977) have demonstrated that the distortions in perovskite can be described by reference to a single tilt Φ about a triad [*111*] axis. This tilt is related to the other tilts through the relationship $\cos(\Phi) = \cos(\Theta) \cdot \cos(\phi)$, and may be expressed with regard to orthorhombic unit cell dimensions as $\Phi=\cos^{-1}(\sqrt{2}\mathbf{c}^2/\mathbf{ab})$. Synthetic loparite exhibits the following tilts $\Theta = 2.3°$, $\phi = 0.9°$, and $\Phi = 2.5°$, which are

minor when compared to a 'standard' distorted orthorhombic perovskite $CaTiO_3$ (Θ = 5.4°, ϕ = 8.4°, and Φ = 10.0°; Buttner and Masden 1992).

4.3 Instrumental Analysis

Compositional Determinations

The exact composition of the phases present in the solid solution series could not be determined by SEM analysis due to the small grain size (<0.1μm) and grain shape (<0.1μm) problems. The compositional data indicate the presence of a normal distribution of compositions about the expected pre-determined calculated composition of each sample. In all, especially the tausonite-rich samples, the content of other phases, in most instances rutile (TiO_2), was minor (<8%).

Powder X-Ray Diffractometry

The *XRD* patterns were collected by methods as described in Chapter 2. *XRD* data are listed in Table 4-2 [a-d], with all reflections with relative intensities of less than 0.5 discarded as being unobserved, although all reflections appear in the *XRD* data plots. For least-squares refinement, all reflections with relative intensities of less than 1 were considered unobserved. Doublets representing both $K_{\alpha 1}$ and $K_{\alpha 2}$ reflections appear as low as 32.4°(2θ) for the tausonite end-member.

Most reflections are represented as doublets (both $K_{\alpha 1}$ and $K_{\alpha 2}$ radiation) to follow the gradual emergence of reflections used to determine the regions where symmetry changes can be observed. Unfortunately the inclusion of the extra reflections complicated

Table 4-2a *XRD* powder pattern reflections and calculated patterns (XRAY and XPOW) for the tausonite-loparite solid solution series (x=1.0-0.8).

	x=1.0				x=0.9				x=0.8			
h k l	*d*-obs.	*d*-calc.	I-obs.	I-calc.	*d*-obs.	*d*-calc.	I-obs.	I-calc.	*d*-obs.	*d*-calc.	I-obs.	I-calc.
1 0 0	3.904	3.905	3.5	3.9	3.906	3.904	4.0	3.7	3.901	3.905	3.4	3.4
1 1 0	2.761	2.761	100.0	100.0	2.761	2.761	100.0	100.0	2.761	2.761	100.0	100
1 1 0	2.760	2.761	46.7	49.7	2.760	2.761	49.6	49.7	2.760	2.761	69.7	49.7
1 1 1	2.254	2.255	22.2	205	2.253	2.254	21.9	20.4	2.254	2.254	19.5	20.3
1 1 1	2.253	2.255	10.2	10.2	2.252	2.254	12.1	10.1	2.253	2.254	14.0	10.1
2 0 0	1.953	1.953	40.7	38.6	1.952	1.952	40.4	38.8	1.953	1.952	35.3	39.0
2 0 0	1.952	1.953	21.3	19.2	1.952	1.952	23.1	19.3	1.952	1.952	25.5	19.4
2 1 0	1.746	1.746	2.3	2.6	1.746	1.746	2.3	2.5	1.746	1.746	2.2	2.4
2 1 0	1.746	1.746	1.3	1.3								
2 1 1	1.594	1.594	37.8	32.8	1.594	1.594	35.2	32.8	1.594	1.594	30.0	32.8
2 1 1	1.594	1.594	19.5	16.3	1.593	1.594	19.6	16.3	1.594	1.594	21.5	16.3
2 2 0	1.381	1.381	21.5	19.0	1.380	1.380	19.2	19.1	1.381	1.381	17.0	19.2
2 2 0	1.380	1.381	11.6	9.4	1.380	1.380	10.9	9.5	1.380	1.381	10.2	9.5
2 2 1	1.302	1.302	1.3	1.4	1.302	1.301	1.3	1.4	1.300	1.302	0.5	1.3
2 2 1	1.302	1.302	0.7	0.7	1.301	1.301	0.6	0.7				
3 1 0	1.235	1.235	14.0	12.2	1.235	1.235	12.5	12.2	1.235	1.235	10.3	12.2
3 1 0	1.235	1.235	7.4	6.1	1.235	1.235	7.1	6.1	1.235	1.235	7.3	6.1
3 1 1	1.177	1.177	4.7	4.7	1.177	1.177	4.2	4.6	1.177	1.177	3.4	4.6
3 1 1	1.177	1.177	2.7	2.3	1.177	1.177	2.0	2.3	1.177	1.177	2.4	2.3
2 2 2	1.127	1.127	6.5	5.6	1.127	1.127	5.6	5.6	1.127	1.127	4.4	5.6
2 2 2	1.127	1.127	3.5	2.8	1.127	1.127	2.6	2.8	1.127	1.127	3.1	2.8
3 2 0	1.083		0.6	0.7	1.083		0.4	0.7	1.083		0.6	0.7
3 2 0	1.083		0.4	0.4								
3 2 1	1.044	1.044	15.8	14.1	1.044	1.043	12.9	14.1	1.044	1.044	10.7	14.0
3 2 1	1.044	1.044	8.1	7.0	1.044	1.043	7.2	7.0	1.044	1.044	6.6	7.0
4 0 0	0.976	0.976	3.1	2.8	0.976	0.976	2.4	2.8	0.976	0.976	1.6	2.8
4 0 0	0.976	0.976	1.8	1.4	0.976	0.976	1.1	1.4	0.976	0.976	1.2	1.4
3 2 2	0.947	0.947	1.1	1.2	0.947	0.947	0.7	1.2	0.947	0.947	0.6	1.2
3 2 2	0.947	0.947	0.4	0.6	0.947	0.947	0.5	0.6	0.947	0.947	0.3	0.6
3 3 0	0.921	0.920	9.3	8.8	0.920	0.920	6.9	8.7	0.920	0.920	5.6	8.7
3 3 0	0.920	0.920	4.5	4.4	0.920	0.920	3.7	4.4	0.920	0.920	3.3	4.4
3 3 1	0.896	0.896	2.4	2.6	0.896	0.896	1.2	2.5	0.896	0.896	1.1	2.5
3 3 1	0.896	0.896	1.1	1.3	0.896	0.896	0.9	1.3	0.896	0.896	0.7	1.3
4 2 0	0.873	0.873	9.7	10.7	0.873	0.873	7.1	10.7	0.873	0.873	5.6	10.7
4 2 0	0.873	0.873	4.4	5.4	0.873	0.873	3.8	5.4	0.873	0.873	3.4	5.4
4 2 1	0.852		0.9	1.4	0.852		0.5	1.3	0.852		0.5	1.2
4 2 1	0.852		0.5	0.7	0.852		0.4	0.7				
3 3 2	0.833	0.833	5.2	6.9	0.832	0.832	3.7	6.9	0.833	0.832	2.9	6.8
3 3 2	0.833	0.833	2.4	3.5	0.832	0.832	2.4	3.5	0.832	0.832	1.5	3.5

Table 4-2b *XRD* powder pattern reflections and calculated patterns (XRAY and XPOW) for the tausonite-loparite solid solution series (x=0.7-0.5).

	x=0.7				x=0.6				x=0.5			
h k l	*d*-obs.	*d*-calc.	I-obs.	I-calc.	*d*-obs.	*d*-calc.	I-obs.	I-calc.	*d*-obs.	*d*-calc.	I-obs.	I-calc.
1 0 0	3.912	3.905	3.1	3.5	3.898	3.896	3.2	2.9	3.890	3.893	2.6	2.6
1 1 0	2.763	2.761	100.0	100.0	2.756	2.755	100.0	100.0	2.754	2.753	100.0	100.0
1 1 1	2.254	2.255	20.0	49.7	2.248	2.250	19.8	20.0	2.248	2.247	19.9	19.9
1 1 1	2.253	2.255	17.5	20.2	2.247	2.250	10.1	10.0	2.247	2.247	11.5	9.9
									1.951		15.7	
2 0 0	1.953	1.952	35.6	39.2	1.949	1.948	27.8	39.0	1.946	1.946	32.7	39.5
2 0 0	1.953	1.952	32.2	19.5					1.946	1.946	17.5	19.6
2 1 0	1.747	1.746	1.6	2.2	1.744	1.743	1.1	2.0	1.742	1.741	1.1	2.0
2 1 1	1.594	1.594	28.3	32.8	1.590	1.591	24.5	32.7	1.590	1.589	26.0	32.7
2 1 1	1.594	1.594	25.5	16.3	1.590	1.591	15.0	16.3	1.589	1.589	17.4	16.2
2 2 0	1.381	1.381	15.6	19.2	1.377	1.378	12.9	19.3	1.377	1.376	13.8	19.3
2 2 0	1.380	1.381	12.4	9.6	1.377	1.378	6.8	9.6	1.377	1.376	9.0	9.6
2 2 1	1.302		0.9	1.3	1.298		0.5	1.2	1.297		0.6	1.1
3 1 0	1.235	1.235	10.2	12.2	1.235	1.232	6.4	12.1	1.231	1.231	6.8	12.1
3 1 0	1.235	1.235	7.8	6.1	1.234	1.232	4.4	6.0				
3 1 1	1.177	1.177	3.1	4.6	1.175	1.175	1.9	4.5	1.174	1.174	2.1	4.4
3 1 1	1.177	1.177	2.2	2.3								
2 2 2	1.127	1.127	4.2	5.6	1.124	1.125	2.8	5.6	1.124	1.124	4.2	5.6
2 2 2	1.127	1.127	3.2	2.8	1.125	1.125	2.2	2.8	1.124	1.124	2.6	2.8
3 2 0	1.083		0.6	0.6					1.079		0.4	0.6
3 2 1	1.044	1.044	9.0	14.0	1.041	1.041	6.6	14.0	1.041	1.040	7.0	13.9
3 2 1	1.044	1.044	7.8	7.0					1.041	1.040	4.4	7.0
4 0 0	0.976	0.976	1.6	2.8	0.975	0.974	1.0	2.8	0.973	0.973	1.2	2.8
4 0 0	0.976	0.976	1.0	1.4	0.975	0.974	0.8	1.4				
3 3 0	0.920	0.920	5.1	8.7	0.919	0.918	2.9	8.7	0.917	0.918	3.7	8.7
3 3 0	0.920	0.920	3.6	4.4					0.917	0.918	2.1	4.4
3 3 1	0.896	0.896	1.1	2.4	0.894		0.5	2.4				
3 3 1	0.895	0.896	0.8	1.1								
4 2 0	0.873	0.873	3.8	10.7	0.872	0.871	2.7	10.8	0.870	0.870	2.9	10.9
4 2 0	0.873	0.873	3.6	5.4					0.870	0.870	1.8	5.5
3 3 2	0.833	0.833	2.4	6.8	0.831	0.831	1.6	6.9	0.830	0.830	2.0	6.9
3 3 2	0.833	0.833	2.0	3.5	0.830	0.831	1.1	3.5	0.830	0.830	1.2	3.5

Table 4-2c *XRD* powder pattern reflections and calculated patterns (XRAY and XPOW) for the tausonite-loparite solid solution series (x=0.4-0.2).

	x=0.4				x=0.3				x=0.2			
h k l	*d*-obs.	*d*-calc.	I-obs.	I-calc.	*d*-obs.	*d*-calc.	I-obs.	I-calc.	*d*-obs.	*d*-calc.	I-obs.	I-calc.
1 0 0	3.886	3.889	2.8	2.4	3.879	3.881	2.9	2.2	3.864	3.874	2.5	1.9
1 1 0	2.749	2.750	100.0	100.0	2.743	2.744	100.0	100.0	2.737	2.739	100.0	100.0
					2.679		0.6					
	2.349		0.7		2.338		0.7		2.336		0.9	
					2.252		3.9					
1 1 1	2.245	2.245	19.4	19.8	2.240	2.241	17.5	19.6	2.235	2.237	17.1	19.5
1 1 1	2.244	2.245	12.5	9.8								
									1.950		5.0	
2 0 0	1.944	1.944	31.0	39.7	1.940	1.941	31.6	39.9	1.936	1.937	33.0	40.0
2 0 0	1.944	1.944	21.6	19.7	1.939	1.941	15.9	19.8	1.935	1.937	15.2	19.9
2 1 0	1.740	1.739	1.1	1.9	1.736	1.736	1.0	1.7	1.733	1.733	1.1	1.6
2 1 0	1.737	1.739	0.7	0.9								
					1.593		4.4		1.592		3.5	
2 1 1	1.587	1.587	27.2	32.6	1.584	1.584	23.8	32.6	1.581	1.582	25.6	32.5
2 1 1	1.587	1.587	16.1	16.2					1.581	1.582	12.0	16.1
					1.380		3.0		1.380		2.1	
2 2 0	1.374	1.375	14.9	19.4	1.373	1.372	10.7	19.4	1.370	1.370	11.6	19.5
2 2 0	1.374	1.375	7.5	9.6					1.370	1.370	4.9	9.7
2 2 1									1.293	1.291	0.7	1.0
					1.234		1.5		1.234		1.0	
3 1 0	1.230	1.230	7.3	12.1	1.227	1.227	6.9	12.1	1.226	1.225	7.1	12.0
3 1 0	1.229	1.230	3.5	6.0					1.225	1.225	3.0	6.0
3 1 1	1.173	1.172	1.7	4.4	1.171	1.170	1.5	4.3	1.169	1.168	1.5	4.3
					1.127		0.8					
2 2 2	1.123	1.123	4.2	5.6	1.121	1.120	2.6	5.7	1.119	1.118	2.5	5.7
2 2 2	1.123	1.123	2.1	2.8								
					1.043		1.5		1.043		1.1	
3 2 1	1.040	1.039	8.3	13.9	1.038	1.037	6.7	13.9	1.035	1.035	6.7	13.8
3 2 1	1.039	1.039	4.8	6.9					1.036	1.035	3.1	6.9
4 0 0	0.973	0.972	1.1	2.8	0.971	0.970	1.0	2.8	0.969	0.969	0.8	2.9
									0.920		0.7	
3 3 0	0.917	0.917	3.5	8.7	0.915	0.915	3.3	8.7	0.913	0.913	3.8	8.7
3 3 1	0.892	0.892	0.6	2.3								
					0.873		0.8		0.873		0.5	
4 2 0	0.869	0.870	3.1	11.0	0.868	0.868	2.5	11.1	0.866	0.866	2.5	11.2
4 2 0	0.869	0.870	1.7	5.5					0.867	0.866	1.4	5.6
3 3 2	0.830	0.829	1.8	6.9	0.827	0.827	1.4	7.0	0.827	0.826	1.4	7.0
3 3 2	0.829	0.829	1.4	3.5								

Table 4-2d *XRD* powder pattern reflections and calculated patterns (XRAY and XPOW) for the tausonite-loparite solid solution series (x=0.1-0.0).

	x=0.1				x=0.0			
h k l	*d*-obs.	*d*-calc.	I-obs.	I-calc.	*d*-obs.	*d*-calc.	I-obs.	I-calc.
1 0 0	3.880	3.879	2.1	1.7	3.872	3.874	1.8	1.5
1 1 0	2.744	2.743	100.0	100.0	2.738	2.739	100.0	100.0
1 1 0	2.742	2.743	42.3	49.7	2.736	2.739	48.7	49.7
	2.339		0.9		2.334		1.3	
1 1 1	2.240	2.240	17.9	19.4	2.236	2.236	16.1	19.2
1 1 1					2.235	2.236	9.3	9.6
					2.063		2.7	
					2.062		1.7	
2 0 0	1.940	1.940	33.3	40.3	1.936	1.937	37.1	40.5
2 0 0	1.939	1.940	16.0	20.0	1.936	1.937	20.7	20.1
2 1 0	1.735	1.735	1.4	1.5	1.732	1.732	1.6	1.4
2 1 0					1.732	1.732	2.6	0.7
2 1 1	1.584	1.584	26.3	32.5	1.581	1.581	30.8	32.4
2 1 1	1.583	1.584	12.6	16.2	1.581	1.581	16.9	16.1
2 2 0	1.372	1.372	13.4	19.6	1.369	1.370	14.8	19.6
2 2 0	1.371	1.372	5.5	9.7	1.369	1.370	7.7	9.8
3 0 0	1.293	1.293	0.5	0.9	1.291	1.291	1.0	0.8
3 1 0	1.227	1.227	7.7	12.0	1.225	1.225	9.5	12.0
3 1 0	1.226	1.227	3.4	6.0	1.225	1.225	5.2	6.0
3 1 1	1.170	1.170	1.7	4.2	1.168	1.168	2.3	4.2
3 1 1					1.168	1.168	1.0	2.1
2 2 2	1.121	1.120	2.7	5.7	1.119	1.118	3.7	5.7
2 2 2					1.118	1.118	1.5	2.8
3 2 1	1.037	1.037	5.8	13.8	1.036	1.035	10.0	13.7
3 2 1	1.037	1.037	3.2	6.9	1.035	1.035	5.0	6.9
4 0 0	0.970	0.970	1.3	2.9	0.969	0.968	1.8	2.9
4 0 0	0.970	0.970	0.6	1.4	0.968	0.968	0.8	1.4
4 1 0					0.940	0.940	0.5	0.7
3 3 0	0.914	0.914	3.6	8.6	0.913	0.913	4.6	8.6
3 3 0	0.914	0.914	1.6	4.3	0.913	0.913	2.5	4.3
3 3 1	0.890	0.890	0.6	2.3	0.889	0.889	0.6	2.2
3 3 1					0.889	0.889	0.5	1.1
4 2 0	0.867	0.867	2.9	11.1	0.866	0.866	3.4	11.2
4 2 0	0.867	0.867	1.4	5.6	0.866	0.866	2.2	5.7
3 3 2	0.827	0.827	1.6	6.9	0.826	0.826	2.5	7.0
3 3 2					0.826	0.826	1.3	3.6

the powder patterns. Some represent minor amounts of residual reactants used in the synthesis (at most 8%), and are typically found in the 10-30° (2θ) range. The intensities of these are enhanced as a consequence of the elevated background in this region. These peaks gradually increase with decreasing tausonite content; possibly amplified by the decrease in overall intensity with decreasing tausonite content.

To simplify correlations between the powder patterns for the whole series, it was necessary to transform the raw *XRD* data (in 2θ) to plots of reflections (Figure 4-1[a-c]). In this manner, changes in symmetry may be correlated more easily than with the raw data. An ICDD database search of *d*-spacings on the tausonite end-member indicated the compound to be tausonite, as would be expected. The majority of the peaks present in all of the other patterns correspond to the pseudo-cubic perovskite peaks. This helped verify that the products were indeed derivatives of the tausonite structure and were perovskite-type compounds (Table 4-2 [a-d]).

4.4 *XRD* Determinations and Least-Squares Refinement of Cell Parameters

The diffraction patterns of the tausonite-loparite solid solution series were indexed against a pseudo-cubic unit cell (tausonite). The powder diffraction pattern of tausonite indicated $m\bar{3}m$ symmetry with no systematic reflections being extinct, consistent with the phase belonging to the space-group $Pm\bar{3}m$. The refinement of the pseudo-cubic unit cell parameters of all members in this solid-solution appear in Table 4-3. Peak positions, intensities and peak widths for a section of the *XRD* pattern which characterises all the phases present (Figure 4-2 and Figure 4-3) were monitored to determine the presence of

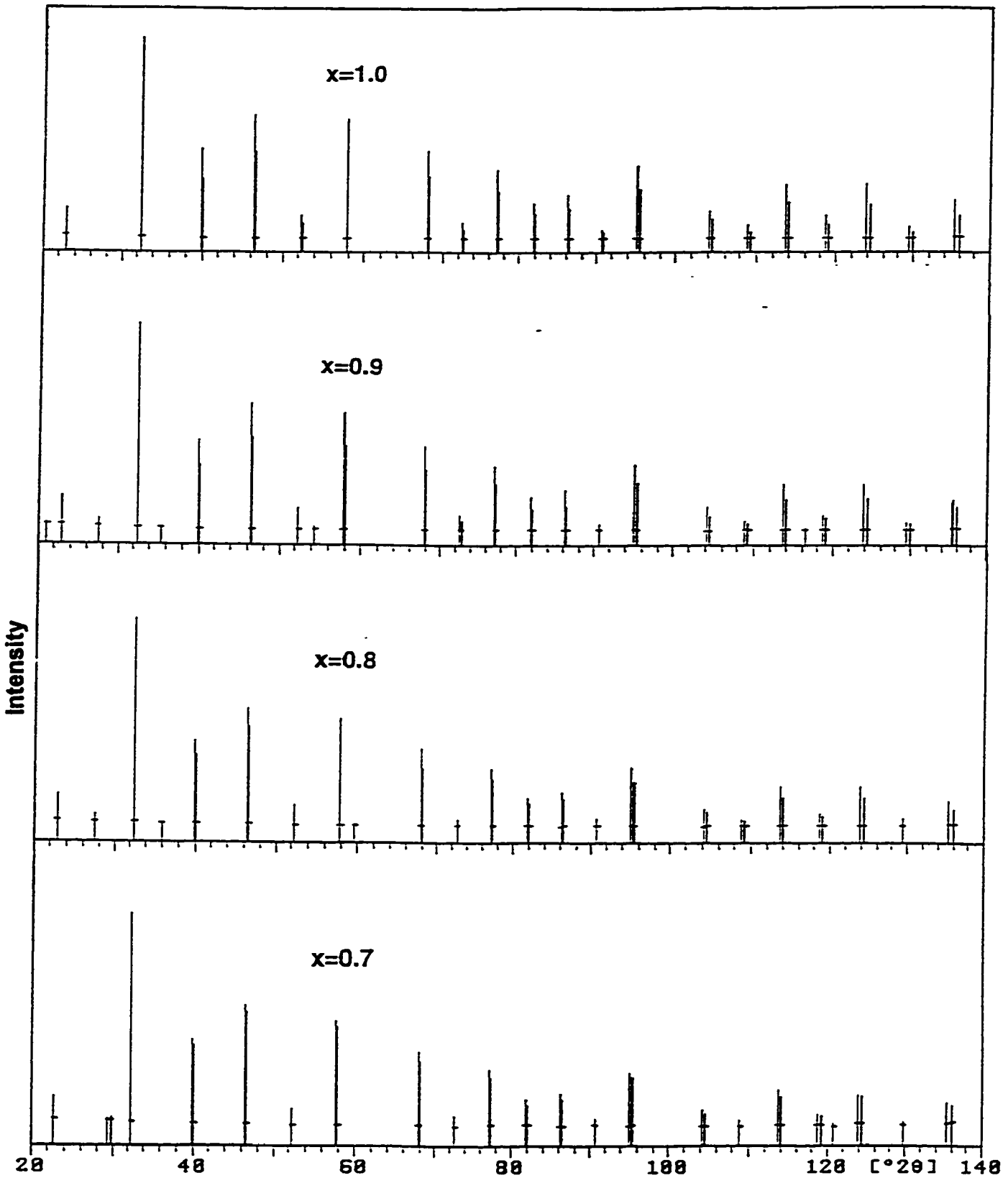

Figure 4-1a *XRD* **diffraction patterns for the tausonite-loparite solid solution series with cubic symmetry ($1.0 \leq x \leq 0.7$); as determined by automated peak search. Intensity is on the y-axes and horizontal dashes crossing the reflections represent the level of background.**

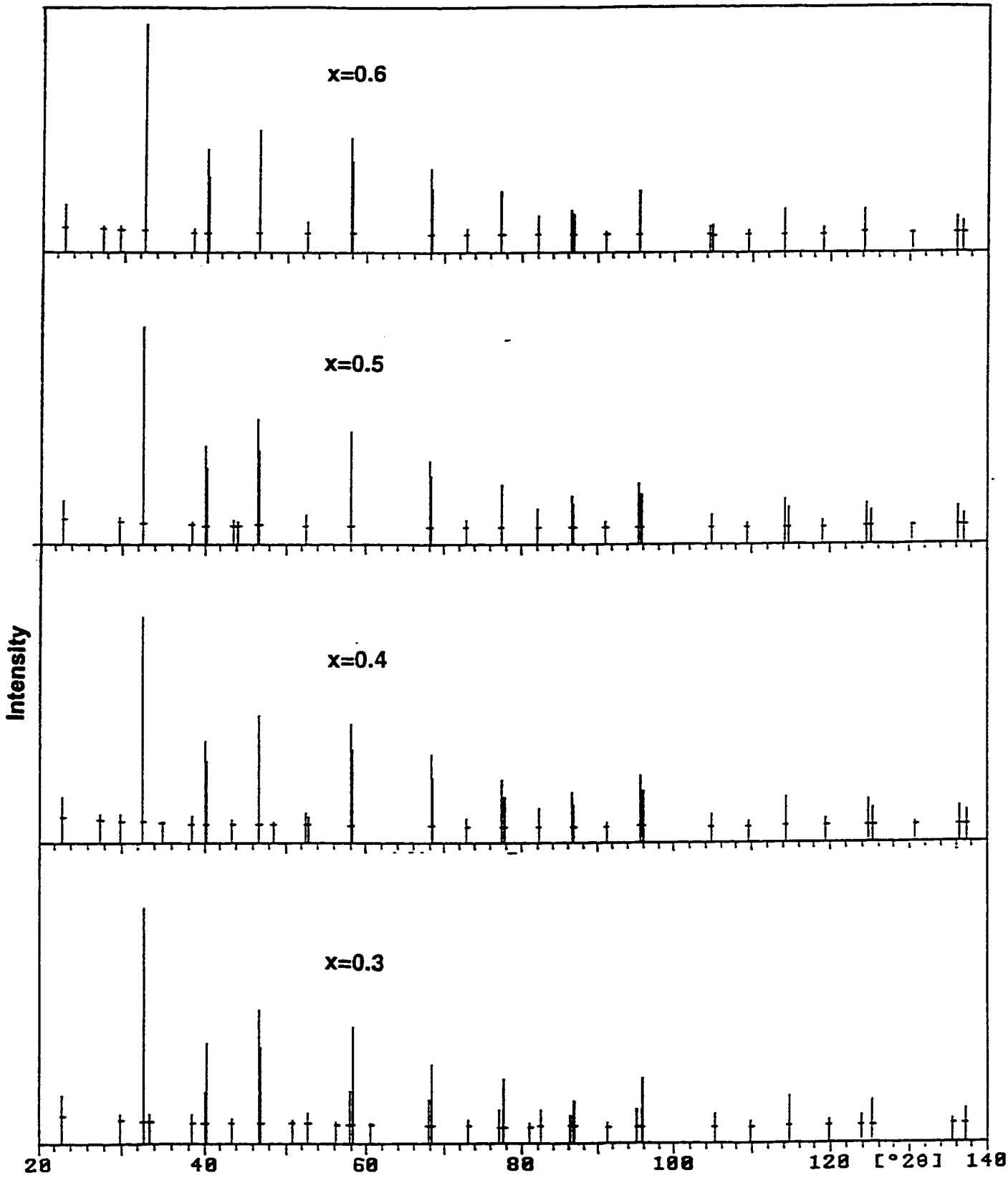

Figure 4-1b *XRD* diffraction patterns for the tausonite-loparite solid solution series with cubic symmetry ($0.6 \leq x \leq 0.3$); as determined by automated peak search. Intensity is on the y-axes and horizontal dashes crossing the reflections represent the level of background.

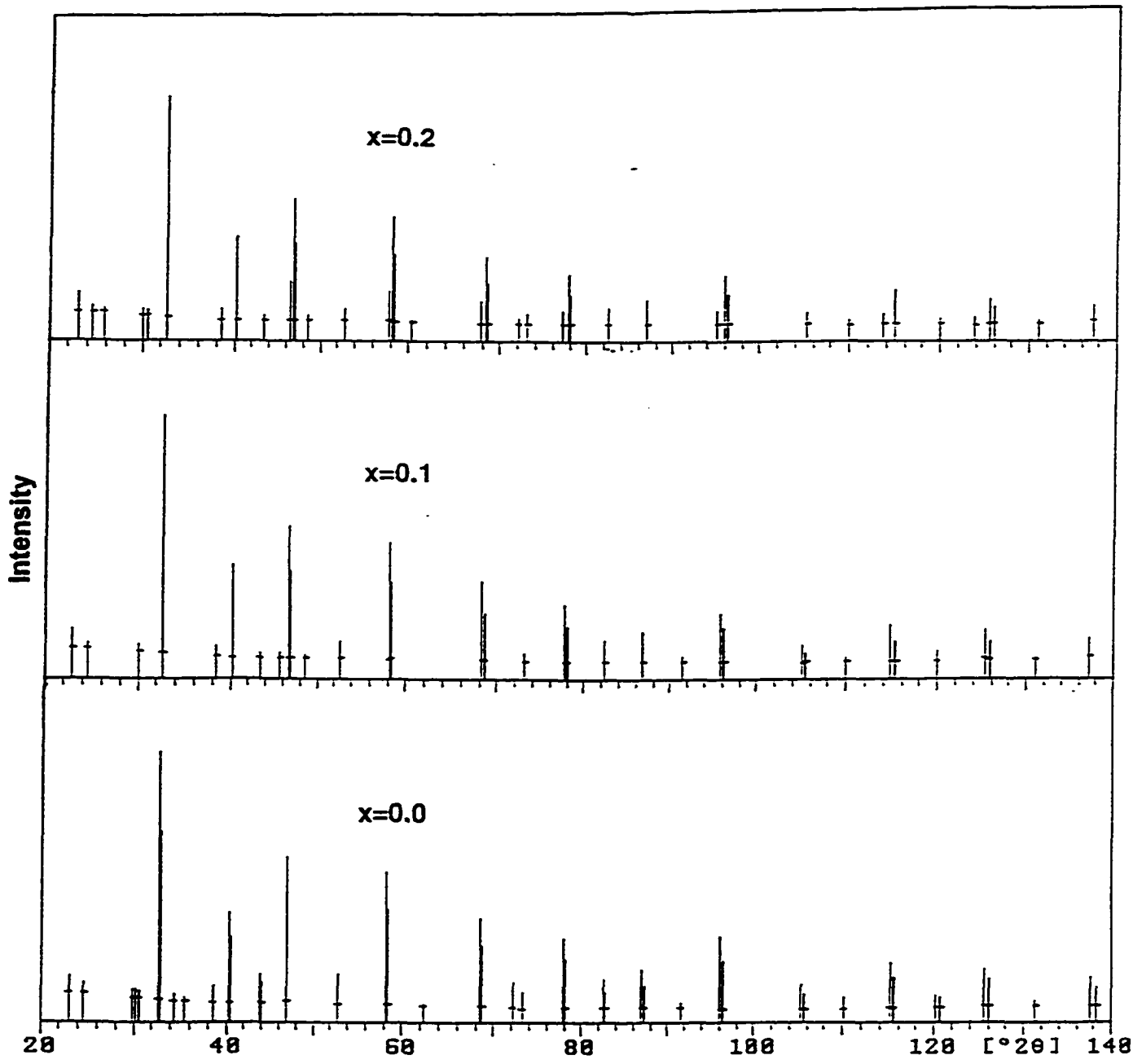

Figure 4-1c *XRD* diffraction patterns for the tausonite-loparite solid solution series with cubic symmetry ($0.2 \leq x \leq 0.0$); as determined by automated peak search. Intensity is on the y-axes and horizontal dashes crossing the reflections represent the level of background.

Table 4-3 Least-squares refinement of perovskite pseudo-cubic unit-cell parameters for the tausonite-loparite solid solution series. Errors refer to least-squares errors in mathematical fit; *XRD* precision and accuracy appear in Chapter 2. Tolerence factors calculated from effective ionic radii (Vainshtein *et al.* 1994).

Composition (x)	a_p (Å)	Error (±)	Volume (Å^3)	Error (±)	Maximum Intensity (Counts)	Rejected Peaks (#/total)	Tolerance Factors (t)
1.0	3.9050	0.0001	59.5493	0.0040	9139	0/39	1.0016
0.9	3.9043	0.0001	59.5163	0.0047	7379	0/36	0.9993
0.8	3.9046	0.0001	59.5312	0.0050	5898	0/35	0.9970
0.7	3.9050	0.0001	59.5462	0.0065	4225	0/32	0.9947
0.6	3.8964	0.0004	59.1551	0.0186	4556	1/27	0.9924
0.5	3.8927	0.0003	58.9859	0.0116	4032	1/30	0.9901
0.4	3.8885	0.0002	58.7958	0.0106	4225	0/30	0.9878
0.3	3.8811	0.0004	58.4595	0.0190	3260	5/28	0.9855
0.2	3.8742	0.0005	58.1496	0.0222	3446	9/30	0.9832
0.1	3.8793	0.0003	58.3815	0.0115	3636	0/29	0.9810
0.0	3.8736	0.0002	58.1232	0.0095	3795	1/38	0.9787

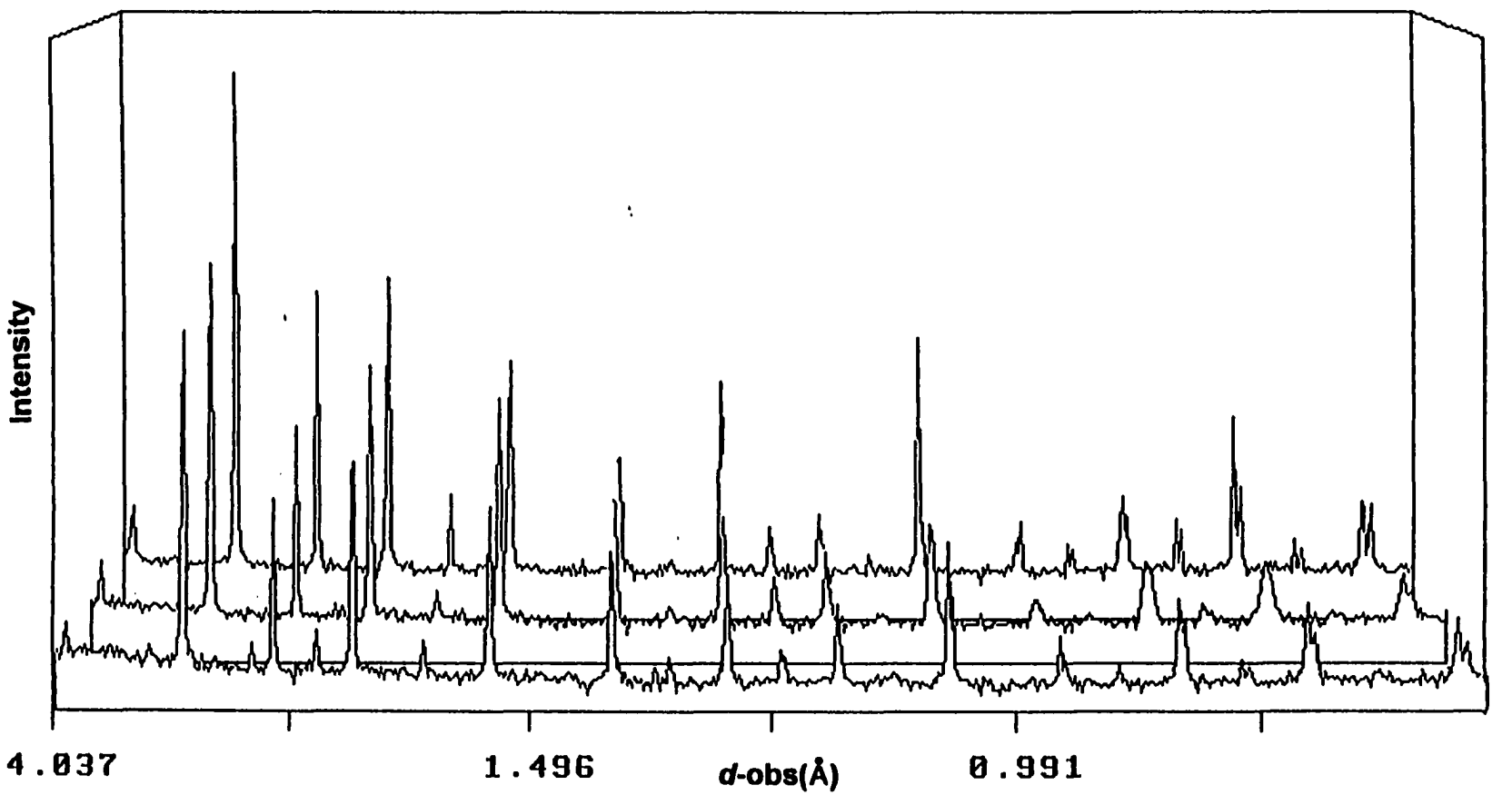

Figure 4-2 Representative *XRD* powder patterns for the three different symmetries of the tausonite-loparite solid solution series. From top to bottom: cubic ($Pm\bar{3}m$) symmetry at the tausonite end-member (x=1.0); tetragonal (*P4/mbm*) symmetry at x=0.5; and orthorhombic (*Pnma*) symmetry at the loparite end-member (x=0.0).

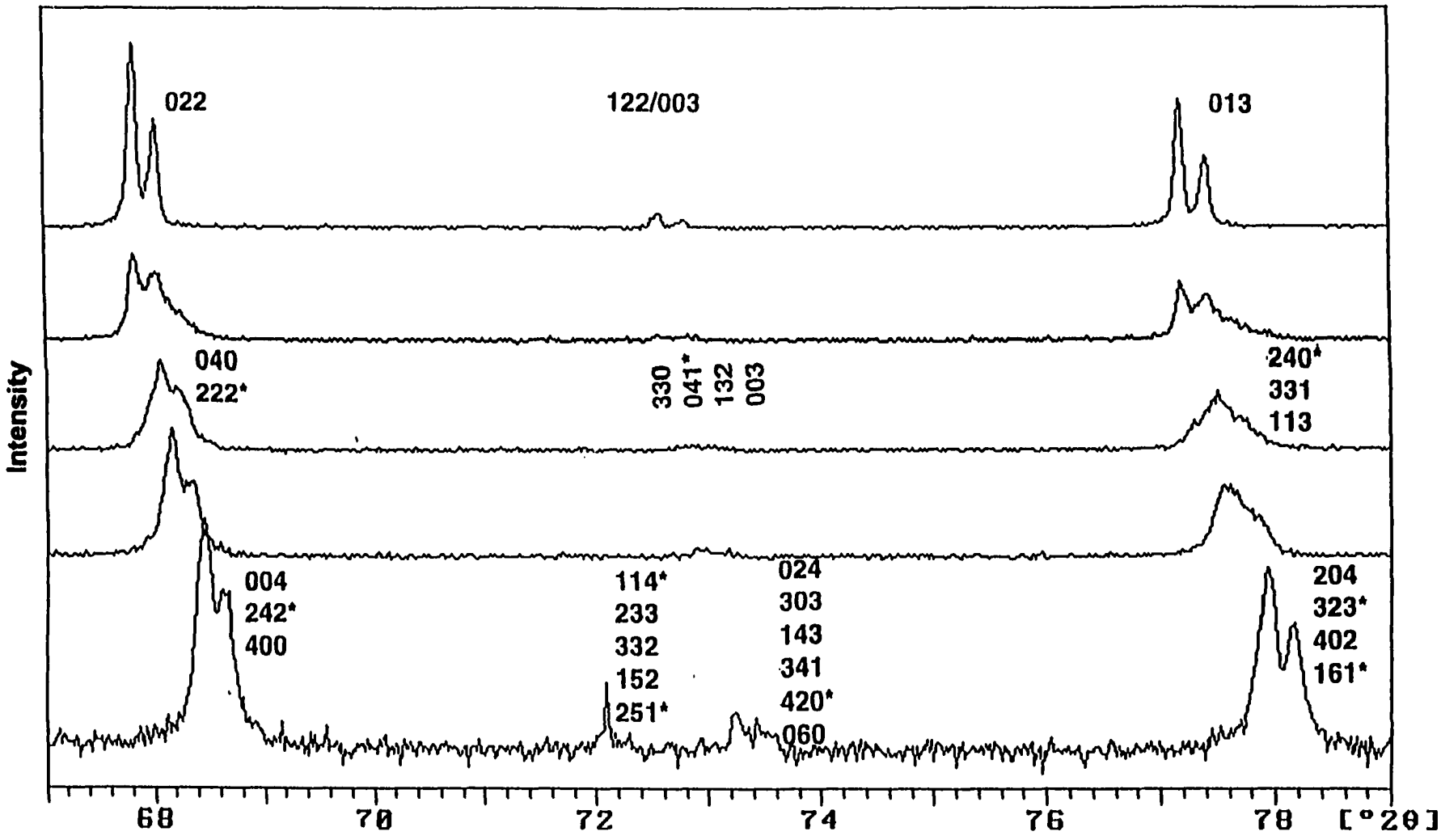

Figure 4-3 Selection of representative *XRD* powder patterns for the three different symmetries and two symmetry transitions, for the tausonite-loparite solid solution series. From top to bottom: cubic ($Pm\bar{3}m$) symmetry at the tausonite end-member (x=1.0); a transition at x=0.7; tetragonal (*P4/mbm*) symmetry at x=0.5; a transition at x=0.3; and orthorhombic (*Pnma*) symmetry at the loparite end-member (x=0.0). The selected 2θ range is 65-80, with only the $K_{\alpha 1}$ reflections having *hkl* values (* *refers to the most intense peak or peak where a number of peaks are unresolved*).

the expected phase transitions. The powder patterns indicate that although these transitions, as described below, do exist, they are very subtle and any peak splittings (described by Zhao *et al.* 1993) are small due to the minor structural distortions exhibited.

The indexed diffraction pattern and the least-squares refinement indicate the presence of two domains in the solid-solution series, and several ranges, where a change in symmetry is suspected. The first domain is characterized by the emergence of no new reflections, from x=1.0 to x=0.7 inclusive. The second domain (x=0.6 to 0.0) is characterized by a return to a normal relative intensity of $K_{\alpha 1}/K_{\alpha 2}$ and by the gradual emergence of a new reflection at approximately 38.5° (2θ) [loparite (*031*), (*112*) and (*211*) reflections], which is always present in some degree. These domains may be best visualised by examination of plots of the *XRD* powder pattern reflections (Figure 4-1[a-c]), through observation of the peak positions and shapes over the entire *XRD* pattern (Figure 4-2), or over a selected range (Figure 4-3).

The first domain (Figure 4-1a) is divided into two ranges. The refinement indicates that at the compositions x=1.0 and x=0.9 (range 1) the powder patterns contain no apparent changes from the ideal cubic perovskite, suggesting the phases are of cubic symmetry. A change in this pattern of reflections occurs over the range x=0.8 to x=0.7 (range 2). In this range most of the reflections have a relative $K_{\alpha 1}/K_{\alpha 2}$ intensity ratio of greater than 0.7 (up to a maximum of ~0.9 at x=0.07), instead of the normal intensity ratio of 0.5. This may indicate a splitting of the reflections towards higher angles (2θ) due to a change in symmetry.

The second domain (Figure 4-1[b,c]) is divided into three additional ranges and is indicative of a definite change from cubic symmetry. Range three (x=0.6 to x=0.4) can be characterized as a return to a normal intensity ratio and the disappearance of the aforementioned splitting. Range four (x=0.3 to x=0.2) is defined by splitting; as before, but with the emergence of the new reflections on the low angle (2θ) side of the reflections (Figure 4-3). The final range (range five, x=0.1 to x=0.0) is consistent with the pattern for an orthorhombic loparite. The aforementioned splitting has disappeared and the new reflection at ~38.5° (2θ), which defines this domain, has established itself (greater than 0.05% relative intensity).

Least-squares refinement of the solid-solution series appears in Table 4-3 and Figure 4-4A is a plot of composition (x) *versus* the cubic unit-cell edge. Figure 4-4B and Figure 4-4C are plots of composition (x) *versus* the pseudo-cubic unit-cell edges (B); and the unit-cell edges (C), as determined by Rietveld refinement. The Table and plots exhibit no deviation, when considering *XRD* precision and accuracy, in the unit cell parameters (a and volume) over the domain x=1.00 to x=0.7. There is a gradual decrease over the compositional range x=0.7 to x=0.0. This supports the existence of previously mentioned domains. The discrepancy at x=0.7 may be a consequence of a profound change from cubic to tetragonal symmetry; and the subsequent change from tetragonal to orthorhombic symmetry is moderate in comparison. These results may indicate that there is no appreciable change in pseudo-cubic unit cell parameters until a point is reached, beyond which the structure can no longer tolerate further substitution of lanthanum and sodium for strontium at the *A*-site (approximately 1/3 substitution).

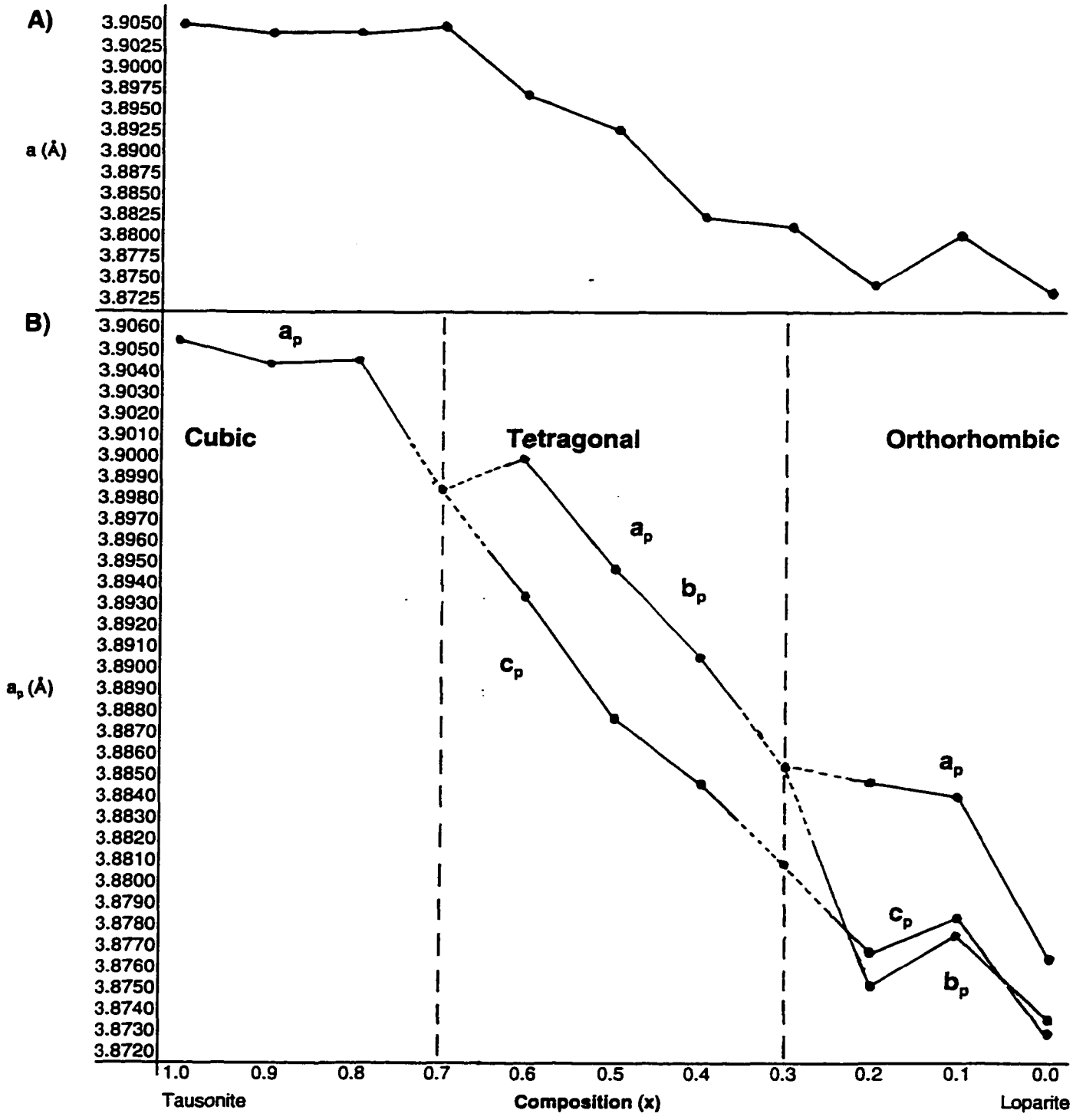

Figure 4-4 Plot of composition *versus*:
A) cubic unit-cell edge (as determined by least-squares refinement),
B) pseudo-cubic unit-cell edges (as calculated from Rietveld refinement), and

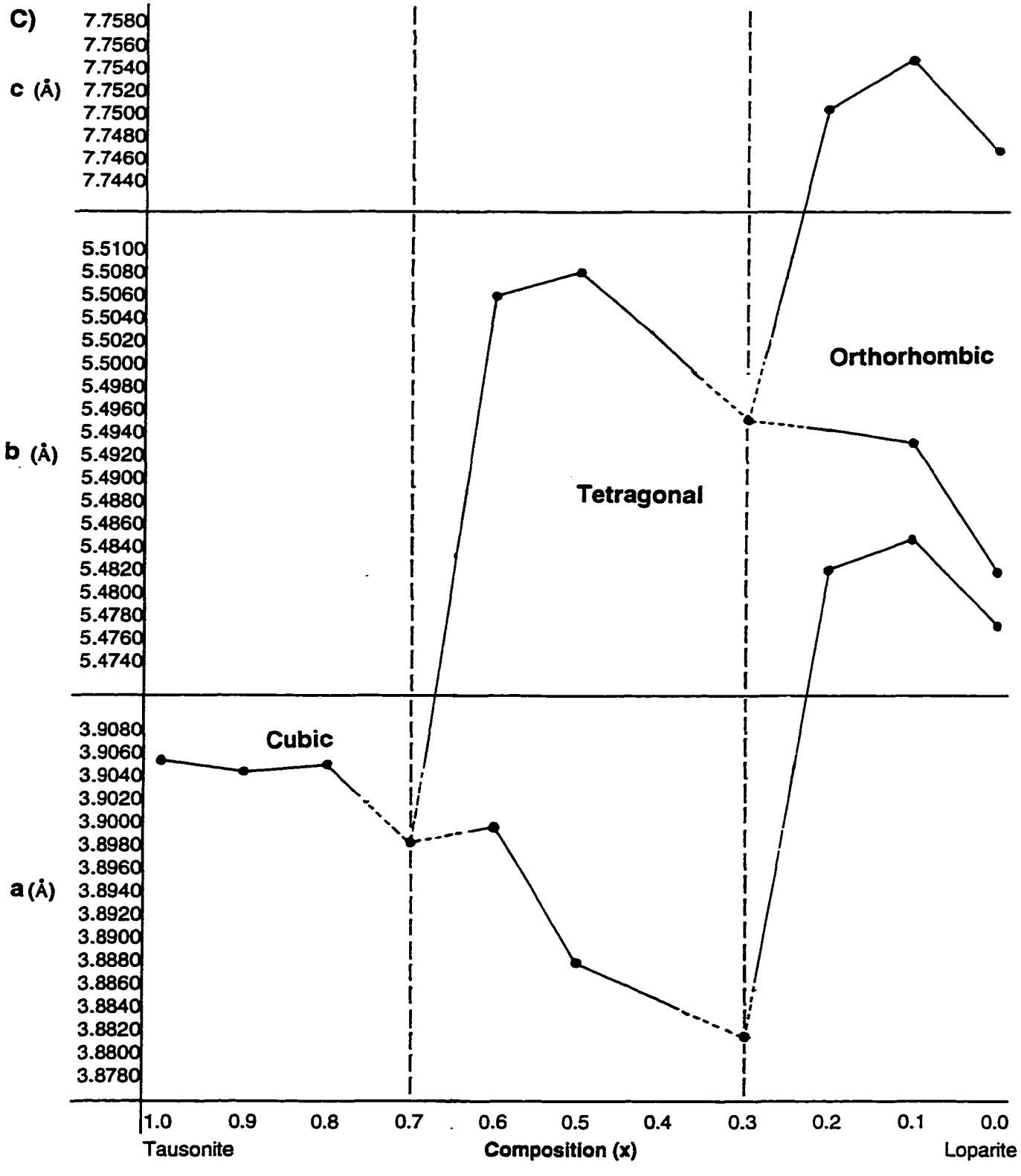

Figure 4-4 Plot of composition *versus*:
C) unit-cell edges (as determined by Rietveld refinement).

The XPOW interactive software (Downs *et al.* 1993) was then used to calculate the relative intensities associated with all Bragg indices for the space group $Pm\bar{3}m$. The results, based on unit cell parameters and atomic coordinates derived for a synthetic tausonite (Mitchell 1996) appear in Table 4-2 (a-d). The XPOW results present an accurate pseudocubic representation of the tausonite-loparite solid solution series patterns observed here.

4.5 Rietveld Refinement and Crystal Structure Determinations

Although the predicted symmetry of the tausonite and loparite end-member apparently proved accurate by least-squares refinement and XPOW, predicting the composition at which a phase transition occurred requires a more detailed structure refinement. All powder patterns were refined by the Rietveld Refinement DBWS-9411 program (Young *et al.* 1995) using the cell parameters listed in Table 4-2. Results are consistent with the phase transitions predicted from least-squares refinement. Results of structure refinements appear in Table 4-4, together with selected criteria-of-fit. As the pattern *R*-factor (*R-p*) and weighted pattern *R*-factor (*R-wp*) are specific for a given refinement only, the progress of the refinement is determined by the values of *S* and *R-Bragg*. The criteria-of-fit are comparable to the limits prescribed in Chapter 3 for the ideal refinement (S <1.5, *R-Bragg* <5, and $D \approx 2.00$). The criteria-of-fit indicate that the best refinements occur in the regions $1.0>x>0.9$, $0.6>x>0.4$ and $0.1<x<0.0$, while the least accurate refinements occur in the regions where a change in symmetry is expected ($0.8>x>0.7$ and $0.3>x>0.2$). The discrepancies in fit are also supported by the plots of the

Table 4-4 Atomic coordinates, positional and thermal parameters, unit-cell dimensions and criteria of fit as determined by the Reitveld refinement program (DBWS-9411), for the tausonite-loparite solid solution series at differing compositions (x).

Parameters		x=1.0	x=0.9	x=0.8	x=0.7	x=0.6	x=0.5	x=0.4	x=0.3	x=0.2	x=0.1	x=0.0
	Space-Group	*Pm3m*	*Pm3m*	*Pm3m*	*Pm3m*	*P4/mbm*	*P4/mbm*	*P4/mbm*	*P4/mbm*	*Pnma*	*Pnma*	*Pnma*
Sr^{2+}	*x*	1/2	1/2	1/2	1/2	0	0	0	0	0.00074	-0.00246	
	y	1/2	1/2	1/2	1/2	1/2	1/2	1/2	1/2	1/4	1/4	
	z	1/2	1/2	1/2	1/2	1/2	1/2	1/2	1/2	-0.00578	-0.00468	
	U(Å²)	0.44581	0.53006	0.64415	0.57448	0.42121	0.25111	0.40782	0.40700	0.53670	0.36194	
	N	0.02083	0.01875	0.01667	0.01458	0.07500	0.06250	0.05000	0.37500	0.10000	0.05000	
Na^{+}	*x*		1/2	1/2	1/2	0	0	0	0	0.00074	-0.00246	-0.00088
	y		1/2	1/2	1/2	1/2	1/2	1/2	1/2	1/4	1/4	1/4
	z		1/2	1/2	1/2	1/2	1/2	1/2	1/2	-0.00578	-0.00468	-0.00624
	U(Å²)		0.53006	0.64415	0.57448	0.42121	0.25111	0.40782	0.40700	0.53670	0.36194	0.27678
	N		0.00147	0.00236	0.00348	0.02733	0.03408	0.04057	0.04683	0.20476	0.23264	0.26230
La^{3+}	*x*		1/2	1/2	1/2	0	0	0	0	0.00074	-0.00246	-0.00088
	y		1/2	1/2	1/2	1/2	1/2	1/2	1/2	1/4	1/4	1/4
	z		1/2	1/2	1/2	1/2	1/2	1/2	1/2	-0.00578	-0.00468	-0.00624
	U(Å²)		0.53006	0.64415	0.57448	0.42121	0.25111	0.40782	0.40700	0.53670	0.36194	0.27678
	N		0.00061	0.00180	0.00276	0.02267	0.02842	0.03443	0.04067	0.19524	0.21736	0.23770
Ti^{4+}	*x*	0	0	0	0	0	0	0	0	1/2	1/2	1/2
	y	0	0	0	0	0	0	0	0	0	0	0
	z	0	0	0	0	0	0	0	0	0	0	0
	U(Å²)	0.18495	0.44071	0.55073	0.49303	0.33642	0.28925	0.36935	0.46156	0.48820	0.39790	0.51637
	N	0.02083	0.02083	0.02083	0.02083	0.12500	0.12500	0.12500	0.12500	0.50000	0.50000	0.50000
O^{2-} (1)	*x*	1/2	1/2	1/2	1/2	0	0	0	0	0.03205	0.01835	0.02822
	y	0	0	0	0	0	0	0	0	1/4	1/4	1/4
	z	0	0	0	0	1/2	1/2	1/2	1/2	0.45783	0.46204	0.48326
	U(Å²)	0.55736	0.83017	0.94611	1.00035	5.92874	-0.70966	-1.38295	-0.50762	-1.53701	-1.13571	-0.42552
	N	0.06250	0.06250	0.06250	0.06250	0.12500	0.12500	0.12500	0.12500	0.50000	0.50000	0.50000
O^{2-} (2)	*x*					0.25445	0.26019	0.24675	0.23903	0.27543	0.25791	0.27514
	y					0.75445	0.76019	0.74675	0.73903	0.01201	-0.01176	0.03333
	z					0	0	0	0	0.24302	0.25214	0.27955
	U(Å²)					-0.34936	2.14854	3.87605	4.01232	5.07452	3.21021	3.21393
	N					0.25000	0.25000	0.25000	0.25000	1.00000	1.00000	1.00000
	Z	1	1	1	1	1	1	1	1	4	4	4
	a_p (Å)	3.9050	3.9044	3.9045	3.8983	3.8954	3.8923	3.8884	3.8839	3.8788	3.8799	3.8741
	a (Å)	3.9050	3.9044	3.9045	3.8983	5.5060	5.5079	5.5018	5.4947	5.4941	5.4930	5.4817
	b (Å)	3.9050	3.9044	3.9045	3.8983	5.5060	5.5079	5.5018	5.4947	7.7502	7.7546	7.7467
	c (Å)	3.9050	3.9044	3.9045	3.8983	3.8996	3.8876	3.8846	3.8810	5.4819	5.4846	5.4771
	Volume (Å³)	59.55	59.52	59.52	59.24	118.22	117.94	117.59	117.17	233.42	233.62	232.59
	S (R-wp/R-exp)	1.39	1.31	1.65	1.61	1.16	1.16	1.18	1.43	1.51	1.33	1.27
	R-Bragg	4.62	5.51	7.91	7.10	3.92	4.23	4.60	5.94	8.40	6.27	6.88

observed and calculated *XRD* patterns (Figure 4-5 and Figure 4-6). Values for the criteria-of-fit appear worse than they actually are due to gross misfits in peak shape, as shown in Figure 4-6, (especially with the use of both $K_{\alpha 1}$ and $K_{\alpha 2}$ reflections) and the rounding-off of certain parameters ($K_{\alpha 1}$ equal to 1.5406Å instead of 1.540562Å). *R-Bragg* (Table 4-4) is higher than expected due to differences in the observed intensities relative to the calculated intensities; which may be a consequence of discrepancies in the peak-shape function; as is the Durbin-Watson statistic (*D*), which is much less (~0.6) than the ideal value (~2.00).

4.5.1 Crystal Structure as a Function of Composition (*x*)

Symmetry transitions are also reflected in the thermal parameters (Table 4-4 and Figure 4-7). Near the expected symmetry transitions, the isotropic temperature factors tend to increase dramatically to a maximum at the transition. This is indicative of an increase in the lateral vibration of the octahedral anions coupled with a sudden volume decrease of the octahedron (Zhao *et al.* 1993). These are manifested in the structural phase transition in the perovskite as a decrease in the tilt angles and a shrinkage of the bond length in the octahedral framework (Zhao *et al.* 1993). Generally, the thermal parameters of the *A*-site cations are greater at x=0 relative to those of the Ti (*B*-site) cation which reflects the greater vibrational freedom for the *A*-site cations in the dodecahedral cavity than for the smaller Ti cation in the octahedron cage of the cubic structure (Zhao *et al.* 1993). The larger isothermal temperature factors associated with *A*-site cations, relative to *B*-site cations, is proportional to the atomic radii of the respective cations.

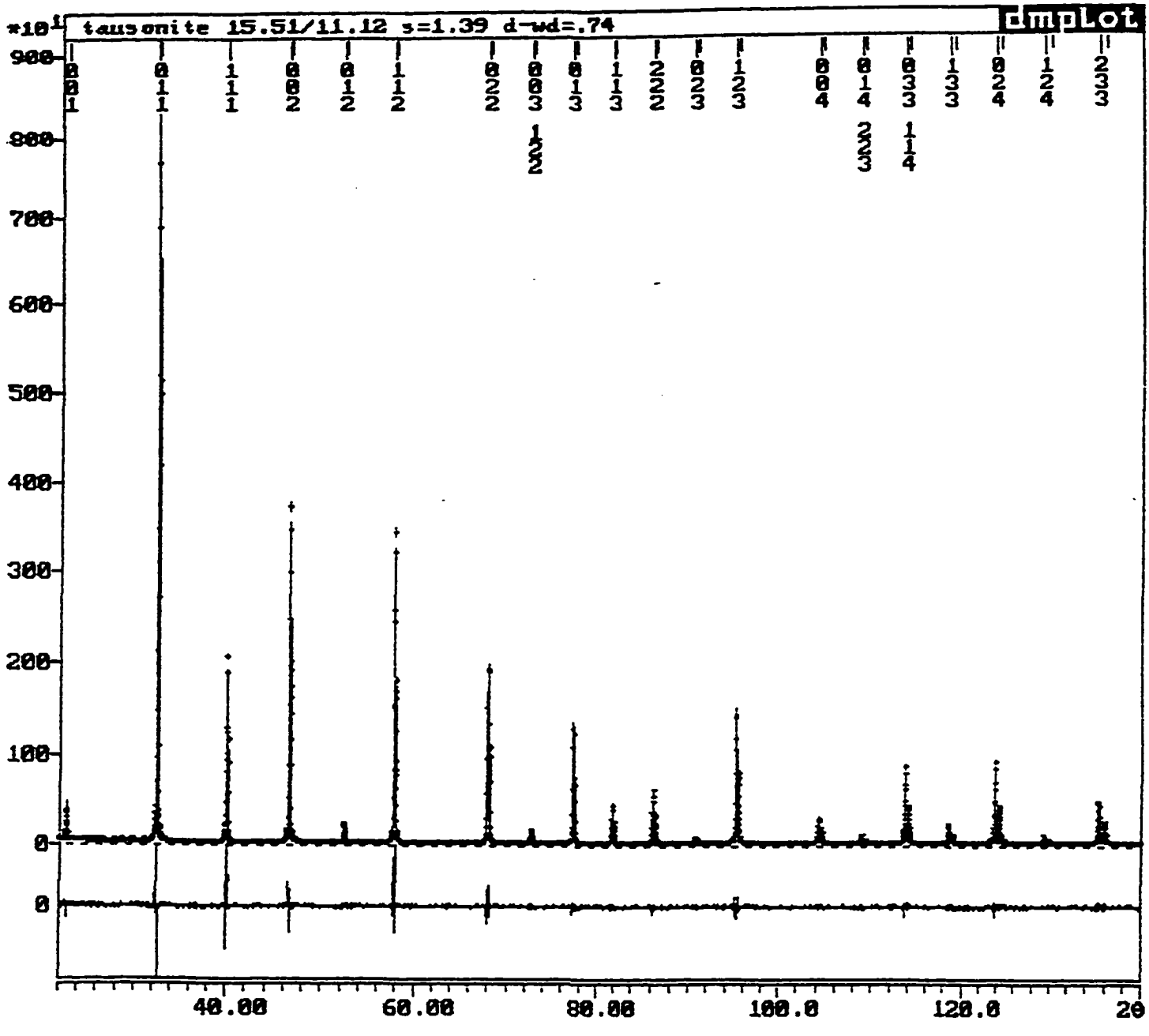

Figure 4-5 Representative fit discrepancy within the Rietveld refinement program (DMPLOT). The plot is of the respective observed (as indicated by data points represented by +), calculated (represented by a line) and residual (at bottom) *XRD* patterns for tausonite (x=1.0).

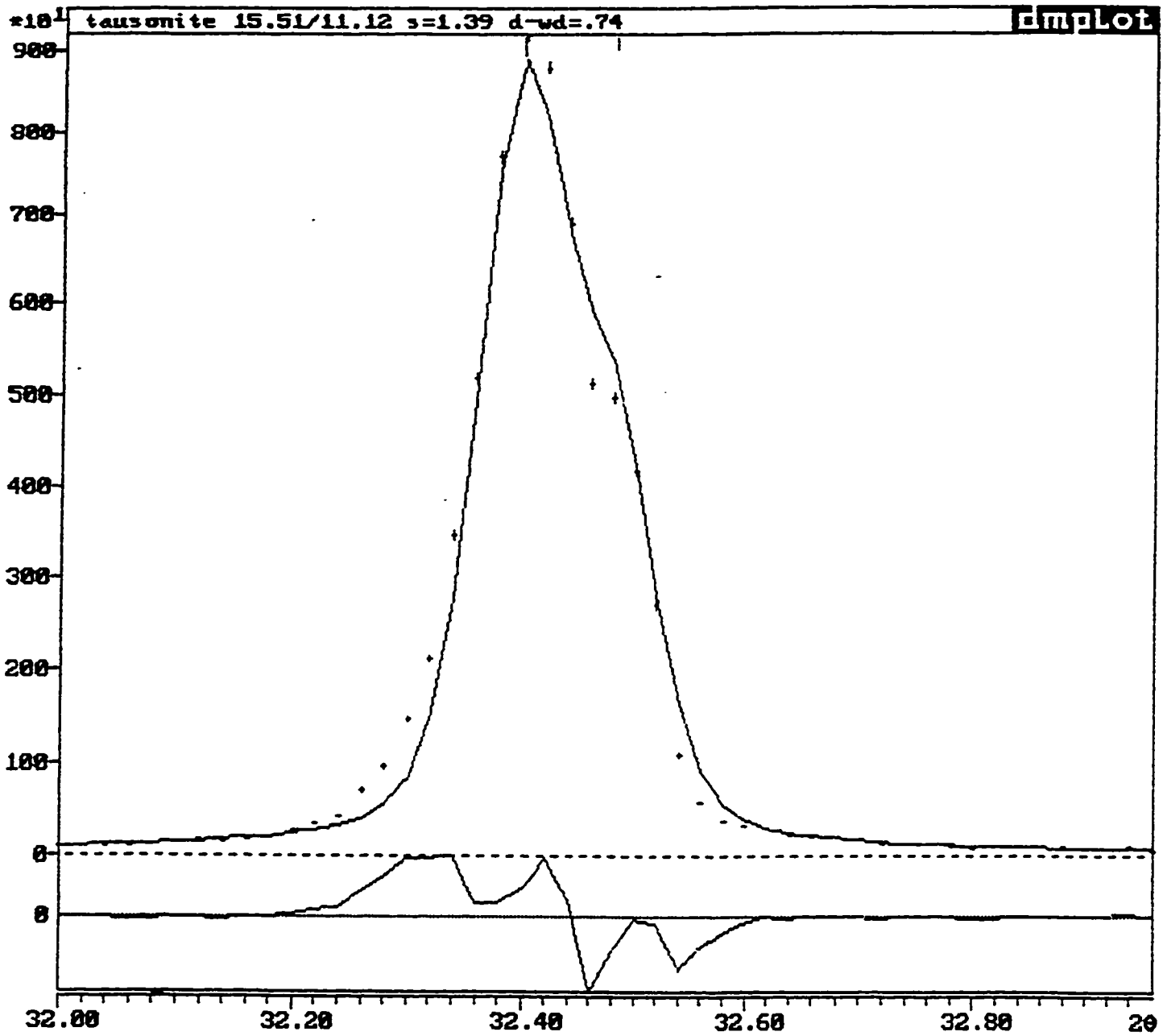

Figure 4-6 Representative fit discrepancy of peak shape within the Rietveld refinement program (DMPLOT). The plot is of the respective observed (as indicated by data points represented by +), calculated (represented by a line) and residual (at bottom) *XRD* patterns for the most intense tausonite reflection.

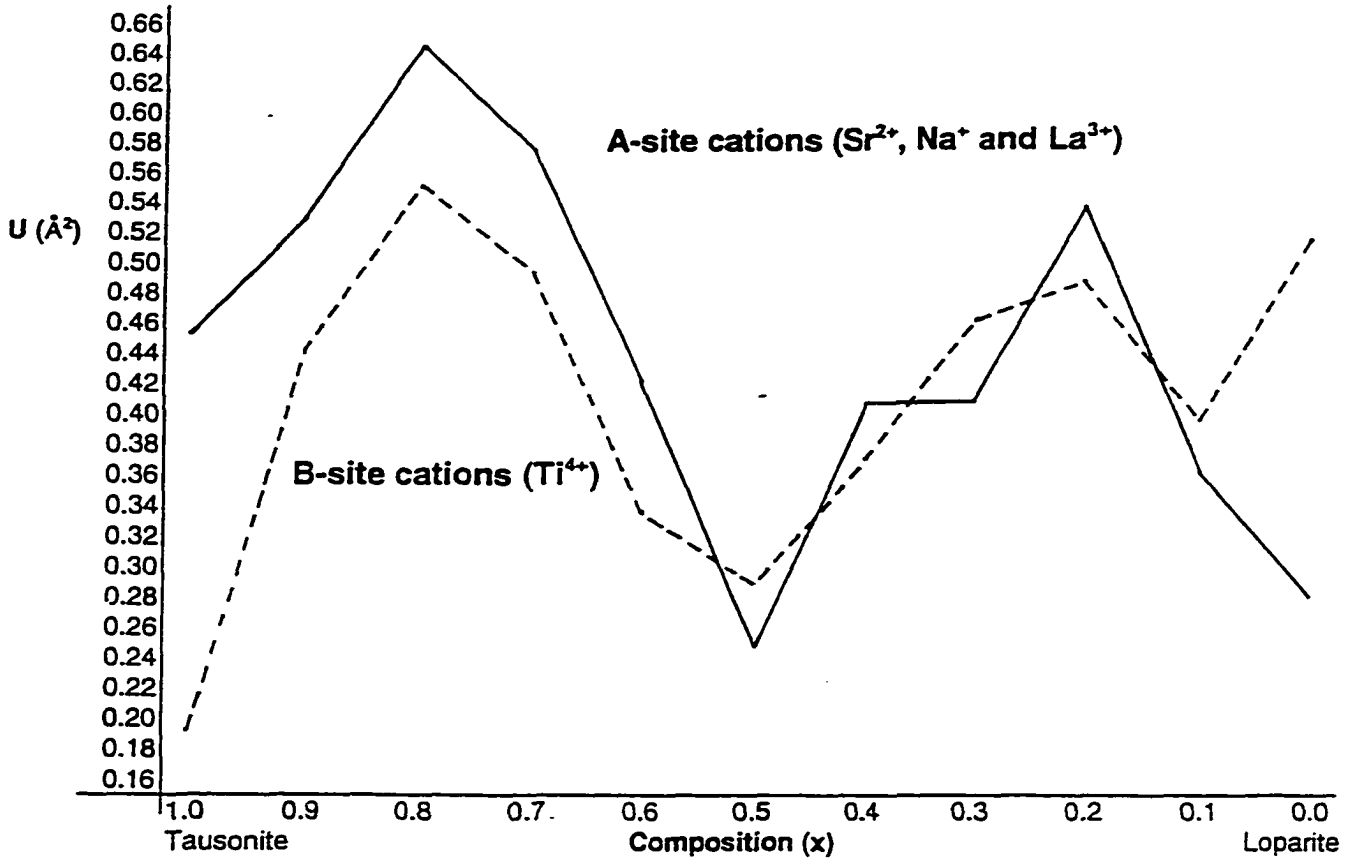

Figure 4-7 Isotropic temperature factors for the *A*-site, the Sr^{2+}, Na^{+} and La^{3+} cations, (represented by the solid line) and the *B*-site, the Ti^{4+} cation (represented by the dashed line).

$Sr_x(NaLa)_{x-1}Ti_2O_6$ structural phase transitions are summarized in a plot of the unit cell parameters as a function of *x* (Figure 4-4[a-c]). The substitution of the divalent Sr^{2+} ions in $SrTiO_3$ by equal amounts of monovalent (Na^+) and trivalent (La^{3+}) cations result in cubic-tetragonal-orthorhombic phase transitions. The disparities in the *XRD* powder patterns for the associated symmetry changes can be viewed in Figure 4-5 and 4-6. Refinements were undertaken using the various space-groups and atomic positions from Woodward (1997a). None of the observed patterns could be assigned to the space-groups characterized by 1:1 cation ordering at the *A*-site.

The phases present at x=1.0 and 0.9 are consistent with the cubic symmetry predictions for tausonite (Galasso 1969). The refinement proved successful (S≈1.35) when using the space group $Pm\bar{3}m$ in the range indicated. The tetragonal perovskite region persists over a composition range of x=0.6 to x=0.4, with the **a** and **c** cell parameters diverging to tetragonal symmetry ($\mathbf{a}\approx\mathbf{a}_p\sqrt{2}$, $\mathbf{c}\approx\mathbf{a}_p$). A successful refinement (S≈1.17) was achieved in this range with the space-group *P4/mbm* (atomic coordinates in Table 4-1).

The orthorhombic perovskite region persists over a composition range of x=0.2 to x=0.0, with **a**, **b** and **c** cell parameters approaching orthorhombic symmetry ($\mathbf{a}\approx\mathbf{a}_p\sqrt{2}$, $\mathbf{b}\approx2\mathbf{a}_p$, and $\mathbf{c}\approx\mathbf{a}_p\sqrt{2}$). Line broadening in this region suggest the structures to be other than cubic or tetragonal; but may in fact be associated with crystallite size. Increasing linewidths with compositional change indicate the patterns to be orthorhombic (barely). The structure is similar to that of loparite-(Ce) (Mitchell 1996) and is isostructural with $CaTiO_3$ (*Pnma* or *Pbnm*). Refinement indicated orthorhombic (*Pnma*) symmetry with

$S \approx 1.30$ and the appearance of peaks indicative of orthorhombic symmetry [(*031*), (*112*) and (*211*)].

4.5.2 Octahedral Tilting and Bond Distortions

The changes in the distorted $ATiO_3$ perovskite structure may be empirically expressed as an amalgamation of the changes in the tilt of the TiO_6 octahedral framework and Ti-O bond length (Zhao *et al.* 1993). The degree of distortion from cubic to tetragonal to orthorhombic symmetry, may be described by the tilting of TiO_6 octahedra, which varies with the tolerance factor (t). Goldschmidt (1926), observed that the perovskite structure is stable if the tolerance factor (t, where $t=(r_A+r_O)/\sqrt{2}\,(r_B+r_O)$, r_A and r_B are the average ionic radii at the *A* and *B*-sites, respectively, and r_O is the ionic radius of oxygen) lies in the range $0.7<t<1.0$. Observed tolerance factors for the tausonite-loparite solid solution series, calculated using ionic radii given by Vainshtein *et al.* (1994), appear in Table 4-3. The observed factors lie at the upper limit (1.0016-0.9787) of this tolerance range indicating that the perovskite structures undergo very little distortion with the substitution of Sr^{2+} by Na^{+} and La^{3+} at the *A*-site. Woodward (1997b) describes octahedral tilting distortions in the perovskite structure together with data for the symmetry and crystallography of the 23 Glazer tilt systems. This allows the space-groups encountered in this synthesis ($Pm\bar{3}m$, *P4/mbm*, and *Pnma*) to be assigned their respective Glazer tilt systems $a^0a^0a^0$, $a^0a^0c^+$, and $a^+b^-b^-$ or $a^+a^-a^-$.

The interatomic bond distances and angles, together with the tilt angles, for the orthorhombic, tetragonal and cubic structures appear in Table 4-5. Table 4-6 contains

Table 4-5 Interatomic attributes for the tausonite-loparite solid solution series, as calculated from a DBWS input control file by the Wyriet program Bond. * distinguishes an identical atom at a different location.

Attributes	x=1.0	x=0.9	x=0.8	x=0.7	x=0.6	x=0.5	x=0.4	x=0.3	x=0.2	x=0.1	x=0.0
Bond Lengths (Å)											
A-O_1 (A)					2.753	2.754	2.751	2.747	2.946	2.927	2.801
A-O_1 (B)									2.547	2.562	2.686
A-O_1 (C)									2.931	2.870	2.903
A-O_1 (D)									2.588	2.643	2.584
A-O_2 (A)	2.762	2.761	2.761	2.757	2.780	2.808	2.767	2.807	2.746	2.855	2.749
A-O_2* (B)					2.730	2.696	2.731	2.686	2.745	2.645	2.780
A-O_2 (C)									2.648	2.687	2.422
A-O_2* (D)									2.849	2.788	3.052
mean *A*-O_1					2.753	2.754	2.751	2.747	2.753	2.751	2.744
mean *A*-O_2	2.762	2.761	2.761	2.757	2.755	2.752	2.749	2.747	2.747	2.744	2.751
mean *A*-$O_{1,2}$	2.762	2.761	2.761	2.757	2.754	2.753	2.750	2.747	2.750	2.747	2.747
Ti-O_1	1.953	1.952	1.952	1.949	1.950	1.944	1.942	1.941	1.959	1.952	1.945
Ti-O_2					1.947	1.949	1.945	1.945	1.818	1.921	1.982
Ti-O_2*									2.070	1.966	1.949
mean Ti-$O_{1,2}$	1.953	1.952	1.952	1.949	1.949	1.947	1.944	1.943	1.949	1.946	1.959
Bond Angles (°)											
O_2-Ti-O_2*	90	90	90	90	90	90	90	90	90.3	89.9	89.2
O_2-Ti-O_1	90	90	90	90	90	90	90	90	94.4	89.7	83.3
O_2*-Ti-O_1	90	90	90	90	90	90	90	90	79.0	86.3	77.1
Ti-O_1-Ti	180	180	180	180	180	180	180	180	162.9	166.4	169.4
Ti-O_2-Ti	180	180	180	180	178.0	175.3	178.5	175.0	173.0	174.1	160.4
Tilt Angles (°)											
[0 0 1]	0.00	0.00	0.00	0.00	0.00	3.45	3.12	2.71	0.00	0.00	0.88
[0 1 0]	0.00	0.00	0.00	0.00	0.00	0.00	0.00	0.00	3.82	3.17	2.35
[1 1 1]	0.00	0.00	0.00	0.00	0.00	0.00	0.00	0.00	3.55	2.92	2.51

Table 4-6 Mean interatomic attributes for the tausonite-loparite solid solution series (calculated from Table 4-5) compared to those of perovskite ($CaTiO_3$; Buttner and Masden 1992). * distinguishes an identical atom at a different location.

Mean Bond Attributes	Cubic (x=1.0-0.7)	Tetragonal (x=0.6-0.3)	Orthorhombic (x=0.2-0.0)	$CaTiO_3$
Bond Lengths(Å)				
$\langle A\text{-}O_1 \rangle$	2.760 Å	2.751 Å	2.896 Å	
$\langle A\text{-}O_1^* \rangle$			2.602 Å	
mean $\langle A\text{-}O_1 \rangle$	2.760 Å	2.751 Å	2.749 Å	2.426 Å
$\langle A\text{-}O_2 \rangle$		2.751 Å	2.753 Å	
$\langle A\text{-}O_2^* \rangle$		2.750 Å	2.741 Å	
mean $\langle A\text{-}O_2 \rangle$		2.751 Å	2.747 Å	2.726 Å
$\langle Ti\text{-}O_1 \rangle$	1.952 Å	1.944 Å	1.950 Å	
$\langle Ti\text{-}O_2 \rangle$		1.947 Å	1.907 Å	
$\langle Ti\text{-}O_2^* \rangle$			1.995 Å	
Mean $\langle Ti\text{-}O \rangle$	1.952 Å	1.946 Å	1.951 Å	1.955 Å
Bond Angles(°)				
$\langle O_2\text{-}Ti\text{-}O_2^* \rangle$	90°	90°	89.8°	89.4°
$\langle O_2\text{-}Ti\text{-}O_1 \rangle$	90°	90°	89.1°	89.6°
$\langle O_2^*\text{-}Ti\text{-}O_1 \rangle$	90°	90°	80.8°	89.3°
$\langle Ti\text{-}O_1\text{-}Ti \rangle$	180°	180°	166.2°	156.9°
$\langle Ti\text{-}O_2\text{-}Ti \rangle$	180°	176.7°	169.2°	155.8°
Tilt Angles(°)				
[001]	0.0°	3.1°	0.3°	5.4°
[010]	0.0°	0.0°	3.1°	8.4°
[111]	0.0°	0.0°	3.0°	10.0°

the mean values; including those for a perovskite standard ($CaTiO_3$, orthorhombic; Buttner and Masden 1992). Perovskite exhibits a larger distortion, with respect to bond attributes, than the perovskite compounds studied in this synthesis. With decreasing tolerance factor *i.e.,* decreasing *x*, the average ⟨*A*-O⟩ bond length decreases; while the average ⟨Ti-O⟩ bond length decreases in the region from *x*=1.0-0.3 and increases in the region *x*=0.2-0.0.

4.6 Conclusions

Analysis of the crystal structures of the tausonite-loparite solid solution series indicates that there is a reduction in symmetry from cubic ($Pm\bar{3}m$) to orthorhombic (*Pnma*), via an intermediate tetragonal (*P4/mbm*) modification. The symmetry changes appear to occur at about ~66.6 and ~33.3 wt% tausonite, and are consistent with formulae of approximately $Sr_2(NaLa)Ti_3O_9$ and $Sr(NaLa)_2Ti_3O_9$, respectively. Discontinuities in lattice parameters with the symmetry reductions indicate that replacement of strontium by equivalent amounts of lanthanum and sodium, in tausonite, represents a compositional, rather than a structural, solid-solution series. The pseudocubic cell parameter $\mathbf{a_p}$ decreases with increasing loparite content (decreasing *x*; Figure 4-4). The [*111*] tilt angle Φ (Φ=0 in $Pm\bar{3}m$) on inception at *x*=0.5 achieves a maximum and decreases thereafter with increasing loparite content. Rietveld refinements indicated that no ordering at the *A*-site exists throughout the solid-solution series.

Chapter 5

STRUCTURE OF THE THORIUM PEROVSKITE

$Na_{2/3}Th_{1/3}TiO_3$

5.1 Introduction and Structure

$Na_{2/3}Th_{1/3}TiO_3$ is a member of the large family of titanium perovskites ($ATiO_3$), but is unusual in that it contains a tetravalent cation (Th^{4+}) at the *A*-site. The thorium cation cannot exist alone at the *A*-site due to its high charge. Thus, sodium is substituted to satisfy the size and charge requirements of the structure. The calculated tolerance factor of $Na_{2/3}Th_{1/3}TiO_3$ is t=0.963 (where r_i=1.21Å for Th_{XII}^{4+}; Vainshtein *et al.* 1994), which indicates reduced symmetry and suggests the space-group is not $Pm\bar{3}m$. This study was undertaken to investigate aspects of the structure of this poorly-characterized Th-bearing perovskite. Subsequent to the commencement of this study, Zhu and Hor (1995) investigated the synthetic perovskite $Na_{0.67}Th_{0.32}TiO_3$ and claimed that it is cubic (a_p=3.8477Å). Zhu and Hor (1995), did not determine any space-group but suggested that superlattice lines in the *XRD* pattern indicate ordering of Na^+ and Th^{4+}. This study is intended to confirm their findings and to attempt to derive a possible space-group.

5.2 Experimental Results

Compositional Determinations

Figure 5-1 shows the SEM/BSE images of the experimental charge. The sample

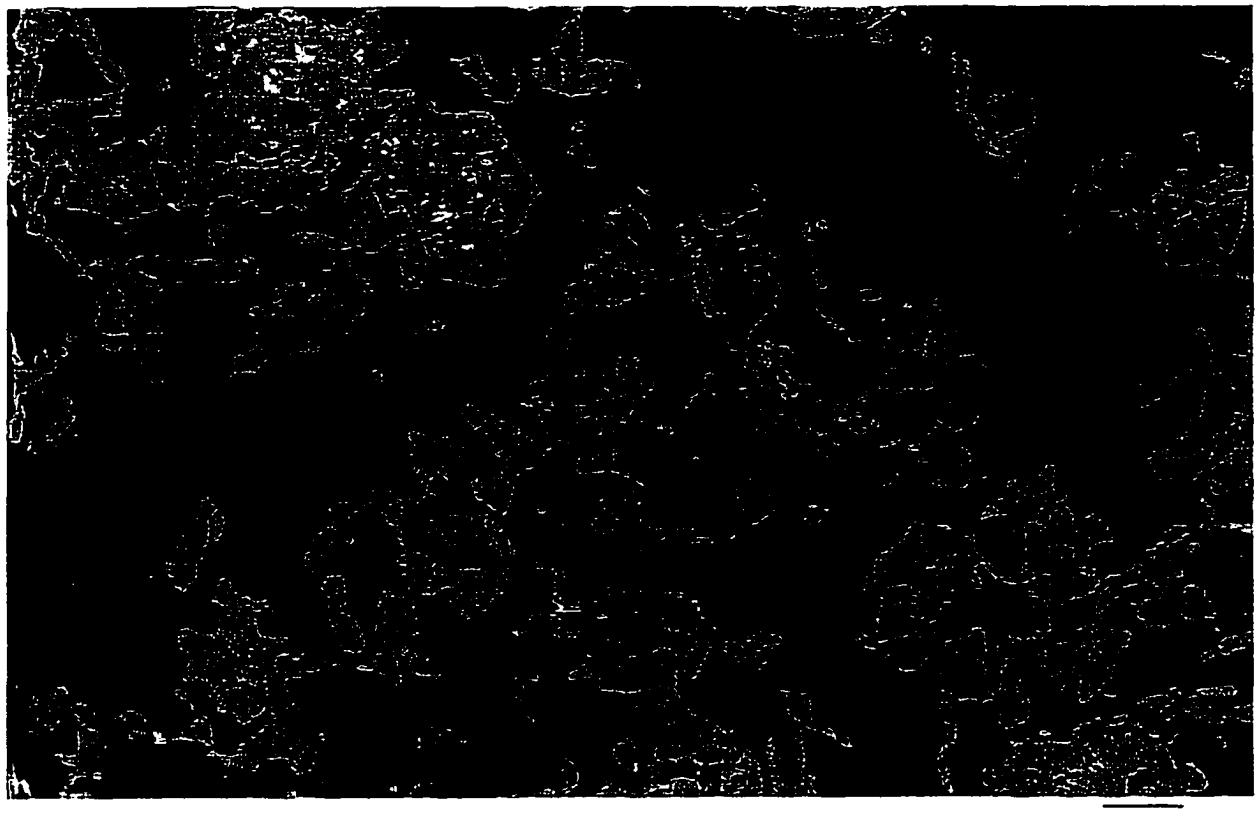

Figure 5-1 SEM/BSE images of the synthesised sodium thorium titanium perovskite. The image exhibits two distinct phases; one of relatively low average atomic number (grey), representing the sodium thorium titanium perovskite ($Na_{2/3}Th_{1/3}TiO_3$); and another of relatively high average atomic number (white), representing thorium dioxide (ThO_2).

consists of two distinct phases; one of relatively low average atomic number (grey), representing the thorium perovskite, and another of high average atomic number (very light), representing thorium dioxide (ThO_2). The thorium perovskite has the general formula $Na_{0.65}Th_{0.35}TiO_3$ and occurs with a modal percentage of approximately 93%; while thorium dioxide (ThO_2) constitutes the remainder (~7%). Unfortunately, the unavailability of a suitable SEM/EDS thorium standard precluded accurate determination of the composition. This resulted in overestimation of Th^{4+}, and hence, high elemental totals for the perovskite phase (~105%) and for thorium dioxide (~110%).

The Ca^{2+} thorium perovskite ($Ca_{.33}Th_{.33}TiO_3$) analogue of this structure could not be synthesised at this temperature (1100°C) and pressure (1 atm.).

Powder X-Ray Diffractometry

The *XRD* powder patterns were collected over the 2θ range 10-140°, with a step size of 0.020 (2θ), which provided 40 reflections. *XRD* data are listed in Table 5-1; all reflections with relative intensities of less than 0.5 were considered unobserved. For least-squares refinement, all reflections with relative intensities of less than 1 were treated as being unobserved. Doublets representing both $K_{\alpha 1}$ and $K_{\alpha 2}$ reflections appear as low as 40°(2θ). Superstructure *d*-spacings, as determined from the *XRD* powder patterns (identified by asterisks in Table 5-1), may be regarded as being only approximate due to the broad nature of the reflections. Those reflections attributed to the impurity (ThO_2) are also identified in Table 5-1.

Table 5-1 *XRD* powder pattern reflections for the synthetic thorium titanium perovskite as compared to that of Zhu and Hor (1995), $La_{2/3}TiO_3$ (Abe and Uchino 1974) and ThO_2 (Leigh and McCartney 1974). The *d*-calc. refers to the *d*-spacings as calculated by the least-squares refinement program (XRAY) and I-calc. refers to the relative intensities as calculated by XPOW. * Refers to broad superstructure lines as identified by Zhu and Hor (1995), and ** refers to those lines identified in this synthesis as possible superstructure lines.

Synthesized $Na_{2/3}Th_{1/3}TiO_3$					$Na_{2/3}Th_{1/3}TiO_3$			$La_{2/3}TiO_3$			ThO_2	
h k l	*d*-obs.	*d*-calc.	I-obs.	I-calc.	*h k l*	*d*-obs.	I-obs.	*h k l*	*d*-obs.	I-obs.	*d*-obs.	I-obs.
*1 0 0***	7.685	7.690	3.9		*	7.693	14	*	7.796	17.6		
2 0 0	3.836	3.845	4.1	4	*1 0 0*	3.847	4	*1 0 0*	3.889	5.8		
*2 1 0***	3.451	3.439	2.5		*	3.441	26	*	3.472	15.7		
	3.224		2.3								3.232	100
2 2 0	2.716	2.719	100.0	100	*1 1 0*	2.720	100	*1 1 0*	2.744	100.0		
*3 0 0***	2.557	2.563	1.1		*	2.565	7	*	2.585	6.1		
2 2 2	2.218	2.220	18.5	20	*1 1 1*	2.221	17	*1 1 1*	2.241	24.5		
2 2 2	2.217	2.220	8.0		*	2.134	3	*	2.155	2.1		
	1.975		1.0								1.978	45
4 0 0	1.921	1.923	31.9	38	*2 0 0*	1.924	46	*2 0 0*	1.94	47.2		
4 0 0	1.921	1.923	15.7	19								
*4 1 0***	1.870	1.865	1.0		*	1.867	10	*	1.88	7.0		
4 2 0	1.719	1.720	2.6	3	*2 1 0*	1.721	5	*2 1 0*	1.74	4.7		
	1.684		1.0		*	1.680	4	*	1.69	3.8	1.687	46
4 2 2	1.569	1.570	37.2	33	*2 1 1*	1.571	48	*2 1 1*	1.59	44.0		
4 2 2	1.569	1.570	18.8	16								
					*	1.540	1					
					*	1.429	3	*	1.44			
4 4 0	1.359	1.359	15.7	19	*2 2 0*	1.361	23	*2 2 0*	1.37			
4 4 0	1.359	1.359	7.1	9								
4 4 2	1.281	1.282	1.6	1	*2 2 1*	1.283	1	*3 0 0*	1.29		1.284	18
6 2 0	1.216	1.216	9.0	12	*3 1 0*	1.217	21	*3 1 0*	1.23			
6 2 0	1.216	1.216	4.0	6								
6 2 2	1.159	1.159	1.9	4	*3 1 1*	1.161	6	*3 1 1*	1.17			
4 4 4	1.110	1.110	4.1	5	*2 2 2*	1.111	9	*2 2 2*	1.12			
4 4 4	1.110	1.110	1.8	3								
6 4 0	1.067	1.066	1.0	1	*3 2 0*	1.067	2					
6 4 2	1.028	1.028	12.2	13	*3 2 1*	1.029	27					
6 4 2	1.028	1.028	5.4	7								
8 0 0	0.962	0.961	1.2	3	*4 0 0*	0.962	4					
8 2 0	0.933	0.933	0.4	0	*4 1 0*	0.934	1					
6 4 4	0.933	0.933	0.4	0	*3 2 2*	0.934	1					
8 2 2	0.907	0.906	3.4	5	*4 1 1*	0.907	7					
8 2 2	0.907	0.906	1.5	3								
6 6 0	0.907	0.906	2.0	3	*3 3 0*	0.907	15					
6 6 0	0.907	0.906	0.9	2								
6 6 2	0.882	0.882	0.7	2								
8 4 0	0.860	0.860	4.2	10								
8 4 0	0.860	0.860	1.9	5								
6 6 4	0.820	0.820	3.2	7								

The *XRD* powder pattern of the perovskite synthesised is similar to those of $Na_{0.67}Th_{0.32}TiO_3$ (Zhu and Hor 1995), $La_{0.5}Li_{0.5}TiO_3$, which is tetragonal (a_p=3.8Å, $a=b=2^{1/2}a_p$, and $c=2a_p$; Várez *et al.* 1995), and $La_{2/3}TiO_3$, which is orthorhombic (a=3.869Å, b=3.882Å, and c=7.782Å; Abe and Uchino 1974). There appear to be many similarities (Table 5-1, indexed reflections) between the positions and intensities of the main peaks for the three perovskite compounds. These main peaks originate from the perovskite (TiO_6) framework. The *XRD* patterns proved to be complex, as indicated by the existence of additional reflections (indicated by asterisks in Table 5-1)). Most of these reflections may be indexed on a double primitive cell ($2a_p$ x $2a_p$ x $2a_p$); as well as tetragonal or orthorhombic cells. The doubled unit cell may represent distortion of the ideal perovskite structure by coordinated tilting of the TiO_6 octahedra resulting from vacancies and/or ordering of Na^+ and Th^{4+} at the *A*-site in eight (*Z*=8) adjacent cells (Varez *et al.* 1995; Zhu and Hor 1995; Smith and Welch 1960).

Least-Squares Refinement of Cell Parameters

The *XRD* pattern for $Na_{2/3}Th_{1/3}TiO_3$ reveals a number of superstructure lines additional to those expected for an ideal perovskite. Splittings of the high-angle reflections, suggesting a gross deviation from strictly cubic symmetry, were not observed (Table 5-1). After exclusion of all superstructure reflections, the diffraction pattern reflections do not suggest $m\bar{3}m$ Laue symmetry, when indexed on a double primitive cell ($2a_p$), with only the reflections having (*hhl*): all odd or even. These data indicate that the observed reflections for thorium perovskite are not consistent with the space-group $Fm\bar{3}m$

(or *Im3*). Least-squares refinement on the double primitive cell indicates **a**=7.6902 ± 0.0007Å, *v*=454.8 ± 0.1Å^3, and *Z*=8. This is very similar to the results of Zhu and Hor (1995), in which a doubling of their unit cell ($2\mathbf{a}_p$) would give **a**=7.6954Å and *v*=455.7Å^3.

5.3 Rietveld Refinement of Thorium Perovskite

Structure Determination

Rietveld refinement (Figure 5-2) proved quite difficult as reflected in the elevated values for the criteria-of-fit (*S*=2.04 and *R-Bragg*=19.00). The refinement discrepancies were partly due to the failure of the Rietveld refinement program (DBWS-9411) to accommodate the two very different peak widths of the main and superstructure reflections, along with inaccuracies due to peak shape. These superstructure reflections, which may be attributed to an ordered microstructure, also generated difficulties in including ThO_2 as an additional phase in the refinement and in obtaining credible ordering parameters for Na^+ and Th^{4+}.

Rietveld refinement results (Table 5-2; where *R-Bragg*=19.00) obtained in this synthesis appear worse than those obtained by Zhu and Hor (1995; *R-Bragg*=7.8). Rietveld refinement by Zhu and Hor (1995) gave results, without addressing refinement parameters and possibly neglecting reflections produced by $K_{\alpha 2}$. As there are no data to support their Rietveld refinement, it may be that the refinement had been purposely biased to allow for more acceptable results, by the exclusion of all the superstructure reflections.

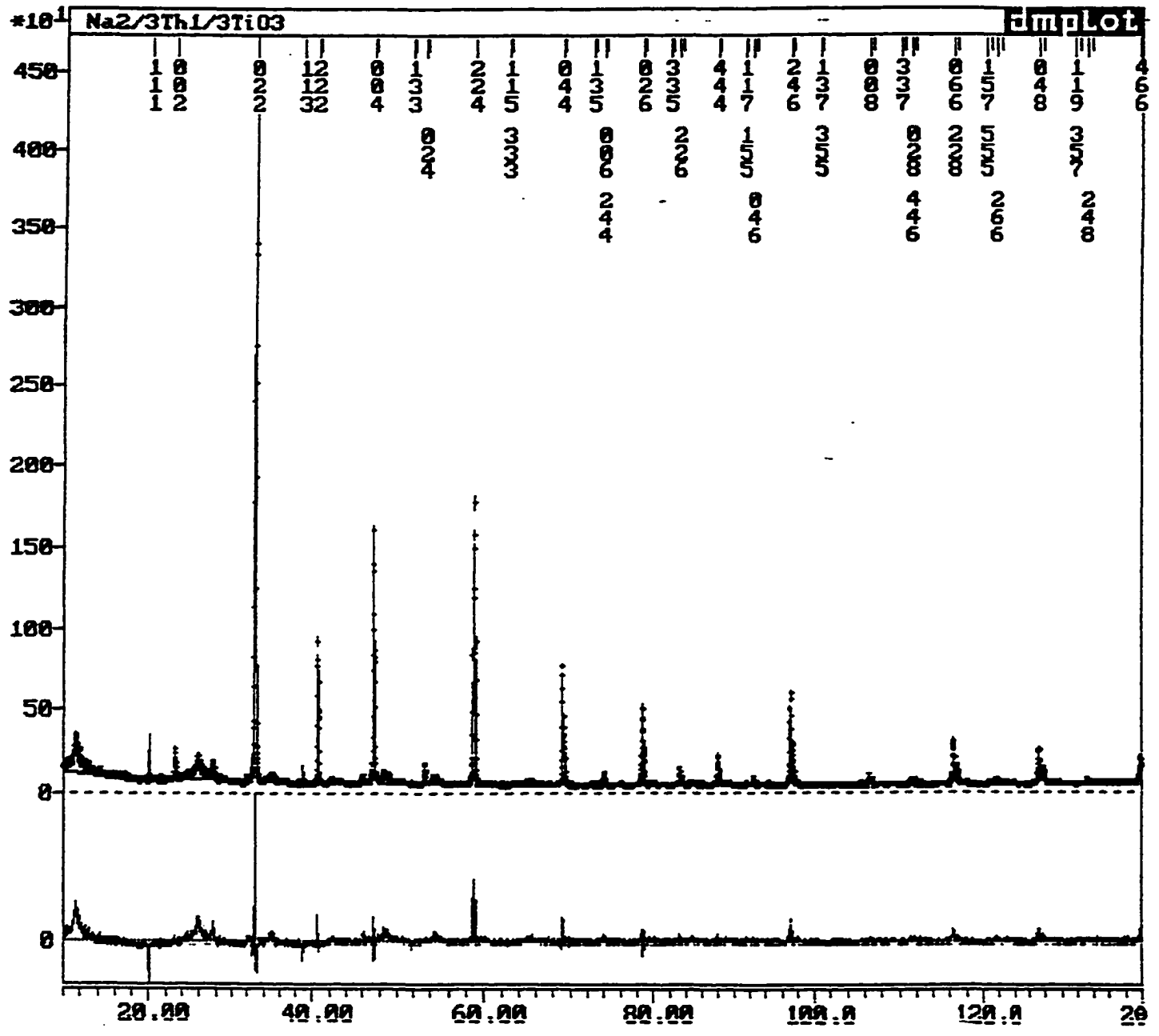

Figure 5-2 DMPLOT for thorium titanium perovskite ($Na_{2/3}Th_{1/3}TiO_3$), of the observed (as indicated by the data points, represented by +), calculated (represented by the line) and residual (at bottom) *XRD* patterns. Criteria of fit for the plot are *S*=2.04 and *R-Bragg*=19.00.

Table 5-2 Atomic coordinates, positional and thermal parameters, unit-cell dimensions and criteria of fit as determined by the Rietveld refinement program (DBWS-9411), for the thorium perovskite ($Na_{2/3}Th_{1/3}TiO_3$), assuming *Fm3̄m* symmetry. The high *R-Bragg* demonstrates that the compound does not belong to this space-group.

Parameters		$Na_{2/3}Th_{1/3}TiO_3$
	Space-Group	*Fm3̄m*
Na^{+} (*4a*)	*x*	*x* (*x*≈0.00000)
	y	0
	z	0
	U(Å^2)	1.00000
	N	0.08543
Th^{4+} (*4b*)	*x*	1/2
	y	1/2
	z	1/2
	U(Å^2)	1.00000
	N	0.00657
Ti^{4+} (8c)	*x*	1/4
	y	1/4
	z	1/4
	U(Å^2)	1.00000
	N	0.04167
O^{-2} (*24d*)	*x*	0
	y	1/4
	z	1/4
	U(Å^2)	4.00000
	N	0.12500
Unit-Cell	*Z*	8
	a_p(Å)	3.8471
	a (Å)	7.6942
	Volume (Å^3)	455.50
	S (*R-wp/R-exp*)	2.04
	R-Bragg	19.00
	D (*D*-statistic)	0.98

The unit cell parameters in this synthesis (a=7.6942Å, v=455.5Å^3) agree closely with those of Zhu and Hor (a=7.6954Å and v=455.7Å^3; 1995), and are better in this respect than those determined by least-squares refinement (a=7.6902Å and v=454.8Å^3). The refined occupancies for Na^+ and Th^{4+} in this synthesis are 0.68 and 0.32, respectively (see Table 5-2), similar to those obtained by Zhu and Hor (1995), which are 0.67 and 0.32, respectively. This effectively maintains the overall valence at the *A*-site of approximately 2, which would be expected for any perovskite with the general formula $ATiO_3$. Bond lengths (as determined by WYRIET; Schneider 1995) within the thorium perovskite structure were calculated to be ⟨*A*-O⟩=2.72Å and ⟨Ti-O⟩=1.93Å, and all interatomic angles are 90°, as expected for a cubic structure.

The thorium perovskite structure consists of a framework of corner-linked TiO_6 polyhedra. Na^+ and Th^{4+} occupy the interstices within this framework in twelve-fold coordination. The presence of weak broad superstructure lines in the *XRD* pattern (Figure 5-2) indicate that ordering of these *A*-site cations is undoubtedly present. Although, the pattern may be indexed on a doubled perovskite unit cell in the space group $Fm\bar{3}m$, the poor quality of the Rietveld refinement in this space-group suggests that the actual space-group must be of lower symmetry; possibly tetragonal or monoclinic. Given the complexity of the powder pattern and the failure of DBWS-9411 to deal adequately with co-existing broad and well-defined reflections, it is considered that solution of this problem is beyond the scope of this work.

5.4 Conclusions

XRD powder pattern results for $Na_{2/3}Th_{1/3}TiO_3$ agree with those determined by Zhu and Hor (1995). The only differences lie in the methods of interpretation of the *XRD* data (Table 5-2). It is concluded that the space-group is not $Fm\bar{3}m$. The structure must have a lower symmetry and potentially exhibits *A*-site ordering; but, further investigation and interpretation is beyond the scope of this work.

Chapter 6

THE PSEUDO-BINARY SYSTEM

$K_2Cr_2Ti_6O_{16}$- $K_2La_2Ti_6O_{16}$

6.1 Introduction

A pseudo-binary system was investigated between a hollandite-group compound ($K_2Cr_2Ti_6O_{16}$) and the *n=3* member of the homologous series $K_2La_2Ti_{3+n}O_{10+2n}$, *i.e.*, $K_2La_2Ti_6O_{16}$. The study was undertaken to determine phase relationships and to evaluate the extent of lanthanum substitution in hollandite. This work examined hollandite-type and other phases over the following compositions; $K_2La_{(2x)}Cr_{(2-2x)}Ti_6O_{16}$ (where x= 0.00, 0.10, 0.20, 0.30, 0.50, 0.75, and 1.00), at temperatures of 1100, 1200 and 1300°C (see Chapter 2). This study provides information relevant to the location and environment of the rare earth cations in natural hollandite-group minerals. Mitchell and Haggerty (1986) have reported up to 2 wt% total REE_2O_3 in hollandites from the New Elands orangeite. In contrast, Mitchell and Bergman (1991) found no appreciable *REE* substitution in the hollandite-group mineral priderite (KTi_8O_{16}), from lamproites. Conclusions have a direct bearing on the ability of synthetic hollandite to immobilize large elements of varying charge and size.

6.2 Experimental Results

The *XRD* powder patterns of compositions investigated were collected over a 2θ range of 10-140°, with a step size of 0.040° (2θ), which provided between 60 to 116

reflections. To perform an adequate Rietveld structure refinement of the hollandite end-member (x=0), it was necessary to collect *XRD* patterns at a step size of 0.020° (2θ). *XRD* data are listed in appendix 2; all reflections with relative intensities of less than 1 were considered as unobserved. The phases present at each composition and temperature investigated, as determined by SEM/EDS analysis, are given in Table 6-1. Figure 6-1 shows representative SEM/BSE images of the experimental charges. The images typically show two distinct phases; one of high average atomic number, that is a lighter colour, represents the perovskite-type phases (P-1, P-2 and P-3) and a darker phase of relatively low average atomic number, representing hollandite (H) and/or potassium hexatitanate (J). At compositions x=0.0-0.5, the darker phase is hollandite; and at compositions x=0.5-1.0, the darker phase is potassium hexatitanate. At x=0.5 and 1100°C hollandite and minor amounts of potassium hexatitanate occur together.

The hollandite-perovskite pseudo-binary phase diagram determined by SEM/EDS (Table 1) and *XRD* (Table 3) appears in Figure 6-2. The phase diagram contains two domains (x=0.0-0.5 and x=0.5-1.0) and four distinct fields (two per domain) as determined from the phase assemblage present. The only phase to persist throughout both domains, is the main perovskite phase (perovskite-1).

The first domain (x=0.0-0.5) is characterized by the presence of hollandite and rutile in decreasing amounts; and contains two distinct fields (x=0.0-0.05; x=0.05-0.5). Perovskite-1, not present in field one, increases in amount as x increases in field two.

In the x=0.0-0.05 field, at the composition of the hollandite end-member, the only phase present is a hollandite-type phase (Figure 6-1A). In the second field (x=0.05-0.5)

Table 6-1 SEM analysis of the hollandite-perovskite pseudo-binary system. Overall modal percentage estimated by relative area approximation. Any composition which could not be analysed due to a small grain size and its proximity to similar grains, is identified by the type of phase only.

Composition	Temp. (°C)	Overall %	Phases Present	Composition (SEM)	Grain Size (μm)
x=0.0	1300	98	Hollandite	$K_{1.51}(Cr_{1.51}Ti_{6.54})_{8.05}O_{16}$	7
		2	Rutile	$(Cr_{0.04}Ti_{0.96})_{1.00}O_2$	5
	1200	100	Hollandite	$K_{1.54}(Cr_{1.63}Ti_{6.37})_{8.00}O_{16}$	6
	1100	100	Hollandite	$K_{1.58}(Cr_{1.57}Ti_{6.43})_{8.00}O_{16}$	5
x=0.1	1300	90	Hollandite	$K_{1.46}(Cr_{1.49}Ti_{6.51})_{8.00}O_{16}$	6
		10	Perovskite-1	$(K_{0.11}La_{0.51})_{0.62}(Cr_{0.10}Ti_{0.97})_{1.07}O_3$	2
	1200	92	Hollandite	$K_{1.49}(Cr_{1.48}Ti_{6.50})_{7.98}O_{16}$	3
		8	Perovskite-1	$(K_{0.16}La_{0.60})_{0.76}(Cr_{0.09}Ti_{0.94})_{1.03}O_3$	1
	1100	95	Hollandite	$K_{1.65}(Cr_{1.52}Ti_{6.39})_{7.91}O_{16}$	2
		5	Perovskite-1		0.5
x=0.2	1300	85	Hollandite	$K_{1.47}(Cr_{1.44}Ti_{6.54})_{7.98}O_{16}$	10
		15	Perovskite-1	$(K_{0.13}La_{0.62})_{0.75}(Cr_{0.03}Ti_{0.99})_{1.02}O_3$	6
	1200	90	Hollandite	$K_{1.53}(Cr_{1.46}Ti_{6.51})_{7.97}O_{16}$	4
		10	Perovskite-1		1
	1100	95	Hollandite	$K_{1.70}(Cr_{1.26}Ti_{6.61})_{7.87}O_{16}$	2
		5	Perovskite-1		0.5
x=0.3	1300	80	Hollandite	$K_{1.48}(Cr_{1.33}Ti_{6.63})_{7.96}O_{16}$	10
		20	Perovskite-1	$(K_{0.33}La_{0.58})_{0.91}(Cr_{0.11}Ti_{0.90})_{1.01}O_3$	6
	1200	85	Hollandite	$K_{1.53}(Cr_{1.46}Ti_{6.52})_{7.98}O_{16}$	4
		15	Perovskite-1	$(K_{0.36}La_{0.55})_{0.93}(Cr_{0.03}Ti_{0.98})_{1.01}O_3$	1.5
	1100	90	Hollandite	$K_{1.72}(Cr_{1.32}Ti_{6.54})_{7.86}O_{16}$	2
		10	Perovskite-1	$(K_{0.12}La_{0.62})_{0.74}(Cr_{0.03}Ti_{0.98})_{1.01}O_3$	1
x=0.5	1300	60	Hollandite	$K_{1.47}(Cr_{1.23}Ti_{6.74})_{7.97}O_{16}$	9
		36	Perovskite-1	$(K_{0.27}La_{0.53})_{0.80}(Cr_{0.03}Ti_{1.02})_{1.05}O_3$	6
		4	Rutile	$Ti_{1.00}O_2$	11
	1200	60	Hollandite	$K_{1.47}(Cr_{1.36}Ti_{6.61})_{7.97}O_{16}$	5
		40	Perovskite-1		1
	1100	60	Hollandite	$K_{1.57}(Cr_{1.48}Ti_{6.40})_{7.88}O_{16}$	2
		35	Perovskite-1	$(K_{0.43}La_{0.49})_{0.92}(Cr_{0.01}Ti_{1.02})_{1.03}O_3$	2
		5	K-Hexatitanate	$K_{1.96}Ti_{5.96}O_{13}$	2
x=0.75	1300	60	K-Hexatitanate	$K_{2.00}Ti_{6.02}O_{13}$	10
		35	Perovskite-1	$(K_{0.29}La_{0.55})_{0.84}(Cr_{0.02}Ti_{1.00})_{1.02}O_3$	5
		5	Perovskite-2	$La_{0.97}Cr_{1.06}O_3$	1
	1200	55	K-Hexatitanate	$K_{2.01}Ti_{6.02}O_{13}$	6
		38	Perovskite-1	$(K_{0.28}La_{0.50})_{0.78}(Cr_{0.11}Ti_{0.97})_{1.08}O_3$	3
		7	Perovskite-2	$La_{0.95}Cr_{1.06}O_3$	0.5
	1100	60	K-Hexatitanate	$K_{1.96}Ti_{6.01}O_{13}$	3
		40	Perovskite-1		1
x=1.0	1300	65	K-Hexatitanate	$K_{2.00}Ti_{6.02}O_{13}$	9
		32	Perovskite-1	$(K_{0.29}La_{0.55})_{0.84}Ti_{1.02}O_3$	4
		3	Perovskite-3		1.5
	1200	60	K-Hexatitanate	$K_{1.96}Ti_{5.99}O_{13}$	8
		35	Perovskite-1	$(K_{0.31}La_{0.53})_{.84}Ti_{1.02}O_3$	3
		5	Perovskite-3	$La_{1.94}Ti_{2.05}O_7$	1.5
	1100	60	K-Hexatitanate	$K_{2.03}Ti_{6.04}O_{13}$	4
		32	Perovskite-1		2
		8	Perovskite-3		0.5

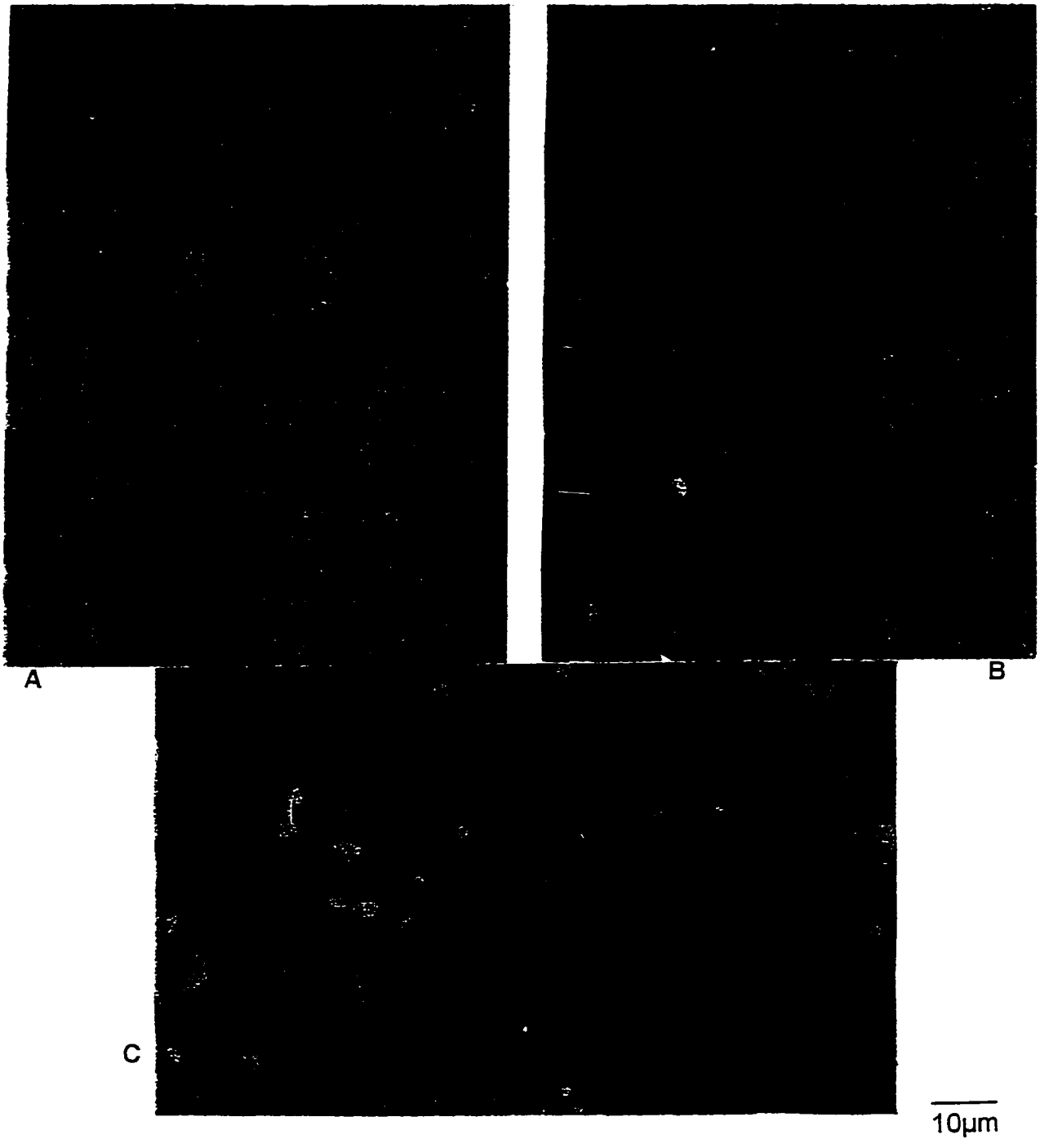

Figure 6-1 SEM/BSE images of representative compositions at a magnification of 1000x.
A) Hollandite (x=0.0)
B) Hollandite-rich (x=0.1-0.5), low-temperature (1100°C).
C) Hollandite-rich (x=0.1), high-temperature (1200°C and 1300°C).
D) Hollandite-rich (x=0.2-0.5) high-temperature (1200°C and 1300°C).
E) Perovskite-rich (x=0.75), high-temperature (1200°C and 1300°C).
F) Perovskite (x=1.0), low-temperature (1100°C).
G) Perovskite (x=1.0), high-temperature (1200°C and 1300°C).

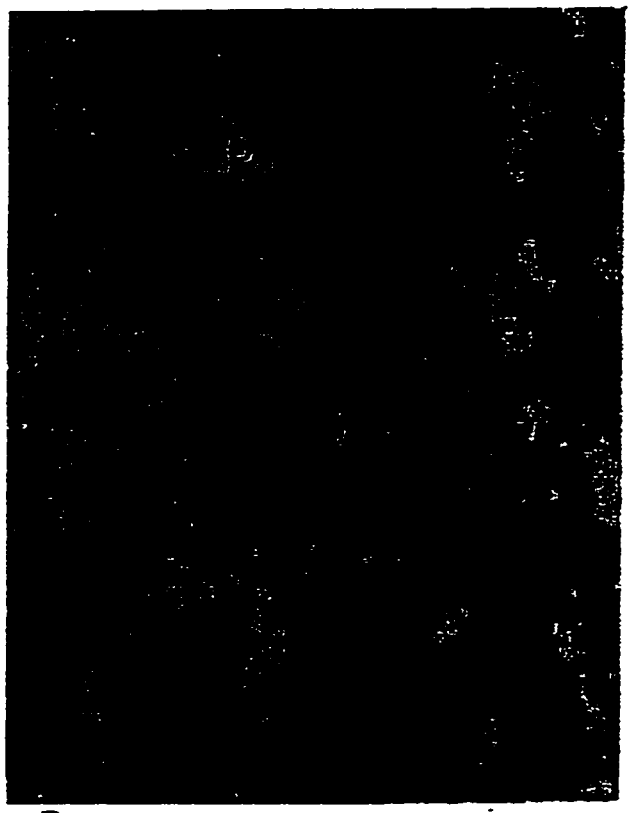

D

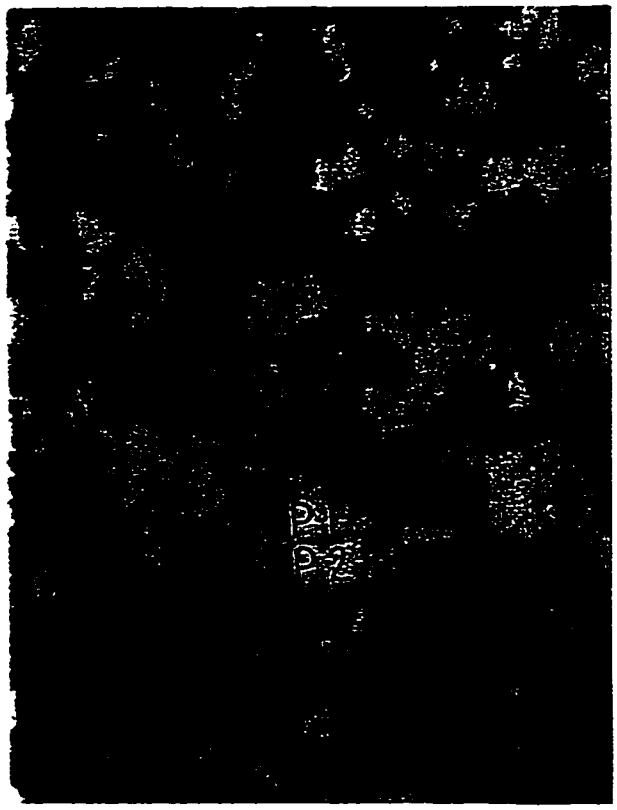

E

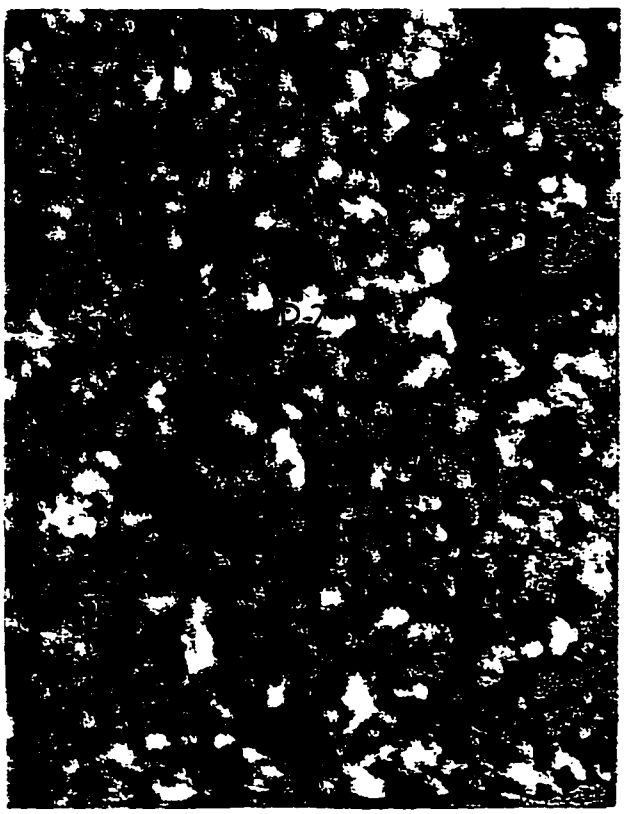

F

G

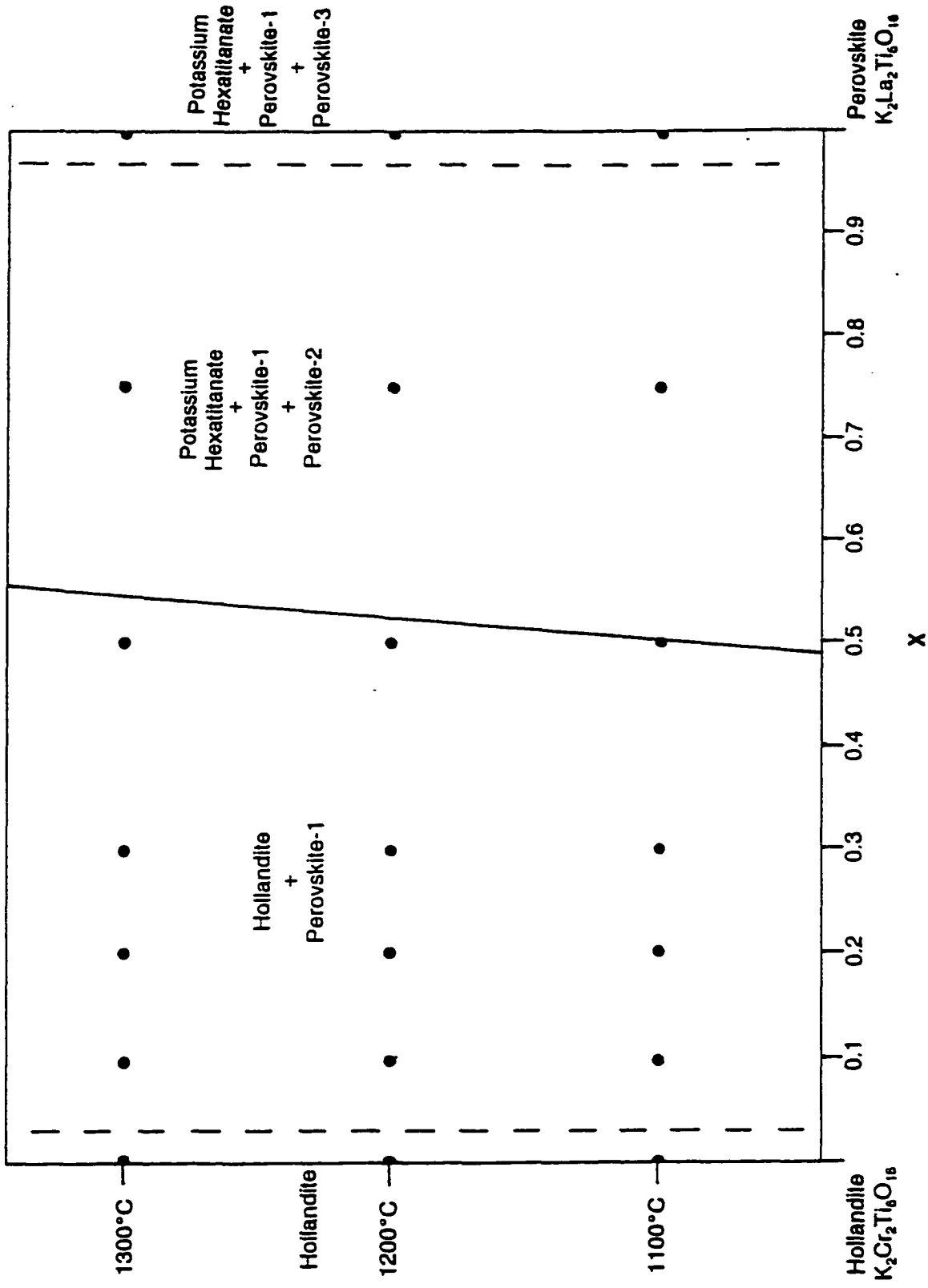

Figure 6-2 Pseudo-binary phase diagram for the system hollandite ($K_2Cr_2Ti_6O_{18}$)-perovskite ($K_2La_2Ti_6O_{18}$), throughout the temperatures 1100°C, 1200°C and 1300°C.

(Figure 6-1B,C and D), the hollandite phase is present in decreasing amounts until it becomes undetectable, by *XRD* and SEM/EDS, at x=0.75. Rutile is accessory to hollandite and is present in all experiments where the hollandite phase exists (at x=0.0-0.5). The occurrence of rutile may be a consequence of oxygen deficiencies or tunnel site vacancies in the hollandite structure (Dubeau and Edgar 1985). Kesson and White (1986a) propose that a bulk composition, like $K_2(Cr,La)_2Ti_6O_{16}$, may have undergone disproportionation to yield $K_{1.54}(Cr_{1.58}Ti_{6.42})_8O_{16}$ and rutile (TiO_2). Most likely the rutile may be a consequence of both. The rutile content appears to increase in abundance with increasing temperature, a feature consistent with hollandite decomposition. The second field, where La^{3+} is introduced, is defined by the appearance of a perovskite-type phase (perovskite-1), which occurs in increasing amounts as x increases to 0.5.

The second domain (x=0.5-1.0) consists of field three (x=0.5-0.95) and field four (x=0.95-1.0), and establishes a limit beyond which it is thermodynamically preferable to stabilize a new assemblage of phases. This assemblage consists of potassium hexatitanate and perovskite-1 in an approximately fixed modal ratio, together with the appearance of two other perovskites (perovskite-2 and perovskite-3). In field three (x=0.5-0.95) (Figure 6-1E), potassium hexatitanate coexists with perovskite-1 and a lanthanum chromium oxide phase (perovskite-2) which is also considered to be a perovskite-type compound. Field four (x=1.0) consists of potassium hexatitanate, perovskite-1 and another perovskite phase (perovskite-3) with a composition similar to $La_2Ti_2O_7$ (Figure 6-1F and G).

6.3 Hollandite

6.3.1 Structure and Space-Group

Compounds with the hollandite-type structure are of great importance due to their physical properties such as ferromagnetism and superionic conductivity (Zhang and Burnham 1994; Genkina *et al.* 1993). Hollandite (KMn_8O_{16}) was first described by Fermor in 1906 from the Kajlidongri manganese mine of central India (Mukherjee 1960).

Hollandites, which are also referred to as the cryptomelane group, have the ideal general formula $A_x B_y C_{(8-z)} O_{16}$, where *A* is a large alkali or alkaline-earth cation (K^+, or Ba^{2+}), *B* is a divalent and/or trivalent cation (V^{3+}, Cr^{3+}, Ce^{3+}, Fe^{3+}, Fe^{2+}, Mn^{4+}, Mn^{2+}, Mg^{2+}, or *REE*), and *C* is usually a transition-metal cation (Ti^{4+} or Nb^{5+}). In natural hollandites there is very limited substitution of *REE* (~2%) at the *B*-site. Ideally *x* and *y* lie between unity and 2, while *z* lies between 0 and 2. The structural formula is complicated by the common occurrence of non-stoichiometry and the presence of elements which occur in more than one valence state (Kesson and White 1986b). Generally, hollandite formulae are conventionally based upon 16 oxygens, which allows for the comparison of different hollandites on the same basis (Mitchell and Meyer 1989). Figure 6-3(a,b) is a depiction of the hollandite structure. The structure (Figure 6-3[a,b]) consists of *A*-site cations situated in 8-fold sites formed by double chains of $(BC)O_6$ octahedra connected through common vertices and edges to comprise a tunnelled framework (Genkina *et al.* 1993). These tunnels, which contain *A*-site cations, are often only partially occupied, a characteristic feature of many hollandites.

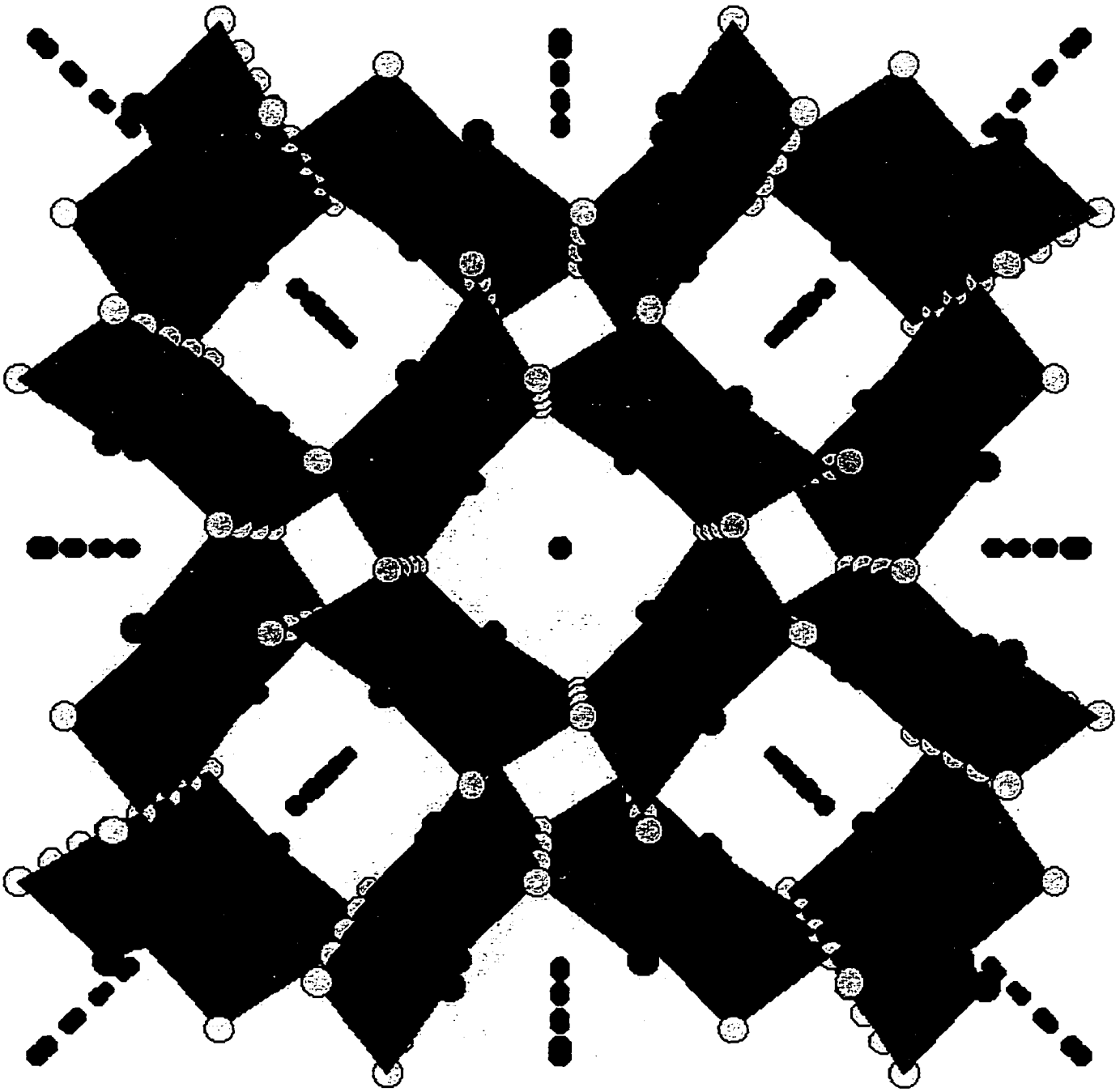

Figure 6-3a Representation of the hollandite structure as projected down the *c*-axis (produced using Atoms for Windows, version 3.2; Dowty 1995). Potassium cations are depicted by blue circles. The $(Ti,Cr)O_6$ octahedra are depicted in green. The oxygens (O_1^A, O_1^B, O_2^A, and O_2^B) are arbitrarily distinguished by subscripts 1 and 2 and are represented by green and yellow circles, respectively.

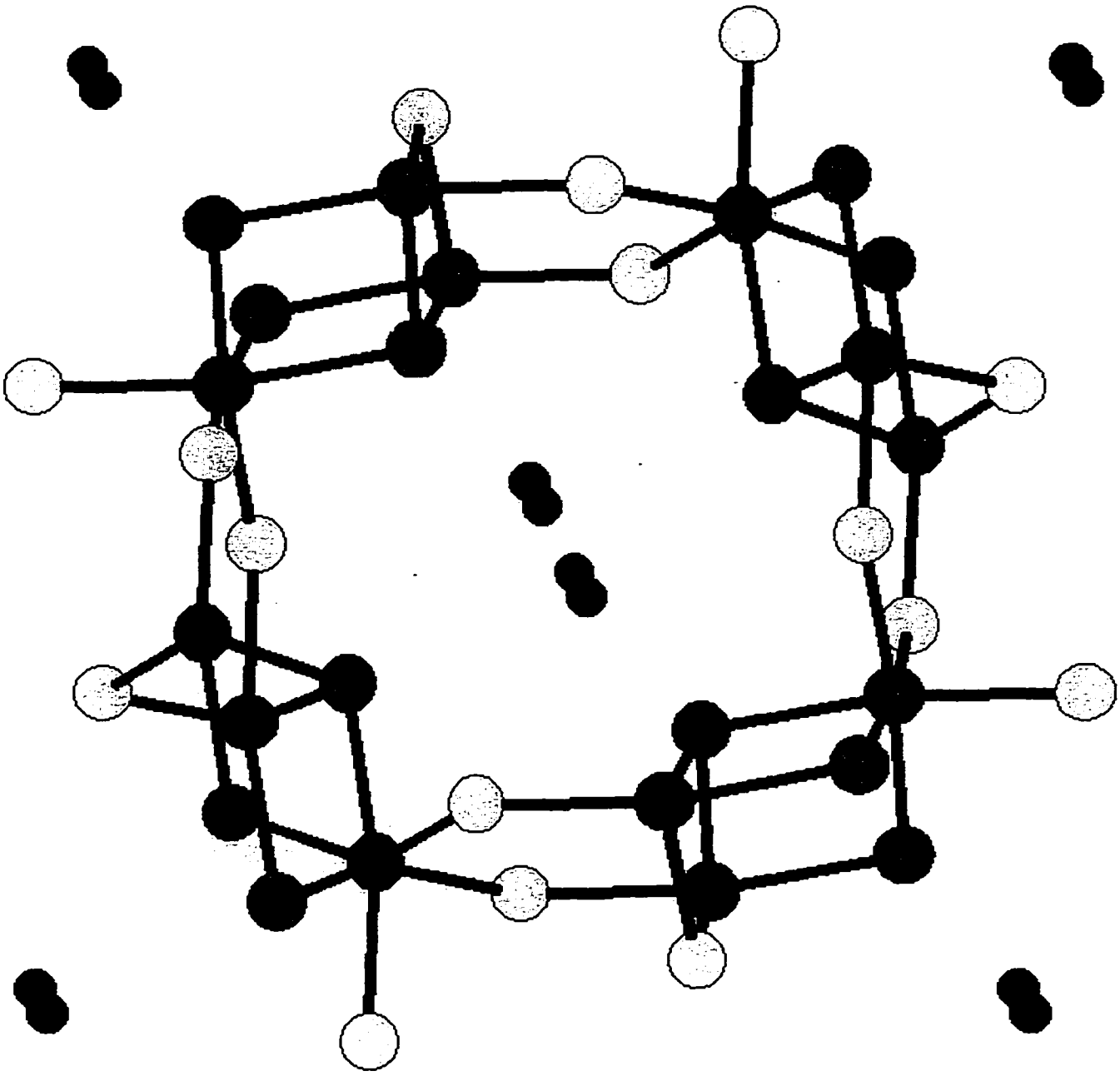

Figure 6-3b Representation of the hollandite structure as projected down the *c*-axis (produced using Atoms for Windows, version 3.2; Dowty 1995). Potassium cations are depicted by blue circles. Chromium and Titanium cations are depicted by pink circles. The oxygens (O_1^A, O_1^B, O_2^A, and O_2^B) are arbitrarily distinguished by subscripts 1 and 2 and are represented by green and yellow circles, respectively.

The ideal hollandite structure is tetragonal (space group *I4/m*), but occasionally, orthorhombic or monoclinic structures occur (Zhang and Burnham 1994). The symmetry of hollandite-type compounds depends on the ratio of the average ionic radius of the octahedral cations to that of the tunnel cations (Zhang and Burnham 1994; Post *et al.* 1982). Zhang and Burham (1994) have derived empirical relationships suggesting that if $r_A > \sqrt{2}\,(r_O + r_B) - r_O$ (where r_A is the average atomic radius of the *A* cation(s), r_B is the average atomic radius of the *B* cation(s) and r_O is the atomic radius of Oxygen), the compound cannot be monoclinic, whereas if $r_A < \sqrt{2}\,(r_O + r_B) - r_O - 0.15$, it cannot be tetragonal. These factors are important, since an increase in the size of the *B* cations will result in distortion of the *B*-O octahedra, resulting in a lowering of the symmetry (Post *et al.* 1982). Post *et al.* (1982) suggest that a monoclinic structure would result when the *A* cation is small, as this initiates twisting of the columns of *B*-O octahedra in order to decrease the volume of the tunnels.

The unit cell size of hollandites is largely dependent on the size of the octahedra, and values of **a** and **c** can be approximated through a comparison of the pseudo-cubic unit cell to the calculated average **a**/**c** ratio (~3.33) for hollandite (Ringwood *et al.* 1967). This ratio reflects the tendency of the octahedra to be elongated parallel to **c** and shortened perpendicular to **c** due to strong cation-cation repulsions across the shared edges in the chains. The unit cell parameter **a** is greater than **c** due to the configuration of the octahedra (Figure 6-3[a,b]). Zhang and Burnham (1994) derived equations based on what they consider to be the main factors determining the unit cell size of any hollandite, which are established by composition alone. The factors are primarily the average *B*-O bond

distance, the charge of the *B* cation, the excess size of the tunnel cation (*A*) relative to the octahedral framework, and the excess size of the *B* cation relative to the octahedral cavity. Zhang and Burnham (1994), calculated the unit cell parameters for one of the proposed end-members, $K_2Ti_6Cr_2O_{16}$ (synthesised in this investigation), to be **a**=10.14 Å and **c**=2.97 Å, and compare these to observed values of **a**=10.125 Å and **c**=2.955 Å. This procedure was applied to the calculation of unit cell parameters for the average composition of the hollandites synthesized in this work [**a**=10.137 Å and **c**= 2.993 Å, ionic radii taken from Shannon and Prewitt (1969)]. Atomic coordinates (Zhang and Burnham 1994), and other crystallographic parameters for an ideal hollandite are given in Table 6-2.

6.3.2 Compositional Determinations

SEM/EDS analysis (Table 6-1) was performed to determine the composition and the cation occupancy of the hollandites, with a structural formula based on 16 oxygen atoms. At x=0.0, the hollandite phase has a composition of approximately $K_{1.54}(Cr_{1.58}Ti_{6.42})_{8.00}O_{16}$. The hollandite compounds exhibit the following approximate formulae; at high temperature (1300°C and 1200°C), $K_{1.50}(Cr_{1.42}Ti_{6.55})_{8.97}O_{16}$, and at 1100°C, $K_{1.64}(Cr_{1.43}Ti_{6.47})_{7.90}O_{16}$ (Table 6-1). The composition of the hollandite phase varies slightly with changing bulk composition (x) and temperature. With increasing x, the number of K^+ cations remains approximately constant, but is accompanied by a slight increase in Ti cations at the *B*-site, a decrease in Cr cations at the *B*-site, and an overall slight decrease in the occupancy of the *B*-site. The decrease in the number of Cr cations at the *B*-site may be related to the

Table 6-2 Table of predicted crystallographic properties of hollandite. Data taken from Zhang and Burnham (1994), Post and Burnham (1986), and International Tables for *X*-Ray Crystallography (1965).

End-member	Hollandite ($K_2Cr_2Ti_6O_{16}$)- Potassium Redledgeite				
Coordination #	8	6	6	2	2
Occupant	K	Cr	Ti	O1	O2
Point Symmetry	*4/m*	*m*	*m*	*m*	*m*
Wyckoff Notation	*2a*	*8h*	*8h*	*8h*	*8h*
Fractional Coordinates:					
x	0	0.3434	0.3434	0.1487	0.5380
y	0	0.1757	0.1757	0.1868	0.1645
z	0	0	0	0	0
Formula Weight	725.5790 g/mole				
Z	1				
Crystal Symmetry	Tetragonal				
Point-Group	*4/m*				
Space-Group	*I4/m* (#87)				
Limiting Reflections (General Only)	*hkl: h+k+l=2n* *hk0: (h+k=2n)* *00l: (l=2n)*				
a (Å)	10.14 Å				
c (Å)	2.97 Å				
volume (Å^3)	305.37 Å^3				

decreasing overall concentration of Cr (increasing *x*, implies decreasing Cr). With increasing temperature all hollandites exhibit a decreased content of potassium, due possibly to increased K^+ loss by volatilization or disproportionation. Titanium content also increases slightly while chromium concentrations remain essentially constant; possibly due to a more efficient breakdown of TiO_2 at higher temperatures.

The compositional data (Table 6-1) indicate an *A*-site occupancy of approximately 75-82%. The *A*-site occupancy indicates that the tunnel sites are only partially filled. *A*-site deficiencies are characteristic of synthetic hollandites which are always non-stoichiometric at low pressure. Tamada *et al.* (1996) conclude that only the high pressure synthesis of hollandite results in full *A*-site occupancy, due to the pressure effectively forcing cations into the tunnels.

6.3.3 Powder *X*-Ray Diffractometry

XRD analysis was undertaken using matched *d*-values of the most intense peaks with those of minerals from the ICDD database. For all temperatures where x=0, the pseudo-binary system consisted of a single hollandite-type phase with a structure similar to: redledgeite ($BaTi_6Cr_2O_{16}$, space-group $I4_1/a$, a=14.300Å, c=5.894Å; Scott and Peatfield 1986); priderite ($(K_{1.2}Ba_{0.4})_{1.6}(Ti_{6.7}Mg_{0.2}Fe_{1.1})_8O_{16}$, space-group I4/m, a=10.140(1)Å, c=2.965(1)Å; Sinclair and McLaughlin 1982; Post *et al.* 1982); and potassium titanium oxide (KTi_8O_{16}, space-group *I4/m*, a=10.1897Å, c=2.9640Å; Bayer and Hoffman 1966).

Of the known minerals, redledgeite has an *XRD* pattern most similar to that of synthetic chromium hollandite (Table 6-3). To identify the hollandite phases throughout

Table 6-3a *XRD* pattern reflections for hollandite (x=0.0) and redledgeite.

1300°C			1200°C			1100°C			Redledgeite		
d-obs.	I-obs.		*d*-obs.	I-obs.		*d*-obs.	I-obs.		*h k l*	*d*-obs.	I-obs.
7.164	41		7.153	37		7.156	35		*1 1 0*	7.161	56
5.066	53		5.061	55		5.061	49		*0 2 0*	5.062	66
3.579	13		3.575	13		3.575	11		*2 2 0*	3.577	12
3.201	100		3.197	100		3.196	100		*1 3 0*	3.198	100
2.531	12		2.529	15		2.529	12		*0 4 0*	2.532	13
2.475	49		2.475	45		2.476	46		*1 2 1*	2.476	46
2.385	2		2.385	4		2.386	2		*3 3 0*	2.385	3
2.264	10		2.262	12		2.262	10		*2 4 0*	2.263	10
2.224	27		2.224	26		2.224	24		*0 3 1*	2.225	23
2.033	3		2.035	2		2.037	2		*3 2 1*	2.037	3
1.987	11		1.985	8		1.984	6		*5 1 0*	1.987	6
1.890	30		1.889	32		1.889	30		*4 1 1*	1.890	26
1.791	2		1.789	2		1.787	2		*4 4 0*	1.787	1
1.738	1		1.736	2		1.736	2		*3 5 0*	1.734	1
1.689	21		1.687	18		1.687	15		*0 6 0*	1.685	14
1.672	6		1.671	4		1.671	5		*0 5 1*	1.670	4
1.586	20		1.585	28		1.587	27		*2 5 1*	1.586	24
			1.585	15					*2 5 1*		
									0 0 2	1.479	6
1.394	26		1.393	18		1.393	18		*5 4 1*	1.394	14
			1.393	10		1.392	9		*5 4 1*		

Table 6-3b *XRD* pattern for hollandite (x=0.1 and x=0.2 respectively), reflections indexed against redledgeite and perovskite reflections (see Table 6-3a and Table 6-3e for associated *d*-values and intensities).

1300°C		1200°C		1100°C		1300°C		1200°C		1100°C		Redledgeite	$La_{2/3}TiO_{2.993}$
d-obs.	I-obs.	*d*-obs.	I-obs.	*d*-obs.	I-obs.	*d*-obs.	I-obs.	*d*-obs.	I-obs.	*d*-obs.	I-obs.	*h k l*	*h k l*
7.806	1									7.688	5		*0 0 1*
7.158	47	7.161	39	7.158	36	7.179	37	7.176	41	7.153	36	*1 1 0*	
5.061	59	5.062	56	5.058	51	5.068	53	5.068	61	5.053	49	*0 2 0*	
		3.889	1			3.886	2	3.901	2	3.883	3		*0 0 2*
3.577	10	3.577	11	3.575	11	3.579	10	3.579	13	3.572	11	*2 2 0*	
3.468	2					3.476	3						*0 1 1*
3.198	100	3.198	100	3.197	100	3.201	100	3.201	100	3.195	100	*1 3 0*	
2.744	21	2.751	17	2.758	14	2.750	41	2.759	41	2.759	28		*1 0 2*
2.530	15	2.530	15	2.528	13	2.533	17	2.532	16	2.528	13	*0 4 0*	
2.475	46	2.476	58	2.477	51	2.477	46	2.477	54	2.475	43	*1 2 1*	
2.383	2	2.385	3	2.384	3	2.386	2	2.386	4	2.384	3	*3 3 0*	
2.263	12	2.262	9	2.261	11	2.265	11	2.264	12	2.261	13	*2 4 0*	
2.242	5					2.245	10						*1 1 2*
2.224	32	2.226	32	2.225	31	2.225	25	2.225	27	2.223	30	*0 3 1*	
2.037	3	2.038	2	2.038	2	2.038	4	2.038	3	2.035	3	*3 2 1*	
1.987	10	1.986	9	1.985	8	1.987	10	1.987	9	1.984	8	*5 1 0*	
1.942	5	1.947	6	1.953	4	1.944	11	1.952	13	1.946	7		*0 2 0*
1.890	35	1.891	34	1.890	35	1.891	40	1.891	37	1.889	33	*4 1 1*	*0 2 1*
1.791	2	1.791	1	1.789	2	1.792	2	1.792	2	1.789	2	*4 4 0*	
1.737	3	1.737	2	1.735	2	1.739	2	1.738	3	1.736	3	*3 5 0*	
1.687	20	1.687	20	1.686	19	1.690	18	1.689	24	1.686	20	*0 6 0*	*1 2 0*
1.670	5	1.670	5	1.672	4	1.673	5	1.672	6	1.669	5	*0 5 1*	
1.586	46	1.586	34	1.586	38	1.587	56	1.587	40	1.586	35	*2 5 1*	
		1.586	20	1.585	16			1.586	19	1.585	19	*2 5 1*	*1 2 2*
1.478	12											*0 0 2*	
1.394	31	1.394	25	1.394	25	1.395	26	1.394	28	1.393	21	*5 4 1*	
1.394	15	1.393	13	1.393	12			1.394	14	1.393	10	*5 4 1*	

Table 6-3c *XRD* pattern for hollandite (x=0.3 and x=0.5 respectively), reflections indexed against redledgeite and perovskite (Abe and Uchino 1974) reflections (see Table 6-3a and Table 6-3e for associated d-values and intensities). Unindexed reflections may represent low intensity reflections that were not acknowledged for the standards.

1300°C		1200°C		1100°C		1300°C		1200°C		1100°C		Redledgeite	$La_{2/3}TiO_{2.993}$
d-obs.	I-obs.	d-obs.	I-obs.	d-obs.	I-obs.	d-obs.	I-obs.	d-obs.	I-obs.	d-obs.	I-obs.	*h k l*	*h k l*
7.844	5			7.688	12			7.695	8	7.695	32		*0 0 1*
7.176	48	7.170	43	7.161	42	7.176	13	7.179	22	7.158	26	*1 1 0*	
				6.417	8			6.401	4	6.403	23		
5.088	64	5.065	54	5.071	53	5.076	22	5.074	36	5.065	37	*0 2 0*	
3.891	3	3.899	4	3.894	8	3.905	4	3.892	7	3.894	18		*0 0 2*
										3.771	9		
3.580	12	3.578	12	3.581	12	3.584	4	3.582	9	3.579	7	*2 2 0*	
3.249	15					3.252	22						
3.202	100	3.200	100	3.201	100	3.205	59	3.204	62	3.200	78	*1 3 0*	
		3.051	1	3.056	10			3.051	7	3.052	27		
				2.988	12			2.984	7	2.984	28		
				2.968	8			2.965	6	2.963	24		
				2.910	2					2.908	13		
2.753	80	2.760	68	2.764	49	2.757	100	2.757	100	2.760	100		*1 0 2*
		2.702	2	2.705	7			2.701	4	2.701	22		
				2.650	1					2.649	8		
2.533	13	2.531	13	2.532	15	2.534	7	2.533	9	2.530	8	*0 4 0*	
2.477	73	2.477	56	2.479	60	2.478	32	2.477	31	2.476	40	*1 2 1*	
2.388	4	2.386	3	2.387	4	2.390	2	2.392	1	2.386	2	*3 3 0*	
						2.302	1						
2.265	16	2.265	15	2.264	12	2.267	8	2.266	8				
2.247	18	2.253	13			2.251	21	2.250	17	2.254	19	*2 4 0*	
2.226	45	2.225	34	2.227	33	2.226	16	2.226	20	2.225	18	*0 3 1*	
				2.103	7			2.100	5	2.099	17		
				2.081	7			2.078	3	2.080	19		
1.988	13	1.987	9	1.987	9	1.989	6	1.987	3	1.987	7	*5 1 0*	
				1.957	11								
1.945	24	1.953	23	1.947	15	1.950	43	1.951	33	1.946	28		*0 2 0*
				1.902	8			1.900	6	1.901	19		
1.891	50	1.891	38	1.891	36	1.892	21	1.890	16	1.888	16	*4 1 1*	*0 2 1*
1.688	29	1.689	21	1.689	19	1.689	26	1.690	13	1.688	15	*0 6 0*	*2 1 1*
1.687	14												
1.671	7	1.672	6	1.673	5	1.672	3	1.672	4	1.666	6	*0 5 1*	
		1.595	19					1.593	27	1.596	23		
1.588	57	1.587	41	1.587	47	1.589	34	1.588	41	1.587	45	*2 5 1*	
1.587	28	1.586	18									*2 5 1*	*1 2 2*
1.395	34	1.394	29	1.394	25	1.395	12	1.395	16	1.394	16	*5 4 1*	
		1.394	14	1.394	13	1.395	8					*5 4 1*	
1.376	11	1.380	10			1.378	17	1.378	13	1.381	10		
1.376	7	1.380	6			1.377	9	1.377	8				
						1.232	13						
						1.232	8						
						1.041	17						

Table 6-3d The *XRD* pattern at x=0.75, reflections indexed against jeppeite (Pryce *et al.* 1984) and perovskite (Abe and Uchino 1974; Khattak and Cox 1977) reflections. Unindexed reflections may represent low intensity reflections that were not acknowledged for the standards.

1300°C		1200°C		1100°C		$(K,Ba)_2Ti_6O_{13}$		$La_{2/3}TiO_{2.993}$		$LaCrO_3$		
d-obs.	I-obs.	*d*-obs.	I-obs.	*d*-obs.	I-obs.	*h k l*	*d*-obs.	*h k l*	*d*-obs.	*h k l*	*d*-obs.	I-obs.
7.705	24	7.705	10	7.695	32	*2 0 0*	7.640	*0 0 1*	7.800			
		7.179	7	7.158	26							
6.408	15	6.412	6	6.403	23	*-2 0 1*	6.370					
5.071	3	5.072	8	5.065	37							
4.496	3	4.505	1	4.494	4	*0 0 2*	4.500					
3.894	11	3.900	6	3.894	18			*0 0 2*	3.890	*1 1 0*	3.880	18
3.777	2			3.771	3	*-4 0 1*	3.730					
3.690	8	3.689	5	3.688	9	*1 1 0*	3.710					
				3.579	7							
3.204	6	3.204	17	3.200	78	*-4 0 2*	3.170					
3.053	22	3.052	9	3.052	27	*3 1 0*	3.070					
2.985	21	2.985	9	2.984	28	*-3 1 1*	2.990					
2.965	17	2.966	8	2.963	24	*-2 0 3*	2.961					
2.800	8	2.799	4	2.794	13	*1 1 2*	2.812					
2.757	100	2.758	100	2.760	100			*1 0 2*	2.744	*1 1 2*	2.745	100
2.702	13	2.702	6	2.701	22	*4 0 2*	2.702					
2.654	3	2.653	1	2.649	4	*2 0 3*	2.649					
2.583	6	2.584	3	2.582	8	*-6 0 1*	2.557					
		2.534	2	2.530	8							
2.477	2	2.477	5	2.476	40							
2.252	20	2.251	16	2.254	19	*5 1 1*	2.236	*1 1 2*	2.241	*0 2 2*	2.246	14
		2.226	2	2.225	18							
2.100	10	2.100	6	2.099	17	*-4 0 4*	2.091					
2.081	13	2.081	5	2.080	19	*6 0 2*	2.074					
				1.987	7							
1.951	27	1.952	31	1.946	28	*-1 1 4*	1.958	*0 2 0*	1.941	*0 0 4*	1.940	30
1.901	14	1.901	6	1.901	19	*-7 1 1*	1.909					
1.885	3			1.888	16	*1 1 4*	1.889	*0 2 1*	1.881			
1.758	4	1.757	2			*5 1 3*	1.762					
1.740	3	1.742	2	1.739	4					*1 3 0*	1.736	6
1.689	2	1.689	3	1.688	15							
1.666	5	1.667	2	1.666	6	*7 1 2*	1.665					
1.602	6											
1.593	26	1.592	28	1.596	23	*-6 0 5*	1.594					
1.588	19	1.587	21	1.587	45			*1 2 2*	1.584	*1 3 2*	1.589	20
1.379	10	1.378	14			*1 1 6*	1.373					
1.375	9	1.378	9			*1 1 6*						
				1.394	16							
				1.381	10					*2 2 4*	1.372	12
		1.233	10			*2 0 7*	1.237					
		1.233	5			*2 0 7*						

Table 6-3e The *XRD* pattern at x=1.0, indexed against jeppeite (Pryce *et al.* 1984) and perovskites (Abe and Uchino 1974; Preuss and Gruehn 1994) standards. Unindexed reflections may represent low intensity reflections that were not acknowledged for the standards.

1300°C		1200°C		1100°C		$(K,Ba)_2Ti_6O_{13}$			$La_{2/3}TiO_{2.993}$			$La_2Ti_2O_7$		
d-obs.	I-obs.	*d*-obs.	I-obs.	*d*-obs.	I-obs.	*h k l*	*d*-obs.	I-obs.	*h k l*	*d*-obs.	I-obs.	*h k l*	*d*-obs.	I-obs.
7.662	13	7.688	8	7.692	12	*2 0 0*	7.640	30	*0 0 1*	7.800	18			
6.380	6	6.401	5	6.408	8	*-2 0 1*	6.370	30				*2 0 0*	6.426	10
				4.489	2	*0 0 2*	4.500	40						
				4.200	9							*-2 1 0*	4.201	40
3.889	4	3.895	5	3.905	4				*0 0 2*	3.890	6			
3.770	2					*-4 0 1*	3.730	23						
3.682	2	3.685	3	3.685	4	*1 1 0*	3.710	10						
				3.392	1							*3 1 0*	3.392	11
				3.218	10							*4 0 0*	3.217	50
				3.169	5	*-4 0 2*	3.170	20				*-1 1 2*	3.172	30
				3.113	3							*2 0 2*	3.112	13
3.046	7	3.051	8	3.050	10	*3 1 0*	3.070	100				*-2 1 2*	2.995	100
2.975	6	2.983	8	2.991	20	*-3 1 1*	2.990	100						
2.960	7	2.963	6	2.963	10	*-2 0 3*	2.961	40						
				2.910	2									
2.794	3					*1 1 2*	2.812	100				*4 1 0*	2.782	50
2.753	100	2.757	100	2.761	100				*1 0 2*	2.744	100	*0 2 0*	2.774	50
2.697	5	2.700	5	2.701	8	*4 0 2*	2.702	40						
				2.677	3							*3 0 2*	2.677	25
		2.647	1	2.649	2	*2 0 3*	2.649	30						
2.576	3	2.567	2	2.583	4	*-6 0 1*	2.557	20				*5 0 0*	2.573	3
2.247	21	2.250	19	2.254	24	*5 1 1*	2.236	10	*1 1 2*	2.241	25	*-1 2 2*	2.253	20
				2.132	2							*-5 1 2*	2.131	17
2.099	5	2.100	4	2.101	9	*-4 0 4*	2.091	60				*-4 2 0*	2.100	25
2.077	8	2.079	5	2.081	6	*6 0 2*	2.074	60				*-3 2 2*	2.071	17
				2.001	1							*6 1 0*	2.000	8
1.948	40	1.952	40	1.953	33	*-1 1 4*	1.958	20	*0 2 0*	1.941	45	*-1 0 4*	1.954	30
				1.924	1	*0 2 0*	1.919	80				*-4 2 2*	1.926	20
1.898	3	1.900	4	1.900	6	*-7 1 1*	1.909	30						
				1.886	4	*1 1 4*	1.889	20	*0 2 1*	1.881	7	*5 2 0*	1.886	30
				1.772	1							*1 1 4*	1.771	15
				1.757	3	*5 1 3*	1.762	20				*-7 0 2*	1.766	11
1.743	3	1.743	2	1.746	2							*7 1 0*	1.744	4
1.665	2			1.666	4	*7 1 2*	1.665	20				*3 0 4*	1.669	20
				1.640	1	*-4 2 2*	1.639	10				*1 3 2*	1.640	11
		1.601	3									*4 3 0*	1.602	13
1.590	33	1.592	35	1.596	25	*-6 0 5*	1.594	10	*1 2 2*	1.584	45			
1.589	17	1.591	17											
1.377	21	1.380	18	1.382	13	*1 1 6*	1.373	20						
		1.380	10											
1.232	12	1.230	12			*2 0 7*	1.237	30						
		1.230	5											
1.041	14	1.042	13											
1.041	7	1.042	7											

the pseudo-binary system, it was necessary to index all reflections up to 60° (2θ) plus all subsequent reflections with greater than 10% relative intensity (Table 6-3a -6-3c). These reflections were then indexed primarily against a synthetic redledgeite standard ($K_2Cr_2Ti_6O_{16}$ synthesized by A.D. Edgar at the University of Western Ontario [at 1400°C and 1atm. in a vertical Pt-furnace]. These data support the findings of the SEM/EDS analysis (Table 6-1). The tables include additional unindexed reflections arising from the presence of the following perovskites $La_{2/3}TiO_{2.993}$ ($0.0<x\geq0.5$) and $La_2Ti_2O_7$, $La_{2/3}TiO_{2.993}$ and TiO_2 ($x>0.5$)

6.3.3.1 Least-Squares Refinement of Cell Parameters For Hollandite-Type Phases

The diffraction patterns of hollandite are consistent with *4/m* Laue symmetry with all reflections having (*hkl*): $h+k+l=2n$, (*hk0*): $h+k=2n$, (*00l*): $l=2n$, (*h00*): $h=2n$, and (*h0l*): $h+l=2n$ extinct, suggesting they belong to the space group *I4/m*. The refinement of the hollandite unit cell parameters appear in Table 6-4.

Figure 6-4 gives plots of bulk composition (x=0.0-0.5) *versus* hollandite unit cell parameters; **a** (Å), **c** (Å) and volume (Å^3). Figure 6-4 shows obvious trends: with increasing temperature (for each x), there is an increase in the **a** unit cell parameter and subsequently in volume, and a slight decrease in **c**; and with increasing composition, there are very slight increases in **a** and slight decreases in **c**, with an overall increase in volume. Any volume changes are obviously more strongly affected by changes in **a**, as it is the

Table 6-4 Least-squares refinement of all hollandite cell parameters for the hollandite-perovskite pseudo-binary system. Errors refer to mathematical "fit" errors as determined by the least-squares refinement program. For *XRD* precision and accuracy see chapter 2.

Comp. (x)	Temp. (°C)	Reflections	a (Å)	Error (±)	c (Å)	Error (±)	vol. (Å^3)	Error (±)
0.0	1300	79	10.1227	0.0005	2.9562	0.0002	302.92	0.03
0.0	1200	68	10.1133	0.0006	2.9579	0.0002	302.53	0.03
0.0	1100	65	10.1095	0.0008	2.9591	0.0003	302.43	0.04
0.1	1300	106	10.1219	0.0004	2.9562	0.0002	302.87	0.02
0.1	1200	98	10.1189	0.0005	2.9576	0.0002	302.84	0.03
0.1	1100	86	10.1137	0.0005	2.9588	0.0002	302.65	0.03
0.2	1300	97	10.1267	0.0005	2.9565	0.0002	303.19	0.03
0.2	1200	96	10.1226	0.0005	2.9572	0.0002	303.01	0.03
0.2	1100	90	10.1137	0.0006	2.9577	0.0003	302.54	0.04
0.3	1300	104	10.1267	0.0007	2.9568	0.0003	303.22	0.04
0.3	1200	100	10.1226	0.0005	2.9571	0.0002	303.00	0.03
0.3	1100	104	10.1197	0.0010	2.9589	0.0004	303.01	0.06
0.5	1300	70	10.1304	0.0010	2.9576	0.0005	303.53	0.06
0.5	1200	82	10.1285	0.0008	2.9572	0.0004	303.37	0.05
0.5	1100	79	10.1194	0.0014	2.9578	0.0007	302.88	0.08

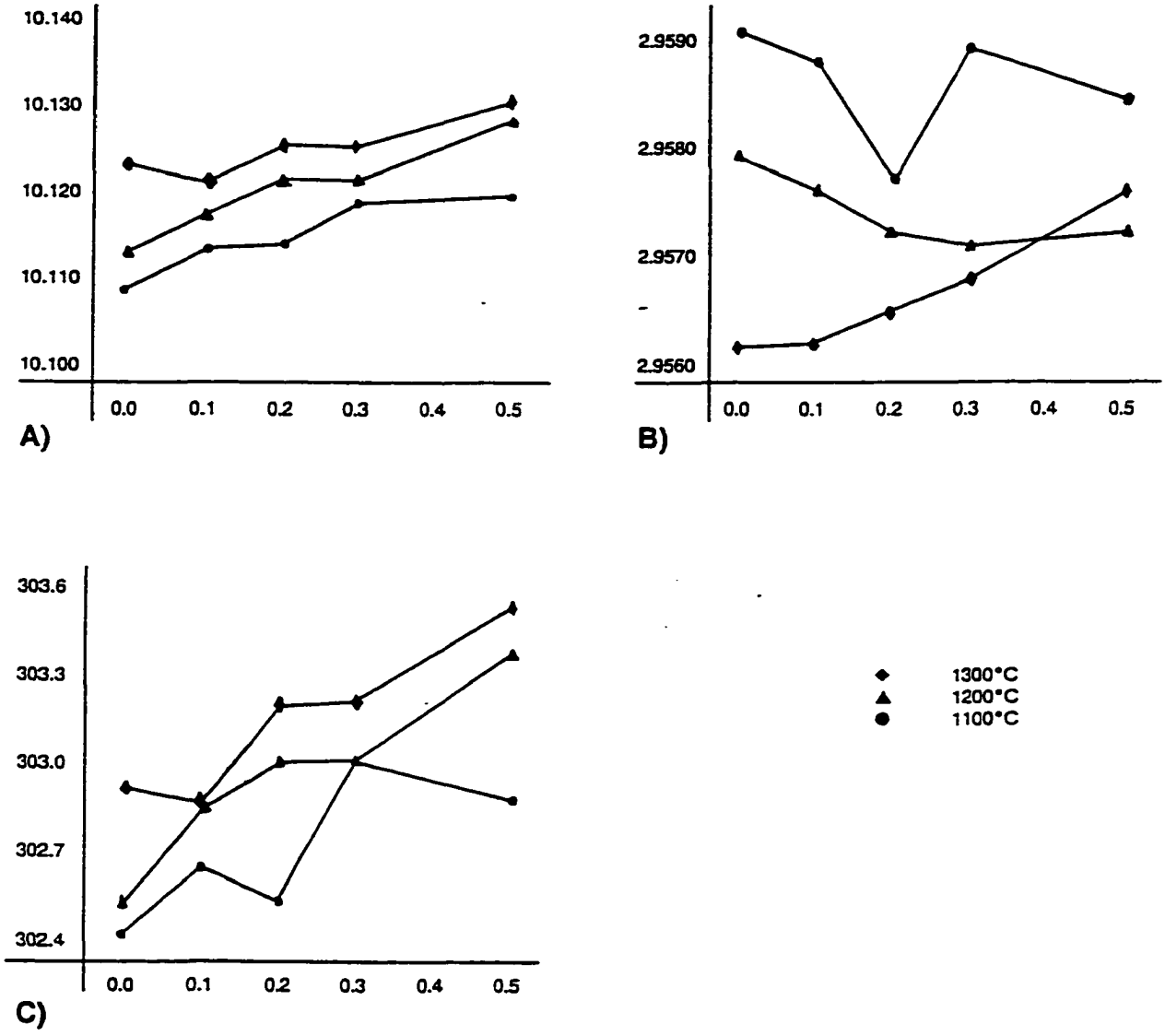

Figure 6-4 Plots of composition (*x*) *versus* unit-cell parameters of hollandite. Error bars have been excluded as the relative errors are equivalent to the area covered by each data point on the graph.

A) Composition (*x*) *versus* unit-cell parameter **a** (Å).
B) Composition (*x*) *versus* unit-cell parameter **c** (Å).
C) Composition (*x*) *versus* volume (Å^3).

larger cell dimension. The hollandites synthesised at 1300°C (with **c** increasing) and at 1100°C and x=0.2 (dip in the plot) are obvious exceptions to the normal trend. These deviations may be due to an ordering mechanism at the *B*-site.

The compositional trends indicate that with an increase in temperature, there is a decrease in the *A*-site (K^+) occupancy, an increase of Ti^{4+} occupancy at the *B*-site, as well as in the occupation of the *B*-site as a whole (which may be a reflection of Ti^{4+} changes in valence). Correlations with temperature and between composition and unit cell parameters, suggest that as the *A*-site (K^+) occupation increases, there is a subsequent increase in **c**; and as the Ti^{4+} occupation of the *B*-site increases, there is a subsequent noticeable increase in **a**.

6.3.4 Rietveld Refinement of Hollandite

Although least-squares refinement of the hollandite phases proved accurate, a more comprehensive structure examination was obtained with Rietveld refinement. All patterns of the essentially pure hollandite compound at x=0.0 and 1300°C, 1200°C, and 1100°C were refined using the starting parameters from Table 6-2. The relative sensitivity of the isotropic temperature factor for K^+, at the atomic coordinates selected, requires that it be set to a value of 1.33. This is most likely a feature of the partial occupancy/disordering that occurs in the *A*-site. Table 6-5 contains the Rietveld atomic parameters, unit cell dimensions and the selected criteria-of-fit. Discrepancies in the criteria-of-fit are directly

Table 6-5 Atomic coordinates, positional and thermal parameters, unit-cell dimensions and criteria of fit as determined by the Rietveld refinement program (DBWS-9411), for the hollandite compound (x=0.00) at the three temperatures. Data for $K_2Cr_8O_{16}$ taken from Tamada *et al.* 1996.

Parameters		$K_2Cr_8O_{16}$	At 1300°C	At 1200°C	At 1100°C
	Space-Group	*I4/M*	*I4/M*	*I4/M*	*I4/M*
K^+	*x*	0	0	0	0
	y	0	0	0	0
	z	1/2	1/2	1/2	1/2
	U(Å^2)	1.33	1.33	1.33	1.33
	N	0.01563	0.01563	0.01563	0.01563
Cr^{3+}	*x*	0.34813	0.35004	0.35022	0.34996
	y	0.16496	0.16679	0.16693	0.16708
	z	0	0	0	0
	U(Å^2)	0.34	0.63415	0.66647	0.65521
	N	0.06250	0.03240	0.02979	0.02325
Ti^{4+}	*x*		0.35004	0.35022	0.34996
	y		0.16679	0.16693	0.16708
	z		0	0	0
	U(Å^2)		0.63415	0.66647	0.65521
	N		0.03010	0.03271	0.03925
O^{-2} (1)	*x*	0.1536	0.15780	0.15588	0.15615
	y	0.2013	0.20663	0.20615	0.20714
	z	0	0	0	0
	U(Å^2)	0.44	-0.49869	-0.69804	-0.63005
	N	0.06250	0.06250	0.06250	0.06250
O^{-2} (2)	*x*	0.5398	0.53961	0.53900	0.53891
	y	0.1633	0.16661	0.16746	0.16673
	z	0	0	0	0
	U(Å^2)	0.48	0.55736	0.56136	0.63005
	N	0.06250	0.06250	0.06250	0.06250
	Z	1	1	1	1
	a (Å)	9.7627	10.1220	10.1114	10.1082
	b (Å)	9.7627	10.1220	10.1114	10.1082
	c (Å)	2.9347	2.9560	2.9579	2.9589
	Volume (Å^3)	279.70	302.86	302.42	302.33
	S (R-wp/R-exp)		1.69	1.66	1.70
	R-Bragg		12.89	11.73	12.67

related to those factors as described in Section 4.6, especially to the overall low intensity reflections of the powder patterns, and most importantly, possibly due to the existence of a disordered structure. These discrepancies are manifested in high *R-Bragg* (~12.5 as compared to expected values of approximately 5) and low Durbin-Watson statistics (not given, but equals about 0.5, as compared to the ideal value of 2.00). These low intensities illustrate the principal reason why the values of *S* (ideal if below 1.5) appear high (~1.68), although they are quite acceptable.

Atomic coordinates and unit cell dimensions (Table 6-4) are similar to the starting parameters and to those of $K_2Cr_8O_{16}$ as determined by Tamada *et al.* (1996). The unit cell dimensions of the hollandites prove consistent with the least-squares refinement, especially for the unit cell parameter **c**. Interatomic bond attributes (lengths and angles) as determined by WYRIET, appear in Table 6-6. These bond attributes correlate well with those of $K_2Cr_8O_{16}$ (Tamada *et al.* 1996).

6.3.5 Structure Description

The polyhedral framework (Figure 6-3[a,b]) of hollandite, consists of K^+ cations situated in 8-fold sites formed by double chains of CrO_6 or TiO_6 octahedra connected through common vertices and edges to comprise a tunnelled framework containing non-stoichiometric amounts of K^+ cations (Genkina *et al.* 1993). It is imperative to note, that there is no significant substitution of La^{3+} in any of the cation sites of these synthetic hollandites.

Table 6-6 Interatomic Bond attributes for the hollandite compound (x=0.00) at the three temperatures, as calculated from a DBWS input control file by the WYRIET program Bond.exe. Data for $K_2Cr_8O_{16}$ taken from Tamada *et al.* 1996.

Bond Attributes [*B*=(Cr,Ti)]	$K_2Cr_8O_{16}$	1300°C	1200°C	1100°C
Bond Lengths (Å)				
$\langle B\text{-}O_1^A \rangle$	1.932 Å	1.987 Å	2.005 Å	2.001 Å
$\langle B\text{-}O_1^B \rangle$ (x2)	1.965 Å	1.967 Å	1.973 Å	1.974 Å
$\langle B\text{-}O_2^B \rangle$ (x2)	1.913 Å	1.958 Å	1.960 Å	1.952 Å
$\langle B\text{-}O_2^A \rangle$	1.871 Å	1.919 Å	1.908 Å	1.909 Å
Mean $\langle B\text{-}O \rangle$	1.927 Å	1.959 Å	1.963 Å	1.960 Å
(BO_6) Octahedral Angles (°)				
$\langle O_1^A\text{-}B\text{-}O_1^B \rangle$ (x2)	82.5	92.8	92.3	92.8
$\langle O_1^A\text{-}B\text{-}O_2^B \rangle$ (x2)	93.5	80.1	80.7	80.6
$\langle O_2^A\text{-}B\text{-}O_2^B \rangle$ (x2)	93.0	92.4	91.7	91.9
$\langle O_1^B\text{-}B\text{-}O_1^B \rangle$	96.6	97.4	97.1	97.1
$\langle O_1^B\text{-}B\text{-}O_2^A \rangle$ (x2)	90.9	94.9	95.4	94.8
$\langle O_1^B\text{-}B\text{-}O_2^B \rangle$ (x2)	81.5	81.8	82.0	81.8
$\langle O_2^B\text{-}B\text{-}O_2^B \rangle$	100.0	98.0	98.0	98.6
Mean $\langle O\text{-}B\text{-}O \rangle$	90.0	90.0	89.9	90.0
Inter-Octahedral Angle (°)				
$\langle O_1^A\text{-}B\text{-}O_2^A \rangle$		168.4	168.4	168.5

B-site octahedra

Rietveld results indicate that position (*8h*) in the space group *I4/m* is jointly occupied by Cr^{3+} and Ti^{4+} and is located within a regular octahedron. No structure refinement has ever detected evidence of ordering on this octahedral site. Post *et al.*, (1982) believe that the presence of lower-valence cations (*e.g.*, Cr^{3+}) in the octahedral site is essential to offset the tiny excess positive charge of the tunnel cations.

A-site tunnel cations

The K^+ cations fit into cavities [(*2a*) position] that are formed by eight O atoms [position (*8h*)], at the corners of a distorted prism (Post *et al.* 1982). Post and Burnham (1986), estimate the (*2a*) position to be normally only two-thirds to three-quarters filled. This is consistent with results from this study where the (*2a*) position is about 75-80% filled. The K^+ cations are distributed along the c-axis and some may be actually shifted from the special position (*2a*) to an off-centered position (*4e*), toward four of the surrounding O atoms, thus reducing positional disorder (Post and Burnham 1986). Genkina *et al.* (1993), suggest that the shift could indicate that the K^+ cations are distributed along the whole conductivity channel or tunnel in order to reduce cation repulsions. Post *et al.* (1982), regard the magnitudes of displacements of the tunnel cations to be dependent on contact-distance considerations, which includes the size, and to a lesser extent, the charge of the *A* cation. A displacement of K^+ is not observed in $K_2Cr_8O_{16}$ (Tamada *et al.* 1996), which has average K-O contact distances to the eight coordinating O atoms of 2.90 Å, close to the predicted value of 2.88 Å. Since K-O contact

distances with a magnitude of 3.018 Å were observed in this study, K^+ displacements may exist in $K_{1.54}(Cr_{1.58}Ti_{6.42})_8O_{16}$.

The occupation of the *A*-site cations over a range of positions within the tunnels of the hollandite structure has been reported by many workers, including Sinclair and McLaughlin (1982), for their work on the priderite structure. Structural refinements of $K_{1.54}(Ti_{7.23}Mg_{0.77})_8O_{16}$ by Weber and Schultz (1983) and Beyeler (1976,) indicate subsidiary sites and positional disorder even though there is only one kind of tunnel cation in the structure. This compound has tunnel sites only 77% filled with the tunnel cations split between a main site (2a) and a subsidiary site displaced 0.74Å along the tunnel. It is not possible to resolve the exact location of K^+ using Rietveld methods alone, and consequently, solution of this problem is considered beyond the scope of this work.

6.4 Perovskite-type Phases

A perovskite-type phase exists throughout the pseudo-binary system with the composition of an *A*-site deficient perovskite (Table 6-1). Two additional composition -dependent perovskite-type phases also occur: one at x=0.75 with the approximate formula $LaCrO_3$; and one at the perovskite end-member (x=1.00) with the approximate formula $La_2Ti_2O_7$. These latter perovskites are always associated with perovskite-1 (see Figure 6-1).

6.4.1 Non-Stoichiometric Perovskite (Perovskite-1)

6.4.1.1 *XRD* Powder Patterns

This phase could not be conclusively identified from its *XRD* powder pattern alone, except for its resemblance to other perovskite-type compounds, and as such is named perovskite-1. An ICDD database search resulted in two possible lanthanum titanium oxide compound matches, ($La_{2/3}TiO_{2.993}$) and ($LaTiO_3$). The first is orthorhombic (**a**=3.869Å, **b**=3.882Å, **c**=7.782Å, a_p=3.881Å, *v*=116.88Å^3; Abe and Uchino 1974). The second compound, $LaTiO_3$ (where Ti is trivalent) is also orthorhombic (**a**=5.601Å, **b**=5.590Å, **c**=7.906Å, a_p=3.955Å, *v*=247.534Å^3; Maclean *et al.* 1979). There appear to be similarities (Table 6-3, indexed reflections) between the main peak positions of $La_{2/3}TiO_{2.993}$ and the perovskite-1 phase encountered in these experiments, but the *XRD* pattern of the latter proved to be more complex, as indicated by the existence of additional unindexed reflections. The main peak positions represent the major perovskite peaks originating from the (TiO_6) framework. Perovskite-1 could not be properly indexed on cubic, tetragonal or orthorhombic symmetry, suggesting that it may have a monoclinic structure. The exact structure determination is beyond the scope of this work.

6.4.1.2 Compositional Determination

The average formula of perovskite-1 is $(K_{0.26}La_{0.55})_{0.81}(Cr_{0.05}Ti_{0.98})_{1.03}O_3$ (Table 6-1); and is considered to be a non-stoichiometric *A*-site deficient perovskite-group compound. This compound increases in modal concentration with decreasing temperature and

increasing composition(x), up to x=0.5. At $x \geq 0.5$ the concentration of perovskite-1 becomes constant (~35%).

6.4.1.3 Structure

Perovskite-1 is obviously non-stoichiometric, and the *XRD* pattern complexity is a reflection of this. It is assumed that the larger Cr and Ti atoms would fill the *B*-site, whereas the smaller K and La cations would occupy the *A*-sites. The structure may be a three-layered perovskite with one layer of vacant *B*-sites for each two layers of occupied *B*-sites (Gopalakrishnan and Bhat 1987). This non-stoichiometry may in fact combine with other complexities such as octahedral tilting, cation off-centring and disordering of cations to produce the observed *XRD* pattern.

6.4.2 Perovskite (-2)

The phase occurring at x=0.75 has the approximate formula $La_{0.95}Cr_{1.05}O_3$, as determined by SEM/EDS. Unfortunately, the grain size was too small (≤1.0μm) to obtain an accurate composition, and the low modal proportions prevented proper determination of its identity by *XRD*. $LaCrO_3$ has a perovskite-type structure (space-group *Pbnm*, **a**=5.512Å, **b**=5.476Å, **c**=7.752Å; Khattak and Cox 1977). When the synthesized phases at x=0.75 are indexed against $LaCrO_3$ (Table 6-3d), the phase is demonstrably present.

6.4.3 Perovskite (-3)

An additional phase occurs at x=1.0, with the approximate formula $La_2Ti_2O_7$ (Table 6-1). Unfortunately, the grain size was much too small (<0.1μm) to obtain an accurate composition, and the low modal proportions prevented a proper determination of its identity by *XRD*. $La_2Ti_2O_7$ is monoclinic (space-group $P2_1$, **a**=7.8-7.6Å, **b**=5.55-5.43Å, **c**=13.01-12.98Å, β≈98°; Preuss and Gruehn 1994). Table 6-3e indicates that when x=1.0 is indexed against $La_2Ti_2O_7$, the occurrence of common reflections support the SEM/EDS compositional analysis.

This phase is similar to a *LREE*-dititanate ($LREE_2Ti_2O_7$) (Preuss and Gruehn 1994). It may be identical in structure to orthorhombic $Ca_2Nb_2O_7$ (space-group $Pn2_1a$, **a**=25.457Å, **b**=5.501Å, **c**=7.692Å; Scheunmann and Muller-Buschbaum 1974). The layered structure consists of a typical perovskite-type structure cut apart at regular intervals, parallel to (*100*), such that the corners of (BO_6) octahedra (which normally share oxygens) are separated to allow the insertion of an oxygen anion.

6.5 Potassium Hexatitanate

For compositions of x=0.75 and 1.00, where the hollandite phase is thermodynamically unfavourable, potassium hexatitanate becomes the stable potassium-bearing titanate. This phase was also detected as a minor phase (5%) at x=0.5 and 1100°C.

6.5.1 Compositional Determination

This phase has an approximate formula $K_{1.99}Ti_{6.01}O_{13}$ (see Table 6-1). It is similar in composition to the synthetic compound dipotassium hexatitanate ($K_2Ti_6O_{13}$; Plumley and Orr 1961), and the mineral jeppeite [$(K,Ba)_2(Ti,Fe)_6O_{13}$; Pryce *et al.* 1984]. Results indicate two important features of potassium hexatitanate: it is the only main phase throughout the pseudo-binary system to be stoichiometric; and it contains no substitution of Cr^{3+} for Ti^{4+} in the (BO_6) structural units. The latter is especially important when nearly all similar minerals, such as jeppeite, exhibit at least some partial substitution of the trivalent cations (Fe^{3+}, V^{3+}, *etc.*,).

6.5.2 *XRD* Powder Patterns

XRD analysis indicates the structure of this phase is consistent with either jeppeite or potassium titanium oxide. Jeppeite is monoclinic (space-group *C2/m*, **a**=15.543Å, **b**=3.8368Å, **c**=9.123Å, β=99.25°, *v*=533.9Å^3; Pryce *et al.* 1984). Dipotassium hexatitanate is also monoclinic (space-group *C2/m*, **a**=15.593Å, **b**=3.796Å, **c**=9.108Å, β=99.78°; Plumley and Orr 1961).

A correlation of reflections for the synthesized hexatitanate with those given by Plumley and Orr (1961) (Table 6-4), verifies the existence of the hexatitanate at *x*=.75 and *x*=1.00. The diffraction pattern reflections of this phase are consistent with *2/m* Laue symmetry with all reflections having (*hkl*): *h+k=2n*, (*hk0*): *h+k=2n*, (*00l*): *l=2n*, (*h0l*): *h=2n*, (*0k0*): *k=2n*, and (*0kl*): *k=2n* extinct. Suggesting it belongs to the space-group *C2/m*. The potassium hexatitanate could not be indexed properly as its *XRD* pattern is weak. This is

due to poor crystallinity of potassium hexatitanate, with respect to the perovskite phases, coupled with strong *X*-ray absorption or scattering by the associated La-rich compound.

6.5.3 Structure

Hexatitanates, of the jeppeite-type, have the general formula $M_2Ti_6O_{13}$ (Z=2) where *M* represents a wide range of monovalent and divalent cations. They have a layered structure (Figure 6-5a) consisting of a framework of edge-sharing and corner-sharing TiO_6 octahedra, which have Ti cations displaced from the centre of the octahedra towards the *M* sites (Bagshaw *et al.* 1977; Cid-Dresdner and Buerger 1962). The monovalent *M* cations occupy tunnel sites coordinated to eight oxygens in a distorted cube and are offset from the centre of this cube towards the central axis of the tunnel, oriented parallel to the **b** axis (Bagshaw *et al.* 1977). The divalent *M* cations exist in a more regular cubic coordination, closer to the centre of the cube. Figure 6-5b illustrates the ideal structure of any hexatitanate (Bagshaw *et al.* 1977). The squares represent the TiO_6 octahedra, and the circles represent *M* atoms in the tunnels (heavy and light lines represent different levels). There is usually a limited substitution of titanium by iron in natural hexatitanates (Mitchell and Bergman 1991); although chromium never substitutes for titanium in this synthesis or in any natural jeppeite-type hexatitanates.

6.6 Conclusions

The pseudo-binary system investigated was characterized by the existence of the following phases (in order of abundance): hollandite $K_{1.54}(Cr_{1.43}Ti_{6.52})_{7.95}O_{16}$; perovskite-1

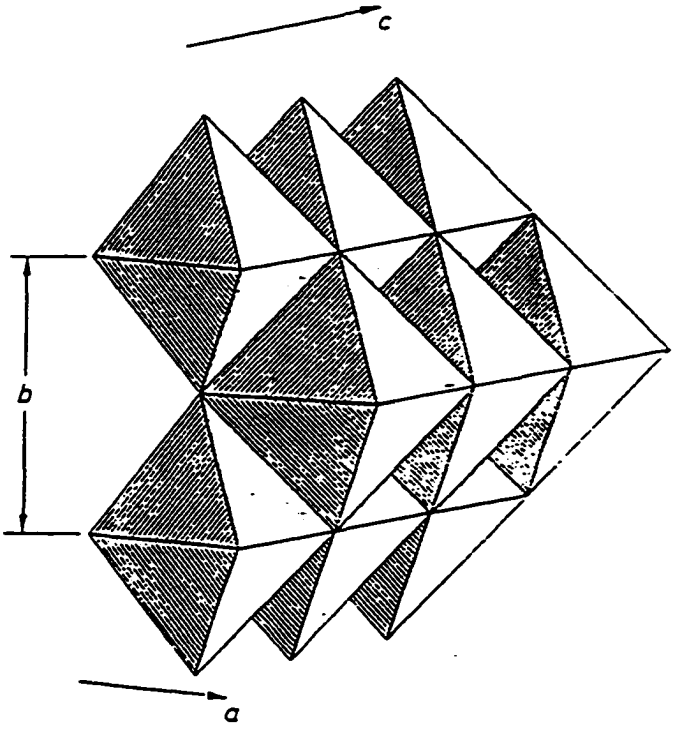

Figure 6-5a Clinographic projection of the structural unit of potassium hexatitanate ($K_2Ti_6O_{13}$; Cid-Dresdner and Buerger 1962).

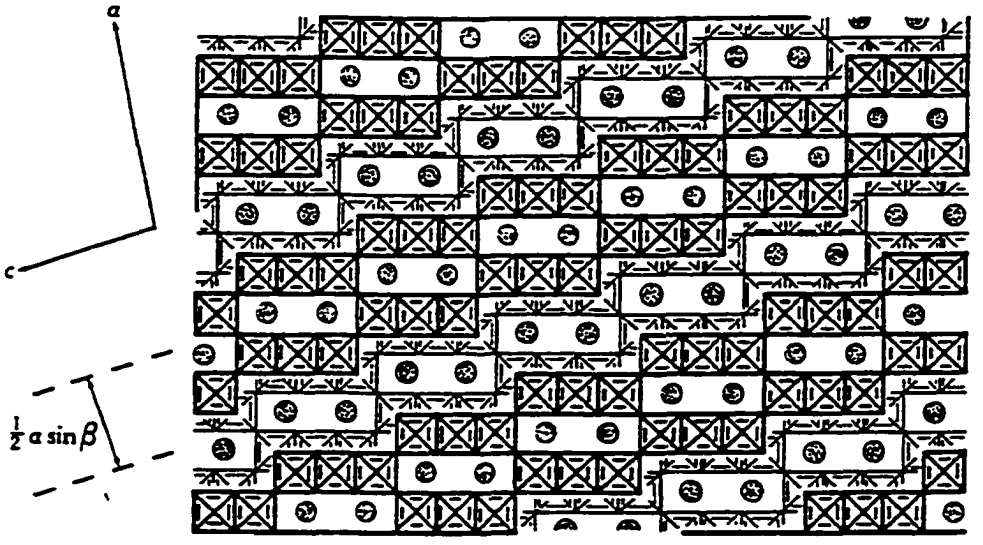

Figure 6-5b The idealized monoclinic hexatitanate ($M_2Ti_6O_{13}$) structure projected on [*010*], (Bagshaw *et al.* 1977).

$[(K_{0.26}La_{0.55})_{0.81}(Cr_{0.05}Ti_{0.98})_{1.03}O_3]$; potassium hexatitanate ($K_2Ti_6O_{13}$); perovskite-2 ($LaCrO_3$); perovskite-3 ($La_2Ti_2O_7$) and a minor amount of rutile (TiO_2). The hollandites have an *A*-site occupancy of approximately 75-82%, and exhibit no significant substitution of La^{3+} at any of the cation sites. Perovskite-1 is considered to be a non-stoichiometric *A*-site deficient perovskite. Two important features are exhibited by potassium hexatitanate; it is the only main phase that is stoichiometric and it contains no substitution of Cr^{3+} in any of the cation sites. Clearly all the Cr^{3+} excluded from the potassium hexatitanate structure is incorporated into perovskite-2.

References

Abe, M. and Uchino, K. (1974). X-Ray Study of the Deficient Perovskite $La_{2/3}TiO_3$. Materials Research Bulletin, 9, 147-156.

Appleman, D.E. and Evans, H.T.Jr. (1973). X-RAY (Least-Squares Refinement program) *U.S. Geological Survey, Compositional Contribution 20.* U.S. National Technical Information Service Document PBZ-16188.

Bagshaw, A.N., Doran, B.H., White, A.H. and Willis, M.C. (1977). Crystal Structure of a Natural Potassium-Barium Hexatitanate Isostructural with $K_2Ti_6O_{13}$. Australian Journal of Chemistry, 30, 1195-1200.

Bayer, G. and Hoffman, W. (1966). Complex Alkali Titanium Oxides $A_x(B_yTi_{8-y})O_{16}$ of the αMnO_2 Structure Type. American Mineralogist, 51, 511-516.

Beran, A., Libowitzky, E., and Armbruster, T. (1996). A Single-Crystal Infrared Spectroscopic and X-Ray-Diffraction Study of Untwinned San Benito Perovskite Containing OH Groups. Canadian Mineralogist, 34, 803-809.

Beyeler, H.U. (1976). Cationic Short-Range Order in the Hollandite $K_{1.54}Mg_{0.77}Ti_{7.23}O_{16}$: Evidence for the Importance of Ion-Ion Interactions in Superionic Conductors. Physical Review Letters, 37, No. 23, 1557-1560.

Bourdillon, A. and Bourdillon, T. (1994). *High Temperature Superconductors: Processing and Science.* Academic Press, San Diego.

Buttner, R.H. and Maslen, E.N. (1992). Electron Difference Density and Vibration Tensors in $SrTiO_3$. Acta Crystallographica, B48, 639-644.

Čeh, M., Kolar, D., and Golič, L. (1987). The Phase Diagram of $CaTiO_3$-$SrTiO_3$. Journal of Solid State Chemistry, 68, 68-72.

Chakhmouradian, A.R. and Mitchell, R.H. (1997). Compositional Variation of Perovskite-Group Minerals from the Khibina Complex, Kola Peninsula. Canadian Mineralogist (in press).

Cid-Dresdner, H. and Buerger, M.J. (1962). The Crystal Structure of Potassium Hexatitanate $K_2Ti_6O_{13}$. Zeitschrift für Jrustakkigraoguem, 117, 411-430.

Downs, R.T., Bartelmehs, K.L., Gibbs, G.V. and Boisen, M.B., Jr. (1993). Interactive Software for Calculating and Displaying X-Ray or Neutron Powder Diffractometer Patterns of Crystalline Materials. American Mineralogist, 78, 1104-1107.

Dowty, E. (1995). ATOMS for Windows, version 3.2 (computer program).

Dubeau, M.L. and Edgar, A.D. (1985). Priderite Stability in the System $K_2MgTi_7O_{16}$-$BaMgTi_7O_{16}$. Mineralogical Magazine, 49, 603-606.

Filip'ev, V.S. and Fesenko, E.G. (1965). Preparation and Structures of Complex Perovskites of Type $Ca_2B'B''O_6$. Soviet Physics-Crystallography, 10, No. 3, 243-247.

Galasso, F. S. (1969). *Structure, Properties, and Preparation of Perovskite Type Compounds*. Oxford: Pergamon Press.

Genkina, E.A., Maksimov, B.A., Dem'yanets, L.N. and Lazarevskaya, O.A. (1993). Synthesis and Structure of a New Compound in the Hollandite Series. Kristallografiya, 38, 66-70.

Glazer, A.M. (1975). Simple Ways of Determining Perovskite Structures. Acta Crystallographica, A31, 756-762.

Glazer, A.M. (1972). The Classification of Tilted Octahedra in Perovskites. Acta Crystallographica, B28, 3384-3392.

Glazer, A.M. and Megaw, H.D. (1972). The Structure of Sodium Niobate (T_2) at 600°C, and the cubic-tetragonal transition in relation to soft-phonon modes. Philosophical Magazine, 25, 1119-1135

Goldschmidt, V.M. (1926). Geochemishe Verteilungsgesetze der Elemente VII. Naturwissenschaften, 14, 477-485.

Gopalakrishnan, J. and Bhat, V. (1987). $A_2Ln_2Ti_3O_{10}$ (a=K or Rb; Ln = La or Rare Earth): A New Series of Layered Perovskites Exhibiting Ion Exchange. Inorganic Chemistry, 26, 4299-4301.

Hazen, R.M. (1988). Perovskites. Scientific American, June, 74-81.

Hazen, R.M. and Navrotsky, A. (1996). Effects of Pressure on Order-Disorder Reactions. American Mineralogist, 81, 1021-1035.

Hu, M., Wenk, H.R. and Sinitsyna, D. (1992). Microstructures in Natural Perovskites. American Mineralogist, 77, 359-373.

Hyde, B.G., O'Keeffe, M. (1973). Relations between the $DO_9(ReO_3)$ Structure Type and Some 'Bronze' and 'Tunnel' Structures. Acta Crystallographica, A29, 243-248.

International Tables for X-ray Crystallography, vol. I. Kynock Press, Birmingham, 1965.

Kay, H.F. and Bailey, P.C. (1957). Structure and Properties of $CaTiO_3$. Acta Crystallographica, 10, 219-226.

Kesson, S.E. and White, T.J. (1986a). Comments on 'Priderite Stability in the System $K_2MgTi_7O_{16}$-$BaMgTi_7O_{16}$'. Mineralogical Magazine, 50, 537-538.

Kesson, S.E. and White, T.J. (1986b). $[Ba_xCs_y][(Ti^{3+},Al)_{2x+y}(Ti^{4+})_{8-2x-y}]O_{16}$ Synroc-Type Hollandites: I. Phase Chemistry. Proceedings of the Royal Society of London, 405A, 73-101.

Khattak, C.P. and Cox, C.P. (1977). Structural Studies of the $(La,Sr)CrO_3$ System. Materials Research Bulletin, 12, 463-472.

Klug, H.P. and Alexander, L.E. (1974). *X-Ray Diffraction Procedures for Polycrystalline and Amorphous Materials*, 2nd ed.; Wiley and Sons, Toronto.

Leigh, H. and McCartney, E. (1974). Redetermination of Lattice Parameter of ThO_2. Journal of the American Ceramic Society, 57, 192.

Liu, X. and Liebermann, R.C. (1993). X-Ray Powder Diffraction Study of $CaTiO_3$ Perovskite at High Temperatures. Physics and Chemistry of Minerals, 20, 171-175.

Loeb, A.L. (1962). A Modular Algebra for the Description of Crystal Structures. Acta Crystallographica, 15, 219-226.

MacLean, D.A., Ng, H-N., Greedan, J.E. (1979). Crystal Structures and Crystal Chemistry of the $RETiO_3$ Perovskites: RE=La, Nd, Sm, Gd, Y. Journal of Solid State Chemistry, 30, 35-44.

McQuarrie, M.C. (1955). Structural Behaviour in the System (Ba, Ca, Sr)TiO_3 and its Relation to Certain Dielectric Characteristics. Journal of the American Ceramic Society, 38, 444-449.

Megaw, H. D. (1973). *Crystal Structures: A Working Approach*. Philadelphia: Saunders.

Merck Index: An Encyclopaedia of Chemicals and Drugs, 9th ed. (Windholz, M. ed.). Merck and Co., Inc., New Jersey, 1976.

Mitchell, R.H. (1996). Perovskites: A Revised Classification Scheme for an Important Rare Earth Host in Alkaline Rocks. *Rare Earth Minerals: Chemistry, Origin and Ore Deposits* (Jones, A.P., Wall, F. and Williams, C.T. eds.); *U.K. Mineralogical Society Series* 6, 41-76.

Mitchell, R.H. (1986). *Kimberlites: Mineralogy, Geochemistry and Petrology*. Plenum Press, New York.

Mitchell, R.H. and Bergman, S.C. (1991). *Petrology of Lamproites*. Plenum Press, New York.

Mitchell, R.H. and Chakhmouradian, A.R. (1996). Compositional Variation of Loparite from the Lovozero Alkaline Complex, Russia. Canadian Mineralogist, 34, 977-990.

Mitchell, R.H. and Haggerty, S.E. (1986). A New K-V-Ba Titanate Related to Priderite from the New Elands Kimberlite, South Africa. Neues Jahrbuch Für Mineralogie Monatohefte,16, 376-384.

Mitchell, R.H. and Meyer, H.O.A. (1989). Niobian K-Ba-Titanates from Micaceous Kimberlite, Star Mine, Orange Free State, South Africa. Mineralogical Society, 53, 451-456.

Mitchell, R.H. and Vladykin, N.V. (1993). Rare Earth Element-Bearing Tausonite and Potassium Barium Titanates from the Little Murun Potassic Alkaline Complex, Yakutia, Russia. Mineralogical Magazine, 57, 651-664.

Mukherjee, B. (1960). Space Group and Cell Dimensions of a specimen of Hollandite. Acta Crystallographica, 13, 164-165.

Náray-Szabó (1943). Der Strukturtyp des Perowskits ($CaTiO_3$). Naturwissenschaften, 31, 202-203.

O'Keefe, M. and Hyde, B.G. (1977). Some Structures Topologically Related to Cubic Perovskite ($E2_1$), ReO3 ($D0_9$) and $Cu_3Au(L1_2)$ Acta Crystallographica, B33, 3802-3813.

Plumley, A.L. and Orr, W.C. (1961). Replacement of Potassium Ions in Solid Potassium Hexatitanate by Sodium Ions from a Chloride Flux. Journal of the American Chemical Society, 83, 1289-1291.

Post, J.E. and Bish, D.L. (1989). Rietveld Refinement of Crystal Structures Using Powder X-Ray Diffraction Data. *Modern Powder Diffraction: Reviews in Mineralogy Vol. 20* (Bish, D.L. and Post, J.E. eds.). Mineralogical Society of America; Washington 277-308.

Post, J.E. and Burnham, C.W. (1986). Modeling Tunnel-Cation Displacements in Hollandites Using Structure-Energy Calculations. American Mineralogist, 71, 1178-1185.

Post, J.E., Von Dreele, R.B. and Buseck, P.R. (1982). Symmetry and Cation Displacements in Hollandites: Structure Refinements of Hollandite, Cryptomelane and Priderite. Acta Crystallographica, B38, 1056-1065.

Preuss, A. and Gruehn, R. (1994). Preparation and Structure of Cerium Titanates: Ce_2TiO_5, $Ce_2Ti_2O_7$, and $Ce_4Ti_9O_{24}$. Journal of Solid State Chemistry, 110, 363-369.

Pryce, M.W., Hodge, L.C. and Criddle, A.J. (1984). Jeppeite, a New K-Ba-Fe Titanate from Walgidee Hills, Western Australia. Mineralogical Magazine, 48, 263-266.

Rietveld, H.M. (1969). A Profile Refinement Method for Nuclear and Magnetic Structures. Journal of Applied Crystallography, 2, 65-71.

Rietveld, H.M. (1967). Line Profiles of Neutron Powder-Diffraction Peaks for Structure Refinement. Acta Crystallographica, 22, 151-152.

Ringwood, A.E. (1985). Disposal of High-Level Nuclear Wastes: a Geological Perspective. Mineralogical Magazine, 49, 159-176.

Ringwood, A.E., Reid, A.F., and Wadstey, A.D. (1967). High-Pressure $KalSi_3O_8$, an Aluminosilicate with Sixfold Coordination. Acta Crystallographica, 23, 1093-1099.

Ruddlesden, S.N. and Popper, P. (1958). The Compound $Sr_3Ti_2O_7$ and its Structure. Acta Crystallographica, 11, 54-55.

Ruddlesden, S.N. and Popper, P. (1957). New Compounds of the K_2NiF_4 Type. Acta Crystallographica, 10, 538-539.

Sasaki, S., Prewitt, C.T., Bass, J.D. and Schulze, W.A. (1987). Orthorhombic Perovskite $CaTiO_3$ and $CdTiO_3$: Structure and Space Group. Acta Crystallographica, C43, 1668-1674.

Scheunemann, K. and Muller-Buschbaum, H.K. (1974). Zur Kristallstruktur von $Ca_2Nb_2O_7$. Journal of Inorganic and Nuclear Chemistry, 36, 1965-1970.

Schneider, M. ·EDV-VERTRIEB (1995). WYRIET version 3.0 Powder Profile Refinement and Structure Analysis Package for Personal Computers.

Scott, J. and Peatfield, G. (1986). Mannardite $[Ba{\cdot}H_2O](Ti_6V_2)O_{16}$, A New Mineral Species, and New Data on Redledgeite. The Canadian Mineralogist, 24, 55.

Shannon, R.D. and Prewitt, C.T. (1969). Effective Ionic Radii in Oxides and Fluorides. Acta Crystallographica, B25, 925.

Sinclair, W. And McLaughlin, G.M. (1982). Structure Refinement of Priderite. Acta Crystallgraphica, B38, 245-246.

Smith, A.J. and Welch, A.J.E. (1960). Some Mixed Metal Oxides of Perovskite Structure. Acta Crystallgraphica, 13, 653-656.

Smith, D.K. and Gorter, S. (1991). Powder Diffraction Program Information, 1990 Program List. Journal of Applied Crystallography, 24, 369-402.

Tamada, O., Yamamoto, N., Mori, T. and Endo, T. (1996). The Crystal Structure of $K_2Cr_8O_{16}$: The Hollandite-Type Full Cationic Occupation in a Tunnel. Journal of Solid State Chemistry, 126, 1-6.

Tejuca, L.G., Fierro, J.L.G. and Tascón, J.M.D. (1989). Structure and Reactivity of Perovskite-Type Oxides. *Advances in Catalysis Vol. 36* (Eley, D.D., Pines, H. and Weisz, P.B. eds.). Academic Press, Inc.; California 237-328.

Tien, T.Y. and Hummel, F.A. (1967). Solid Solutions in the System $SrTiO_3$-(La_2O_3:$3TiO_2$). Transactions of the British Ceramic Society, 66, 233-245.

Vainshtein, B., Fridkin. V.M., and Indenbom, V. (1994). *Structure of Crystals, 2nd edition*. Springer Verlag, New York.

Várez, A., García-Alvarado, F., Morán, E. and Alario, F. (1995). Microstructural Study of $La_{0.5}Li_{0.05}TiO_3$. Journal of Solid State Chemistry, 118, 78-83.

Veksler, I.V. and Teptelev, M.P. (1990). Conditions for Crystallization and Concentration of Perovskite-Type Minerals in alkaline Magmas. Lithos, 26, 177-189.

Vlasov, K.A. (1966). *Geochemistry and Mineralogy of Rare Elements and Genetic Types of Their Deposits. II. Mineralogy of Rare Elements.* Israel Program for Scientific Translations, Jerusalem, Israel.

Vorob'yev, Ye.I., Konev, A.A., Malyshonok, Yu.V., Afonina, G.F. and Sapozhnikov, A.N. (1984). Tausonite, $SrTiO_3$, A New Mineral of the Perovskite-Group. International Geology Review, 462-465.

Weber, H.P. and Schultz, H. (1983). Atomic Disorder and Thermal Behaviour of a Synthetic Potassium Hollandite. Geological Society of America. Abstracts with Programs, 15, 715.

Woodward, P.M. (1997a). Octahedral Tilting in Perovskites. I. Geometrical Considerations. Acta Crystallographica, B53, 32-43.

Woodward, P.M. (1997b). Octahedral Tilting in Perovskites. II. Structure Stabilizing Forces. Acta Crystallographica, B53, 44-66.

Young, R.A. (1995). *The Rietveld Method: International Union of Crystallography Monographs on Crystallography 5*; Oxford University Press; Toronto.

Young, R.A., Sakthivel, A., Moss, T.S. and Paiva-Santos, C.O. (1995). User's Guide to Program DBWS-9411 (Release 30.3.95) for Rietveld Analysis of X-Ray and Neutron Powder Diffraction Patterns. Journal of Applied Crystallography, 28, 366-367.

Zhang, J. and Burnham, C.W. (1994). Hollandite-Type Phases: Geometric Consideration of Unit-Cell Size and Symmetry. American Mineralogist, 79, 168-174.

Zhao, Y., Weidner, D.J., Parise, J.B. and Cox, D.E. (1993). Thermal Expansion and Structural Distortion of Perovskite-Data for $NaMgF_3$ Perovskite. Part I. Physics of the Earth and Planetary Interiors, 76, 1-16.

Zhu, W.J. and Hor, P.H. (1995). A New Titanium Perovskite Oxide, $Na_{2/3}Th_{1/3}TiO_3$. Journal of Solid State Chemistry, 120, 208-209.

APPENDIX

A.1 Rietveld Refinement Setup

The setup of the DBWS-9411 program is relatively simple. The distribution package (from the user's guide by Young *et al.* 1995) for the PC version of DBWS 9411 includes the source code, a user's guide and test case data and input control files. The package, written for a MS-DOS environment, includes the following files on magnetic media in five subdirectories, and should be saved on drive C:

1) Subdirectory FOR, the DBWS-9411 source code (DB1.FOR, DB2.FOR, and DB3.FOR) in three parts, and a file (PARAM.INC) needed at compilation time for specifying the user's choice of sizes of the five most-likely-to-be-redimensioned arrays.

2) Subdirectory QTEST, contains the files necessary for a quartz test case, which has alumina as a minor phase.

3) Subdirectory FTEST, contains the files necessary for a fluorapatite test case.

4) Subdirectory DMPLOT, contains the files used for operation of this proprietary program offered as a SHAREWARE item.

5) Subdirectory SPLOT, contains the files used for the operation of the SHAREWARE plotting program.

The best refinement requires manipulation of the PC's files CONFIG.SYS (addition of DEVICE=C:\DOS\EMM386.EXE NOEMS) to activate drivers and AUTOEXEC.BAT (addition of PATH C:\DBWS9411;C:\DBWS9411\DMPLOT; C:\DBWS9411\SPLOT ,and DOSKEY) to set paths for the running of the execute commands in any directory. Now

simply typing DOSKEY at the DOS prompt toggles the function on or off. Although not necessary, this facilitates the refinement by allowing for the repetition of the various commands required.

Preceding any structure refinement, a separate subdirectory for each set of data, similar to QTEST and FTEST, must be setup within the directory C:\DBWS9411 (see appendix). This directory will contain all observed data input files, input control files and output data files related to a specific compound or member of a solid-solution series. With the setup of the preceding subdirectory, and the previous manipulation of the CONFIG.SYS and AUTOEXEC.BAT files, it is now possible to run the refinement of any compound within the confines of the established subdirectory.

The observed data input files (Young *et al.* 1995) are of two types, one type (TAPE 4, also referred to as FORT 4) contains the measured *XRD* data for the compound under investigation and the other type (TAPE 3, also referred to as FORT 3) contains the measured *XRD* background, which is optional. The compound data can be in any of the following formats:

A) Constant incident flux and a single detector collecting *X*-ray (JOBTYP= 0) or neutron (JOBTYP= 1) data at equal increments of two-theta (INSTRM= 0).

B) Varying incident *X*-ray flux (synchrotron x-radiation) and a single detector collecting data (JOBTYP= 0, INSTRM= 1) in equal increments of two-theta.

C) Fixed wavelength, constant intensity neutron beam incident and multiple diffracted-beam detectors (JOBTYP= 1, INSTRM= 1), but not all detectors contributing to the count at every step.

Line 1 (3F8, A56)

1 F8 START -beginning angle (2θ).

2 F8 STEP -step size (2θ).

3 F8 STOP -last angle (2θ).

A56 DATAID -data identification.

Line N (8(F7.0, 1X)) -the data from the start angle to the stop angle.

Codewords are used within the ICF for all parameters which are to be refined. Codewords consists mainly of two parts, the designation of a matrix position for the parameter, and the specification of the fraction of the calculated shift that is to be applied to the parameter. They have the form *SDDDC.CC* where *DDD* specifies the matrix position, *C.CC* specifies what fraction (multiple) of the calculated shift is to be applied to update the parameter, and *S* is the sign (+ or -) desired for the applied shift, default is (+). It is also possible to set a group 'relaxation' factor to be applied to the calculated shifts for all parameters in each of four different groups of parameters (*line 5*, 2-F4-5-F4).

A.2 XRD Patterns For The $K_2Cr_2Ti_6O_{16}$-$K_2La_2Ti_6O_{16}$ Pseudo-Binary System

The following are the raw *XRD* patterns for the $K_2Cr_2Ti_6O_{16}$-$K_2La_2Ti_6O_{16}$ pseudo-binary system. The observed *d*-values appear in the *d*-obs. column, where the associated wavelengths are $K_{\alpha 1}$=1.541863Å, for all single reflections up to 60 (2θ), and $K_{\alpha 1}$=1.540562Å and $K_{\alpha 1}$ =1.544390Å for all others. The calculated *d*-values appear in the *d*-calc. column; determined by least-squares refinement (Appleman and Evans 1973). The observed relative intensities appear in the I-obs. column; reflections with relative intensities below 1 were regarded as being unobserved. The *hkl* values refer only to hollandite-type phases, and their associated calculated relative intensities appear in I-calc. (as determined by XPOW). For x=0.5, the calculated relative intensities have been scaled relative to the most intense hollandite line at approximately d=3.2Å (*130*).

x=0.0 at 1300°C

hkl	D-obs.	D-calc.	I-obs.	I-calc.	hkl	D-obs.	D-calc.	I-obs.	I-calc.
1 1 0	7.164	7.158	41	51	3 7 2	0.988	0.988	3	5
0 2 0	5.066	5.061	53	54	3 7 2	0.988	0.988	1	2
2 2 0	3.579	3.579	13	10	4 9 1	0.971	0.971	1	1
1 3 0	3.201	3.201	100	100	1 2 3	0.963	0.963	3	3
0 4 0	2.531	2.531	12	14	1 2 3	0.963	0.963	1	1
1 2 1	2.475	2.475	49	67	4 10 0	0.940	0.940	1	1
3 3 0	2.385	2.386	2	4	4 10 0	0.940	0.940	1	1
2 4 0	2.264	2.264	10	8	6 6 2	0.928	0.928	2	3
0 3 1	2.224	2.224	27	37	5 7 2	0.921	0.921	2	1
3 2 1	2.033	2.036	3	4	5 7 2	0.921	0.921	1	0
5 1 0	1.987	1.985	11	8	1 4 3	0.914	0.914	3	3
4 1 1	1.890	1.889	30	37	1 4 3	0.915	0.914	1	1
4 4 0	1.791	1.789	2	2	1 9 2	0.892	0.892	3	4
3 5 0	1.738	1.736	1	2	1 9 2	0.892	0.892	2	2
0 6 0	1.689	1.687	21	23	7 9 0	0.888	0.888	3	3
0 5 1	1.672	1.670	6	3	7 9 0	0.888	0.888	2	2
6 2 0	1.602	1.601	2	2	0 11 1	0.879	0.879	1	1
2 5 1	1.586	1.586	20	41	2 5 3	0.873	0.873	4	6
0 0 2	1.478	1.478	8	11	2 5 3	0.873	0.873	2	3
0 0 2	1.477	1.478	4	5	10 6 0	0.868	0.868	1	1
1 6 1	1.448	1.450	2	1	2 11 1	0.866	0.866	6	10
1 7 0	1.431	1.432	3	3	2 11 1	0.866	0.866	4	5
0 2 2	1.419	1.419	4	2	11 4 1	0.830	0.830	4	8
0 2 2	1.418	1.419	2	1	11 4 1	0.830	0.830	2	4
4 6 0	1.404	1.404	2	2	10 2 2	0.824	0.824	1	3
5 4 1	1.394	1.394	26	28					
1 3 2	1.342	1.342	6	9					
7 3 0	1.329	1.329	7	6					
7 3 0	1.329	1.329	4	3					
0 4 2	1.276	1.276	4	2					
0 4 2	1.276	1.276	2	1					
3 3 2	1.258	1.257	1	2					
2 7 1	1.258	1.258	1	1					
4 2 2	1.238	1.238	1	2					
6 6 0	1.193	1.193	3	3					
6 6 0	1.193	1.193	2	1					
5 6 1	1.186	1.187	1	1					
1 5 2	1.186	1.186	1	1					
7 5 0	1.177	1.177	2	2					
1 8 1	1.156	1.156	4	4					
1 8 1	1.156	1.156	2	2					
8 4 0	1.132	1.132	1	1					
1 9 0	1.118	1.118	5	4					
1 9 0	1.118	1.118	2	2					
0 6 2	1.112	1.112	7	8					
0 6 2	1.112	1.112	4	4					
3 9 0	1.067	1.067	2	2					
1 7 2	1.029	1.028	3	4					
1 7 2	1.029	1.028	1	2					
4 6 2	1.018	1.018	2	1					
0 10 0	1.012	1.012	1	1					
5 8 1	1.009	1.009	4	4					
5 8 1	1.009	1.009	2	2					
10 2 0	0.993	0.993	1	1					

x=0.0 at 1200°C

hkl	D-obs.	D-calc.	I-obs.	I-calc.	hkl	D-obs.	D-calc.	I-obs.	I-calc.
110	7.153	7.151	37	49	572	0.920	0.920	2	2
020	5.061	5.057	55	55	572	0.920	0.920	1	1
220	3.575	3.576	13	11	143	0.915	0.915	2	3
130	3.197	3.198	100	100	143	0.915	0.915	1	1
040	2.529	2.528	15	14	192	0.891	0.891	2	4
121	2.475	2.475	45	64	192	0.891	0.891	1	2
330	2.385	2.384	4	4	790	0.887	0.887	1	3
240	2.262	2.261	12	11	253	0.873	0.873	4	6
031	2.224	2.223	26	38	253	0.873	0.873	2	3
321	2.035	2.035	2	4	2111	0.865	0.865	5	12
510	1.985	1.983	8	8	2111	0.865	0.865	2	6
411	1.889	1.888	32	37	453	0.836	0.836	4	8
440	1.789	1.788	2	2	453	0.836	0.836	3	4
350	1.736	1.734	2	2	1141	0.829	0.829	2	8
060	1.687	1.686	18	23					
051	1.671	1.670	4	3					
620	1.599	1.599	1	2					
251	1.585	1.585	28	40					
251	1.585	1.585	15	20					
002	1.479	1.479	9	11					
161	1.449	1.449	3	4					
170	1.429	1.430	2	2					
022	1.420	1.419	4	2					
022	1.419	1.419	2	1					
460	1.402	1.402	1	1					
541	1.393	1.393	18	27					
541	1.393	1.393	10	14					
132	1.342	1.342	6	9					
132	1.342	1.342	4	5					
730	1.328	1.328	4	3					
042	1.277	1.277	3	2					
042	1.277	1.277	2	1					
332	1.257	1.257	1	2					
271	1.257	1.257	1	2					
660	1.192	1.192	2	3					
561	1.186	1.186	2	1					
152	1.186	1.186	1	1					
750	1.176	1.176	1	2					
181	1.155	1.155	2	4					
190	1.117	1.117	2	3					
062	1.112	1.112	5	8					
062	1.111	1.112	3	4					
262	1.086	1.086	1	1					
172	1.028	1.028	3	1					
172	1.028	1.028	1	1					
462	1.018	1.018	2	1					
462	1.017	1.018	1	1					
581	1.008	1.008	2	4					
581	1.008	1.008	1	2					
372	0.988	0.988	2	4					
372	0.988	0.988	1	2					
123	0.963	0.963	2	3					
123	0.963	0.963	1	1					
662	0.928	0.928	1	3					

x=0.0 at 1100°C

h k l	D-obs.	D-calc.	I-obs.	I-calc.	*h k l*	D-obs.	D-calc.	I-obs.	I-calc.
1 1 0	7.156	7.149	35	49	*1 4 3*	0.915	0.915	1	2
0 2 0	5.061	5.055	49	54	*1 9 2*	0.891	0.891	1	5
2 2 0	3.575	3.574	11	11	*7 9 0*	0.886	0.887	1	3
1 3 0	3.196	3.197	100	100	*7 9 0*	0.886	0.887	1	2
0 4 0	2.529	2.527	12	14	*2 5 3*	0.873	0.873	4	6
1 2 1	2.476	2.476	46	64	*2 5 3*	0.873	0.873	2	3
3 3 0	2.386	2.383	2	4	*2 11 1*	0.865	0.865	4	8
2 4 0	2.262	2.261	10	8	*2 11 1*	0.864	0.865	2	4
0 3 1	2.224	2.224	24	37	*4 5 3*	0.837	0.837	3	8
3 2 1	2.037	2.035	2	4	*4 5 3*	0.837	0.837	3	4
5 1 0	1.984	1.983	6	8	*11 4 1*	0.829	0.829	2	8
4 1 1	1.889	1.888	30	23					
4 4 0	1.787	1.787	2	14					
3 5 0	1.736	1.734	2	2					
0 6 0	1.687	1.685	15	23					
0 5 1	1.671	1.669	5	3					
6 2 0	1.598	1.598	1	2					
2 5 1	1.587	1.585	27	40					
0 0 2	1.480	1.480	7	11					
1 6 1	1.449	1.449	3	5					
1 7 0	1.430	1.430	2	3					
0 2 2	1.420	1.420	3	2					
4 6 0	1.402	1.402	2	2					
5 4 1	1.393	1.393	18	27					
5 4 1	1.392	1.393	9	14					
1 3 2	1.343	1.343	6	11					
1 3 2	1.342	1.343	3	5					
7 3 0	1.327	1.327	3	6					
0 4 2	1.277	1.277	3	2					
3 3 2	1.257	1.257	1	2					
2 7 1	1.257	1.257	1	1					
3 3 2	1.257	1.257	1	1					
2 7 1	1.257	1.257	1	1					
4 2 2	1.238	1.238	1	2					
6 6 0	1.191	1.191	1	3					
5 6 1	1.186	1.186	2	1					
1 5 2	1.186	1.186	1	1					
1 8 1	1.154	1.155	2	4					
1 9 0	1.117	1.116	2	3					
0 6 2	1.112	1.112	5	8					
0 6 2	1.112	1.112	3	4					
2 6 2	1.086	1.086	1	1					
2 6 2	1.086	1.086	1	0					
1 7 2	1.028	1.028	3	5					
1 7 2	1.028	1.028	2	3					
4 6 2	1.018	1.018	1	1					
4 6 2	1.018	1.018	1	1					
5 8 1	1.008	1.008	3	4					
3 7 2	0.988	0.988	2	5					
1 2 3	0.964	0.964	2	3					
6 6 2	0.928	0.928	1	3					
6 6 2	0.928	0.928	1	2					
5 7 2	0.920	0.920	1	2					
1 4 3	0.915	0.915	2	3					

x=0.1 at 1300°C

h k l	D-obs.	D-calc.	I-obs.	I-calc.	h k l	D-obs.	D-calc.	I-obs.	I-calc.
0 0 0	7.806	0.000	1		0 6 2	1.112	1.112	4	4
1 1 0	7.158	7.157	47	54	3 8 1	1.100	1.100	1	1
0 2 0	5.061	5.061	59	59	3 8 1	1.100	1.100	1	0
2 2 0	3.577	3.579	10	10	2 6 2	1.086	1.086	2	1
0 0 0	3.468	0.000	2		2 6 2	1.086	1.086	1	0
1 3 0	3.198	3.201	100	100	3 9 0	1.067	1.067	2	2
0 0 0	2.744	0.000	21		3 9 0	1.067	1.067	1	1
0 4 0	2.530	2.530	15	15	0 0 0	1.038	0.000	2	
1 2 1	2.475	2.475	46	66	1 7 2	1.029	1.028	4	4
3 3 0	2.383	2.386	2	4	1 7 2	1.028	1.028	2	2
2 4 0	2.263	2.263	12	11	4 6 2	1.018	1.018	3	1
0 0 0	2.242	0.000	5		4 6 2	1.018	1.018	2	0
0 3 1	2.224	2.223	32	37	0 10 0	1.012	1.012	1	1
3 2 1	2.037	2.036	3	4	5 8 1	1.009	1.009	4	4
5 1 0	1.987	1.985	10	8	5 8 1	1.009	1.009	2	2
0 0 0	1.942	0.000	5		10 2 0	0.993	0.993	1	1
4 1 1	1.890	1.889	35	38	3 7 2	0.988	0.988	2	5
4 4 0	1.791	1.789	2	2	3 7 2	0.988	0.988	1	2
3 5 0	1.737	1.736	3	2	4 9 1	0.971	0.971	1	1
0 6 0	1.687	1.687	20	23	4 9 1	0.971	0.971	1	1
0 5 1	1.670	1.670	5	1	1 2 3	0.963	0.963	3	3
6 2 0	1.601	1.600	2	2	1 2 3	0.963	0.963	1	1
2 5 1	1.586	1.586	46	41	4 10 0	0.940	0.940	1	1
0 0 2	1.478	1.478	12	11	4 10 0	0.940	0.940	1	0
0 0 2	1.477	1.478	5	5	6 6 2	0.928	0.928	2	3
1 6 1	1.450	1.450	3	4	6 6 2	0.928	0.928	1	2
1 7 0	1.432	1.431	3	3	5 7 2	0.921	0.921	2	2
1 7 0	1.431	1.431	1	1	5 7 2	0.921	0.921	1	1
0 2 2	1.419	1.419	4	2	1 4 3	0.915	0.914	3	3
4 6 0	1.404	1.404	2	2	1 4 3	0.914	0.914	2	1
5 4 1	1.394	1.394	31	28	1 9 2	0.892	0.892	3	4
5 4 1	1.394	1.394	15	14	1 9 2	0.892	0.892	2	2
0 0 0	1.373	0.000	2		7 9 0	0.888	0.888	3	3
1 3 2	1.342	1.342	5	9	7 9 0	0.888	0.888	2	2
1 3 2	1.342	1.342	4	4	0 11 1	0.877	0.879	1	1
7 3 0	1.329	1.329	6	7	0 11 1	0.878	0.879	0	0
7 3 0	1.329	1.329	3	3	2 5 3	0.873	0.873	6	6
0 4 2	1.276	1.276	6	2	2 5 3	0.873	0.873	3	3
0 4 2	1.276	1.276	3	1	10 6 0	0.868	0.868	1	2
3 3 2	1.257	1.256	1	1	2 11 1	0.866	0.866	8	9
2 7 1	1.257	1.258	1	1	2 11 1	0.866	0.866	4	4
0 0 0	1.253	0.000	1		12 0 0	0.843	0.843	1	1
8 2 0	1.228	1.227	2	1	7 7 2	0.841	0.841	1	1
6 6 0	1.193	1.193	3	3	7 7 2	0.841	0.841	1	0
6 6 0	1.193	1.193	2	1	4 5 3	0.836	0.836	6	8
5 6 1	1.186	1.187	1	2	4 5 3	0.836	0.836	3	4
1 5 2	1.186	1.186	0	1	0 0 0	0.835	0.000	3	
7 5 0	1.177	1.177	2	2	0 0 0	0.835	0.000	2	
1 8 1	1.155	1.156	5	4	11 4 1	0.830	0.830	5	8
1 8 1	1.155	1.156	3	2	11 4 1	0.830	0.830	2	4
8 4 0	1.132	1.132	1	1	10 2 2	0.824	0.824	1	3
1 9 0	1.118	1.118	5	4	10 2 2	0.824	0.824	1	2
1 9 0	1.118	1.118	2	2					
0 6 2	1.112	1.112	6	8					

x=0.1 at 1200°C

h k l	D-obs.	D-calc.	I-obs.	I-calc.	h k l	D-obs.	D-calc.	I-obs.	I-calc.
1 1 0	7.161	7.155	39	53	1 9 0	1.117	1.117	2	2
0 2 0	5.062	5.059	56	57	0 6 2	1.112	1.112	6	8
0 0 0	3.889	0.000	1		0 6 2	1.112	1.112	3	4
2 2 0	3.577	3.578	11	10	3 8 1	1.100	1.099	1	1
1 3 0	3.198	3.200	100	100	2 6 2	1.086	1.086	1	2
0 0 0	2.751	0.000	17		3 9 0	1.067	1.067	1	1
0 4 0	2.530	2.530	15	15	0 0 0	1.040	0.000	2	
1 2 1	2.476	2.476	58	65	1 7 2	1.029	1.028	4	4
3 3 0	2.385	2.385	3	4	1 7 2	1.029	1.028	2	2
2 4 0	2.262	2.263	9	11	4 6 2	1.018	1.018	2	1
0 3 1	2.226	2.224	32	37	4 6 2	1.018	1.018	1	1
0 0 0	2.103	0.000	6		0 10 0	1.012	1.012	1	1
3 2 1	2.038	2.036	2	4	5 8 1	1.008	1.008	4	4
5 1 0	1.986	1.984	9	8	5 8 1	1.008	1.008	2	2
0 0 0	1.947	0.000	6		10 2 0	0.992	0.992	1	1
4 1 1	1.891	1.889	34	37	3 7 2	0.988	0.988	3	5
4 4 0	1.791	1.789	1	2	3 7 2	0.988	0.988	1	2
3 5 0	1.737	1.735	2	2	4 9 1	0.970	0.971	1	1
0 6 0	1.687	1.686	20	23	1 2 3	0.963	0.963	3	2
0 5 1	1.670	1.670	5	3	1 2 3	0.963	0.963	1	1
6 2 0	1.600	1.600	2	2	4 10 0	0.940	0.940	1	1
2 5 1	1.586	1.586	34	41	4 10 0	0.939	0.940	0	1
2 5 1	1.586	1.586	20	21	6 6 2	0.928	0.928	2	3
0 0 2	1.479	1.479	7	11	6 6 2	0.928	0.928	1	2
1 6 1	1.449	1.450	4	5	5 7 2	0.921	0.921	2	2
1 7 0	1.431	1.431	3	3	1 4 3	0.915	0.915	3	3
0 2 2	1.420	1.419	3	2	1 9 2	0.891	0.892	3	4
4 6 0	1.404	1.403	2	2	1 9 2	0.892	0.892	1	2
5 4 1	1.394	1.394	25	28	7 9 0	0.887	0.887	2	3
5 4 1	1.393	1.394	13	14	7 9 0	0.887	0.887	1	2
0 0 0	1.374	0.000	2		0 11 1	0.878	0.878	1	1
1 3 2	1.343	1.342	6	9	0 11 1	0.878	0.878	0	1
1 3 2	1.342	1.342	3	5	2 5 3	0.873	0.873	5	6
7 3 0	1.329	1.329	6	6	2 5 3	0.873	0.873	3	3
7 3 0	1.328	1.329	3	3	10 6 0	0.868	0.868	1	1
0 4 2	1.277	1.277	4	2	2 11 1	0.865	0.865	7	10
0 4 2	1.277	1.277	2	1	2 11 1	0.865	0.865	4	5
3 3 2	1.257	1.257	2	2	4 5 3	0.836	0.836	5	8
2 7 1	1.257	1.258	2	2	4 5 3	0.836	0.836	3	4
3 3 2	1.257	1.257	1	1	12 2 0	0.833	0.832	1	1
2 7 1	1.257	1.258	1	1	11 4 1	0.830	0.830	4	8
4 2 2	1.238	1.238	1	2	11 4 1	0.830	0.830	2	4
8 2 0	1.230	1.227	2	0	10 2 2	0.824	0.824	1	3
6 6 0	1.193	1.193	3	3	10 2 2	0.824	0.824	1	2
6 6 0	1.192	1.193	1	1					
5 6 1	1.186	1.187	2	2					
1 5 2	1.186	1.186	1	1					
5 6 1	1.186	1.187	1	1					
1 5 2	1.186	1.186	0	0					
7 5 0	1.176	1.176	2	2					
7 5 0	1.176	1.176	1	1					
1 8 1	1.155	1.155	4	4					
1 8 1	1.155	1.155	2	2					
1 9 0	1.117	1.117	3	4					

x=0.1 at 1100°C

hkl	D-obs.	D-calc.	I-obs.	I-calc.	hkl	D-obs.	D-calc.	I-obs.	I-calc.
110	7.158	7.151	36	44	390	1.066	1.066	1	1
020	5.058	5.057	51	50	000	1.043	0.000	1	
220	3.575	3.576	11	11	172	1.028	1.028	4	5
130	3.197	3.198	100	100	172	1.028	1.028	2	2
000	2.758	0.000	14		462	1.018	1.018	2	1
040	2.528	2.528	13	13	462	1.018	1.018	1	1
121	2.477	2.476	51	63	000	1.011	0.000	1	
330	2.384	2.384	3	4	581	1.008	1.008	3	4
240	2.261	2.261	11	12	581	1.008	1.008	2	2
031	2.225	2.224	31	37	372	0.988	0.988	2	5
321	2.038	2.036	2	5	372	0.988	0.988	1	2
510	1.985	1.983	8	8	123	0.964	0.964	2	2
000	1.953	0.000	4		123	0.963	0.964	1	1
411	1.890	1.888	35	36	662	0.928	0.928	2	3
440	1.789	1.788	2	2	662	0.928	0.928	1	1
350	1.735	1.734	2	2	572	0.921	0.920	2	2
060	1.686	1.686	19	22	143	0.915	0.915	2	3
060	1.685	1.686	9	11	143	0.915	0.915	1	1
051	1.672	1.670	4	3	192	0.891	0.891	2	4
251	1.586	1.586	38	40	192	0.891	0.891	1	2
251	1.585	1.586	16	20	790	0.887	0.887	3	3
002	1.480	1.479	9	10	790	0.887	0.887	1	1
002	1.479	1.479	4	5	253	0.873	0.873	4	6
161	1.449	1.449	4	4	253	0.873	0.873	3	3
170	1.431	1.430	2	2	2111	0.865	0.865	6	10
022	1.420	1.420	3	2	2111	0.865	0.865	3	5
022	1.419	1.420	2	1	453	0.836	0.837	4	7
460	1.403	1.403	2	2	453	0.836	0.837	3	3
541	1.394	1.393	25	28	000	0.833	0.000	1	
541	1.393	1.393	12	14	1141	0.829	0.829	3	8
000	1.380	0.000	2		1141	0.829	0.829	1	4
132	1.343	1.343	6	9	1022	0.824	0.824	1	3
730	1.328	1.328	5	6					
730	1.328	1.328	3	3					
042	1.277	1.277	3	2					
042	1.277	1.277	2	1					
332	1.257	1.257	2	1					
271	1.257	1.258	2	1					
332	1.257	1.257	1	1					
271	1.257	1.258	1	1					
422	1.234	1.238	2	1					
660	1.192	1.192	3	3					
561	1.186	1.186	2	1					
152	1.186	1.186	1	1					
561	1.186	1.186	1	0					
152	1.186	1.186	1	0					
750	1.176	1.176	2	2					
181	1.155	1.155	3	4					
181	1.155	1.155	1	2					
190	1.117	1.117	3	3					
062	1.112	1.112	6	8					
062	1.112	1.112	3	4					
262	1.086	1.086	1	1					
262	1.086	1.086	1	0					

x=0.2 at 1300°C

hkl	D-obs.	D-calc.	I-obs.	I-calc.	hkl	D-obs.	D-calc.	I-obs.	I-calc.
1 1 0	7.179	7.161	37	54	3 9 0	1.067	1.067	1	1
0 2 0	5.068	5.063	53	58	0 0 0	1.039	0.000	4	
0 0 0	3.886	0.000	2		1 7 2	1.030	1.029	4	4
2 2 0	3.579	3.580	10	10	1 7 2	1.029	1.029	2	2
0 0 0	3.476	0.000	3		4 6 2	1.018	1.018	2	1
1 3 0	3.201	3.202	100	100	4 6 2	1.018	1.018	1	1
0 0 0	2.750	0.000	41		0 10 0	1.013	1.013	2	1
0 4 0	2.533	2.532	17	15	5 8 1	1.009	1.009	3	4
1 2 1	2.477	2.476	46	65	5 8 1	1.009	1.009	1	2
3 3 0	2.386	2.387	2	4	10 2 0	0.993	0.993	1	1
2 4 0	2.265	2.264	11	11	3 7 2	0.989	0.989	4	5
0 0 0	2.245	0.000	10		3 7 2	0.989	0.989	2	2
0 3 1	2.225	2.224	25	37	0 0 0	0.965	0.000	2	1
3 2 1	2.038	2.036	4	4	1 2 3	0.963	0.963	3	3
5 1 0	1.987	1.986	10	8	1 2 3	0.963	0.963	1	1
0 0 0	1.944	0.000	11		0 0 0	0.946	0.000	1	
4 1 1	1.891	1.889	40	37	4 10 0	0.940	0.940	2	2
4 4 0	1.792	1.790	2	2	6 6 2	0.929	0.929	2	3
3 5 0	1.739	1.737	2	2	6 6 2	0.929	0.929	1	2
0 6 0	1.690	1.688	18	23	5 7 2	0.921	0.921	3	2
0 5 1	1.673	1.671	5	3	5 7 2	0.921	0.921	2	1
6 2 0	1.602	1.601	2	2	1 4 3	0.915	0.915	4	3
2 5 1	1.587	1.587	56	41	1 4 3	0.915	0.915	2	1
0 0 2	1.479	1.478	9	11	1 9 2	0.892	0.892	4	4
0 0 2	1.478	1.478	5	5	1 9 2	0.892	0.892	2	2
1 6 1	1.451	1.451	3	4	7 9 0	0.888	0.888	4	3
1 7 0	1.432	1.432	3	3	7 9 0	0.888	0.888	2	2
0 2 2	1.419	1.419	4	2	0 11 1	0.879	0.879	1	1
4 6 0	1.405	1.404	3	2	0 11 1	0.879	0.879	1	1
5 4 1	1.395	1.395	26	28	2 5 3	0.873	0.873	5	6
0 0 0	1.375	0.000	6		2 5 3	0.873	0.873	3	3
1 3 2	1.342	1.342	6	9	10 6 0	0.868	0.868	3	2
7 3 0	1.330	1.330	6	7	2 11 1	0.866	0.866	8	10
7 3 0	1.329	1.330	2	3	2 11 1	0.866	0.866	4	5
0 4 2	1.277	1.277	4	2	7 7 2	0.841	0.841	2	1
0 4 2	1.277	1.277	3	1	4 5 3	0.836	0.836	7	8
3 3 2	1.259	1.257	1	1	4 5 3	0.836	0.836	3	4
2 7 1	1.259	1.259	1	1	11 4 1	0.830	0.830	5	8
4 2 2	1.238	1.238	1	2	11 4 1	0.830	0.830	2	4
8 2 0	1.230	1.228	2	0	0 0 0	0.828	0.000	1	
6 6 0	1.194	1.193	3	3	0 0 0	0.828	0.000	1	
5 6 1	1.186	1.187	1	1	10 2 2	0.824	0.824	1	3
5 1 2	1.186	1.186	0	0	10 2 2	0.824	0.824	1	2
7 5 0	1.177	1.177	3	2					
1 8 1	1.156	1.156	4	4					
1 8 1	1.156	1.156	2	2					
1 9 0	1.118	1.118	4	4					
1 9 0	1.118	1.118	2	2					
0 6 2	1.112	1.112	6	8					
0 6 2	1.112	1.112	3	4					
8 3 1	1.100	1.100	1	1					
2 6 2	1.086	1.086	2	1					
2 6 2	1.086	1.086	1	0					
3 9 0	1.067	1.067	2	2					

x=0.2 at 1200°C

hkl	D-obs.	D-calc.	I-obs.	I-calc.	hkl	D-obs.	D-calc.	I-obs.	I-calc.
1 1 0	7.176	7.158	41	50	3 9 0	1.067	1.067	1	1
0 2 0	5.068	5.061	61	56	0 0 0	1.042	0.000	4	
0 0 0	3.901	0.000	2		1 7 2	1.029	1.028	3	4
2 2 0	3.579	3.579	13	11	1 7 2	1.029	1.028	2	2
1 3 0	3.201	3.201	100	100	4 6 2	1.018	1.018	2	1
0 0 0	2.759	0.000	41		4 6 2	1.018	1.018	1	1
0 4 0	2.532	2.531	16	14	0 10 0	1.012	1.012	1	1
1 2 1	2.477	2.476	54	65	5 8 1	1.009	1.009	5	4
3 3 0	2.386	2.386	4	4	5 8 1	1.009	1.009	2	2
2 4 0	2.264	2.263	12	11	10 2 0	0.992	0.993	1	1
0 3 1	2.225	2.224	27	37	3 7 2	0.988	0.988	3	5
3 2 1	2.038	2.036	3	4	3 7 2	0.988	0.988	2	2
5 1 0	1.987	1.985	9	8	4 9 1	0.971	0.971	1	1
0 0 0	1.952	0.000	13		1 2 3	0.963	0.963	3	3
4 1 1	1.891	1.889	37	37	1 2 3	0.963	0.963	2	1
4 4 0	1.792	1.789	2	2	4 10 0	0.940	0.940	1	1
3 5 0	1.738	1.736	3	2	4 10 0	0.940	0.940	1	1
0 6 0	1.689	1.687	24	23	6 6 2	0.928	0.928	2	3
0 5 1	1.672	1.671	6	3	6 6 2	0.928	0.928	1	2
0 0 0	1.594	0.000	12		5 7 2	0.921	0.921	3	2
2 5 1	1.587	1.586	40	41	5 7 2	0.921	0.921	2	1
2 5 1	1.586	1.586	19	20	1 4 3	0.915	0.915	2	3
0 0 2	1.479	1.479	9	11	1 4 3	0.915	0.915	2	1
1 6 1	1.449	1.450	2	4	1 9 2	0.892	0.892	3	4
1 7 0	1.432	1.432	3	3	1 9 2	0.891	0.892	1	2
0 2 2	1.419	1.419	3	2	7 9 0	0.888	0.888	3	3
0 2 2	1.419	1.419	2	1	7 9 0	0.888	0.888	1	2
4 6 0	1.404	1.404	2	2	0 11 1	0.879	0.879	1	1
5 4 1	1.394	1.394	28	28	0 11 1	0.878	0.879	1	0
5 4 1	1.394	1.394	14	14	2 5 3	0.873	0.873	5	6
0 0 0	1.379	0.000	6		2 5 3	0.873	0.873	3	3
1 3 2	1.343	1.342	5	9	10 6 0	0.868	0.868	1	1
1 3 2	1.342	1.342	3	5	2 11 1	0.866	0.866	7	10
7 3 0	1.329	1.329	7	6	2 11 1	0.866	0.866	4	5
7 3 0	1.329	1.329	4	3	7 7 2	0.841	0.841	1	1
0 4 2	1.277	1.277	4	2	4 5 3	0.836	0.836	5	8
0 4 2	1.277	1.277	2	1	4 5 3	0.836	0.836	3	4
3 3 2	1.258	1.257	1	2	8 6 2	0.835	0.835	3	3
2 7 1	1.258	1.258	1	2	11 4 1	0.830	0.830	5	8
0 0 0	1.234	0.000	3		11 4 1	0.830	0.830	2	4
6 6 0	1.193	1.193	3	3	10 2 2	0.824	0.824	1	3
6 6 0	1.193	1.193	2	1	10 2 2	0.824	0.824	1	2
5 6 1	1.186	1.187	1	2					
1 5 2	1.186	1.186	1	1					
7 5 0	1.177	1.177	3	3					
1 8 1	1.156	1.156	5	4					
1 8 1	1.156	1.156	2	2					
5 3 2	1.126	1.126	2	2					
1 9 0	1.118	1.118	5	3					
1 9 0	1.118	1.118	3	2					
0 6 2	1.112	1.112	6	8					
0 6 2	1.112	1.112	3	4					
2 6 2	1.086	1.086	2	1					
3 9 0	1.067	1.067	1	2					

x=0.2 at 1100°C

h k l	D-obs.	D-calc.	I-obs.	I-calc.	h k l	D-obs.	D-calc.	I-obs.	I-calc.
0 0 0	7.688	0.000	5		1 8 1	1.155	1.155	3	4
1 1 0	7.153	7.151	36	41	1 8 1	1.155	1.155	2	2
0 0 0	6.387	0.000	3	48	0 0 0	1.127	0.000	1	
0 2 0	5.053	5.057	49		1 9 0	1.117	1.117	3	3
0 0 0	4.483	0.000	1		0 6 2	1.112	1.112	5	8
0 0 0	3.883	0.000	3		0 6 2	1.112	1.112	3	4
0 0 0	3.685	0.000	2		2 6 2	1.086	1.086	1	1
2 2 0	3.572	3.576	11	11	2 6 2	1.086	1.086	1	0
1 3 0	3.195	3.198	100	100	0 0 0	1.043	0.000	2	
0 0 0	2.986	0.000	4		0 0 0	1.043	0.000	2	
0 0 0	2.982	0.000	5		1 7 2	1.028	1.028	3	1
0 0 0	2.963	0.000	3		1 7 2	1.028	1.028	2	1
0 0 0	2.759	0.000	28		4 6 2	1.018	1.018	2	1
0 0 0	2.699	0.000	2		4 6 2	1.018	1.018	1	1
0 4 0	2.528	2.528	13	13	5 8 1	1.008	1.008	3	4
1 2 1	2.475	2.475	43	61	5 8 1	1.008	1.008	1	2
3 3 0	2.384	2.384	3	3	3 7 2	0.988	0.988	2	5
2 4 0	2.261	2.261	13	12	1 2 3	0.963	0.963	2	3
0 3 1	2.223	2.223	30	37	1 2 3	0.963	0.963	1	1
0 0 0	2.100	0.000	2		6 6 2	0.928	0.928	1	3
0 0 0	2.080	0.000	2		6 6 2	0.928	0.928	1	1
3 2 1	2.035	2.035	3	5	5 7 2	0.921	0.920	2	2
5 1 0	1.984	1.983	8	8	1 4 3	0.915	0.915	3	3
0 0 0	1.953	0.000	7		1 4 3	0.915	0.915	1	1
0 0 0	1.946	0.000	7		1 9 2	0.891	0.891	2	4
4 1 1	1.889	1.888	33	35	7 9 0	0.887	0.887	2	3
4 4 0	1.789	1.788	2	2	7 9 0	0.887	0.887	1	1
3 5 0	1.736	1.734	3	2	2 5 3	0.873	0.873	4	6
0 6 0	1.686	1.686	19	22	2 5 3	0.873	0.873	2	3
0 5 1	1.669	1.670	5	4	2 11 1	0.865	0.865	6	10
0 0 0	1.593	0.000	8		2 11 1	0.865	0.865	3	5
2 5 1	1.586	1.585	35	39	4 5 3	0.836	0.836	4	8
2 5 1	1.585	1.585	19	20	4 5 3	0.837	0.836	2	4
0 0 0	1.496	0.000	1		0 0 0	0.833	0.000	1	
0 0 2	1.479	1.479	7	10	11 4 1	0.830	0.829	3	8
0 0 2	1.478	1.479	4	5	11 4 1	0.830	0.829	1	4
1 6 1	1.449	1.449	3	5					
1 7 0	1.430	1.430	2	2					
0 2 2	1.419	1.419	3	2					
4 6 0	1.402	1.403	2	2					
5 4 1	1.393	1.393	21	26					
5 4 1	1.393	1.393	10	13					
0 0 0	1.380	0.000	3						
1 3 2	1.342	1.342	5	9					
7 3 0	1.328	1.328	5	6					
0 4 2	1.277	1.277	3	2					
0 4 2	1.276	1.277	2	1					
3 3 2	1.257	1.257	2	1					
2 7 1	1.257	1.257	1	1					
4 2 2	1.235	1.238	2	2					
6 6 0	1.192	1.192	3	3					
5 6 1	1.186	1.186	2	1					
1 5 2	1.186	1.186	1	1					
7 5 0	1.176	1.176	3	2					

x=0.3 at 1300°C

hkl	D-obs.	D-calc.	I-obs.	I-calc.	hkl	D-obs.	D-calc.	I-obs.	I-calc.
000	7.844	0.000	5		181	1.156	1.156	7	4
110	7.176	7.161	48	53	181	1.156	1.156	2	2
020	5.068	5.063	64	58	840	1.132	1.132	1	1
000	3.891	0.000	3		000	1.123	0.000	5	
220	3.580	3.580	12	10	190	1.118	1.118	5	4
000	3.518	0.000	16		062	1.112	1.112	11	8
000	3.480	0.000	6		062	1.112	1.112	6	4
000	3.249	0.000	15		831	1.100	1.100	1	2
130	3.202	3.202	100	100	000	1.094	0.000	1	
000	2.753	0.000	80		622	1.086	1.086	2	1
000	2.598	0.000	2		390	1.065	1.067	2	2
040	2.533	2.532	13	15	000	1.040	0.000	7	
121	2.477	2.476	73	65	000	1.039	0.000	4	
330	2.388	2.387	4	4	172	1.029	1.029	4	4
240	2.265	2.264	16	11	462	1.018	1.018	3	1
000	2.247	0.000	18		462	1.018	1.018	2	1
031	2.226	2.224	45	37	0100	1.013	1.013	2	1
000	2.190	0.000	1		581	1.009	1.009	6	4
321	2.038	2.036	3	4	581	1.009	1.009	3	2
510	1.988	1.986	13	8	1020	0.993	0.993	2	1
000	1.945	0.000	24		372	0.989	0.989	3	5
411	1.891	1.889	50	37	372	0.989	0.989	2	2
440	1.791	1.790	2	2	491	0.971	0.971	2	1
530	1.740	1.737	3		123	0.963	0.963	4	3
060	1.688	1.688	29	23	123	0.963	0.963	2	1
060	1.687	1.688	14	12	000	0.944	0.000	1	
051	1.671	1.671	7	3	662	0.929	0.929	2	3
000	1.624	0.000	2		662	0.929	0.929	1	2
251	1.588	1.587	57	40	572	0.921	0.921	3	2
251	1.587	1.587	28	20	000	0.919	0.000	3	
002	1.479	1.478	9	11	143	0.915	0.915	5	3
161	1.448	1.451	5	5	143	0.914	0.915	1	1
170	1.432	1.432	3	3	192	0.892	0.892	4	4
022	1.419	1.419	4	2	192	0.892	0.892	3	2
022	1.419	1.419	2	1	790	0.888	0.888	4	3
460	1.405	1.404	3	2	790	0.888	0.888	3	2
541	1.395	1.395	34	28	0111	0.879	0.879	1	1
000	1.376	0.000	11		000	0.877	0.000	3	
000	1.376	0.000	7		253	0.873	0.873	7	6
132	1.342	1.342	9	9	253	0.873	0.873	5	3
730	1.330	1.330	7	7	1060	0.868	0.868	4	1
701	1.298	1.299	1	1	1060	0.868	0.868	2	1
042	1.277	1.277	4	2	2111	0.866	0.866	7	10
042	1.277	1.277	3	1	2111	0.865	0.866	3	5
800	1.265	1.266	1	0	772	0.841	0.841	1	1
332	1.259	1.257	2	2	453	0.836	0.836	7	8
271	1.259	1.259	2	2	453	0.836	0.836	3	4
422	1.238	1.238	2	2	1141	0.830	0.830	6	8
820	1.230	1.228	7	0	1141	0.830	0.830	3	4
660	1.193	1.193	6	3	1022	0.824	0.824	1	3
561	1.186	1.187	2	1					
512	1.186	1.186	1	0					
750	1.177	1.177	2	2					
000	1.173	0.000	2						

x=0.3 at 1200°C

hkl	D-obs.	D-calc.	I-obs.	I-calc.	hkl	D-obs.	D-calc.	I-obs.	I-calc.
1 1 0	7.170	7.158	43	50	1 9 0	1.118	1.118	2	2
0 2 0	5.065	5.061	54	56	0 6 2	1.112	1.112	7	8
0 0 0	3.899	0.000	4		0 6 2	1.112	1.112	3	4
2 2 0	3.578	3.579	12	11	2 6 2	1.086	1.086	2	1
1 3 0	3.200	3.201	100	100	2 6 2	1.086	1.086	1	0
0 0 0	3.051	0.000	1		3 9 0	1.067	1.067	1	2
0 0 0	2.974	0.000	2		0 0 0	1.043	0.000	7	
0 0 0	2.760	0.000	68		0 0 0	1.043	0.000	5	
0 0 0	2.702	0.000	2		1 7 2	1.029	1.028	3	4
0 4 0	2.531	2.531	13	14	1 7 2	1.029	1.028	2	2
1 2 1	2.477	2.476	56	64	4 6 2	1.018	1.018	3	1
3 3 0	2.386	2.386	3	4	0 10 0	1.012	1.012	2	1
2 4 0	2.265	2.263	15	11	5 8 1	1.009	1.009	4	4
0 0 0	2.253	0.000	13		5 8 1	1.009	1.009	2	2
0 3 1	2.225	2.224	34	37	3 7 2	0.988	0.988	3	5
3 2 1	2.039	2.036	2	4	0 0 0	0.976	0.000	1	
5 1 0	1.967	1.965	9	8	4 9 1	0.971	0.971	1	1
0 0 0	1.953	0.000	23		1 2 3	0.963	0.963	3	3
4 1 1	1.891	1.889	38	37	1 2 3	0.963	0.963	2	1
4 4 0	1.791	1.789	3	2	0 0 0	0.946	0.000	1	
0 0 0	1.747	0.000	2		4 10 0	0.940	0.940	1	1
0 6 0	1.689	1.687	21	23	6 6 2	0.928	0.928	2	3
0 5 1	1.672	1.671	6	3	6 6 2	0.928	0.928	1	2
0 0 0	1.595	0.000	19		5 7 2	0.921	0.921	3	2
2 5 1	1.587	1.586	41	41	1 4 3	0.915	0.915	3	3
2 5 1	1.586	1.586	18	20	1 4 3	0.915	0.915	2	1
0 0 2	1.479	1.479	10	11	8 8 0	0.895	0.895	1	1
0 0 2	1.478	1.479	4	5	1 9 2	0.892	0.892	3	4
1 6 1	1.450	1.450	4	4	1 9 2	0.892	0.892	1	2
1 7 0	1.432	1.432	3	3	7 9 0	0.888	0.888	3	3
0 2 2	1.419	1.419	4	2	7 9 0	0.888	0.888	1	2
4 6 0	1.404	1.404	2	2	2 5 3	0.873	0.873	7	6
5 4 1	1.394	1.394	29	28	2 5 3	0.873	0.873	5	3
5 4 1	1.394	1.394	14	14	10 6 0	0.868	0.868	2	1
0 0 0	1.380	0.000	10		2 11 1	0.866	0.866	7	10
0 0 0	1.379	0.000	7		2 11 1	0.866	0.866	4	5
1 3 2	1.342	1.342	7	9	12 0 0	0.843	0.844	1	1
1 3 2	1.342	1.342	3	5	7 7 2	0.841	0.841	1	1
3 7 0	1.329	1.329	8	6	4 5 3	0.836	0.836	5	8
0 4 2	1.277	1.277	5	2	4 5 3	0.836	0.836	3	4
0 4 2	1.277	1.277	2	1	8 6 2	0.835	0.835	2	3
3 3 2	1.258	1.257	1	2	0 0 0	0.832	0.000	2	
2 7 1	1.258	1.258	1	1	0 0 0	0.832	0.000	1	
3 3 2	1.257	1.257	1	3	11 4 1	0.830	0.830	4	8
2 7 1	1.257	1.258	1	1	11 4 1	0.830	0.830	2	4
6 6 0	1.193	1.193	3	3	10 2 2	0.824	0.824	1	3
5 6 1	1.186	1.187	1	1					
5 1 2	1.186	1.186	1	1					
7 5 0	1.177	1.177	4	2					
7 5 0	1.177	1.177	2	1					
1 8 1	1.156	1.156	4	4					
1 8 1	1.156	1.156	2	2					
5 3 2	1.127	1.126	3	1					
1 9 0	1.118	1.118	3	3					

x=0.3 at 1100°C

h k l	D-obs.	D-calc.	I-obs.	I-calc.	h k l	D-obs.	D-calc.	I-obs.	I-calc.
0 0 0	7.688	0.000	12		0 4 2	1.278	1.277	4	2
1 1 0	7.161	7.156	42	42	0 4 2	1.277	1.277	2	1
0 0 0	6.417	0.000	8		3 3 2	1.258	1.257	2	2
0 2 0	5.071	5.060	53	48	2 7 1	1.258	1.258	2	1
0 0 0	3.894	0.000	8		3 3 2	1.257	1.257	1	1
0 0 0	3.894	0.000	6		2 7 1	1.257	1.258	1	1
2 2 0	3.581	3.578	12	11	4 2 2	1.236	1.238	4	2
1 3 0	3.201	3.200	100	100	0 0 0	1.230	0.000	4	
0 0 0	3.056	0.000	10		6 6 0	1.192	1.193	3	3
0 0 0	2.988	0.000	12		5 6 1	1.186	1.187	1	1
0 0 0	2.968	0.000	8		5 1 2	1.186	1.186	1	1
0 0 0	2.910	0.000	2		7 5 0	1.176	1.176	3	2
0 0 0	2.803	0.000	6		1 8 1	1.156	1.156	3	4
0 0 0	2.764	0.000	49		1 8 1	1.156	1.156	2	2
0 0 0	2.705	0.000	7		5 3 2	1.127	1.126	1	1
0 0 0	2.650	0.000	1		1 9 0	1.118	1.118	3	3
0 0 0	2.586	0.000	3		0 6 2	1.112	1.112	6	8
0 4 0	2.532	2.530	15	13	0 6 2	1.112	1.112	3	4
1 2 1	2.479	2.477	60	63	2 6 2	1.087	1.086	1	1
3 3 0	2.387	2.385	4	4	3 9 0	1.067	1.067	1	1
2 4 0	2.264	2.263	12	12	0 0 0	1.044	0.000	3	
0 3 1	2.227	2.224	33	36	0 0 0	1.037	0.000	2	
0 0 0	2.103	0.000	7		1 7 2	1.029	1.029	4	4
0 0 0	2.081	0.000	7		1 7 2	1.029	1.029	2	2
3 2 1	2.040	2.036	4	5	4 6 2	1.018	1.018	2	1
5 1 0	1.987	1.985	9	8	0 10 0	1.012	1.012	2	1
0 0 0	1.957	0.000	11		5 8 1	1.008	1.008	4	4
0 0 0	1.947	0.000	15		5 8 1	1.009	1.008	2	2
0 0 0	1.902	0.000	8		3 7 2	0.989	0.989	3	5
4 1 1	1.891	1.889	36	35	3 7 2	0.989	0.989	2	2
4 4 0	1.792	1.789	1	2	4 9 1	0.970	0.971	2	1
0 0 0	1.758	0.000	3		1 2 3	0.964	0.964	3	3
3 5 0	1.738	1.736	4	2	1 2 3	0.964	0.964	2	1
0 6 0	1.689	1.687	19	22	6 6 2	0.929	0.928	1	3
0 5 1	1.673	1.671	5	3	5 7 2	0.921	0.921	3	2
0 0 0	1.667	0.000	4		0 0 0	0.918	0.000	3	
2 5 1	1.587	1.586	47	39	1 4 3	0.915	0.915	4	3
0 0 0	1.553	0.000	1		1 4 3	0.915	0.915	2	2
0 0 0	1.531	0.000	3		1 9 2	0.892	0.892	2	4
0 0 0	1.496	0.000	2		7 9 0	0.887	0.888	3	3
0 0 2	1.480	1.479	9	11	2 5 3	0.873	0.873	6	6
1 6 1	1.451	1.450	3	4	2 5 3	0.873	0.873	3	3
1 7 0	1.432	1.431	2	2	2 11 1	0.865	0.866	8	9
0 2 2	1.419	1.420	2	2	2 11 1	0.865	0.866	4	5
0 0 0	1.410	0.000	3		4 5 3	0.836	0.837	4	7
4 6 0	1.403	1.403	5	2	4 5 3	0.837	0.837	3	4
5 4 1	1.394	1.394	25	26	0 0 0	0.833	0.000	2	
5 4 1	1.394	1.394	13	13	11 4 1	0.830	0.830	4	8
0 0 0	1.382	0.000	5		11 4 1	0.830	0.830	2	4
0 0 0	1.377	0.000	4		10 2 2	0.824	0.824	1	3
1 3 2	1.343	1.343	7	8					
1 3 2	1.343	1.343	4	4					
7 3 0	1.329	1.329	5	6					
7 0 1	1.294	1.299	1	1					

x=0.5 at 1300°C

hkl	D-obs.	D-calc.	I-obs.	I-calc.	hkl	D-obs.	D-calc.	I-obs.	I-calc.
110	7.176	7.163	13	32	000	0.974	0.000	3	
020	5.076	5.065	22	34	123	0.963	0.963	2	2
000	3.905	0.000	4		000	0.945	0.000	1	
220	3.584	3.582	4	6	000	0.918	0.000	8	
000	3.252	0.000	22		000	0.918	0.000	4	
130	3.205	3.204	59	59	000	0.901	0.000	1	
000	2.757	0.000	100		253	0.873	0.873	4	4
040	2.534	2.533	7	9	000	0.871	0.000	9	
121	2.478	2.477	32	38	000	0.871	0.000	5	
330	2.390	2.388	2	2	2111	0.866	0.866	5	6
000	2.302	0.000	1		2111	0.866	0.866	3	3
240	2.267	2.265	8	7	000	0.850	0.000	1	
000	2.251	0.000	21		1200	0.844	0.844	1	1
031	2.226	2.225	16	22	453	0.837	0.837	3	5
000	2.190	0.000	4		1141	0.831	0.831	8	5
510	1.989	1.987	6	5	1141	0.831	0.831	3	2
000	1.950	0.000	43						
411	1.892	1.890	21	22					
440	1.790	1.791	1	1					
350	1.742	1.737	3	1					
060	1.689	1.688	26	14					
051	1.672	1.672	3	2					
000	1.626	0.000	1						
251	1.589	1.587	34	24					
002	1.480	1.479	6	6					
002	1.479	1.479	4	3					
161	1.451	1.451	1	2					
022	1.418	1.420	1	1					
541	1.395	1.395	12	16					
541	1.395	1.395	8	8					
000	1.378	0.000	17						
000	1.377	0.000	9						
000	1.360	0.000	2						
132	1.342	1.343	2	5					
730	1.329	1.330	1	4					
042	1.277	1.277	2	1					
332	1.258	1.257	1	2					
271	1.258	1.259	1	2					
000	1.232	0.000	13						
000	1.232	0.000	8						
660	1.194	1.194	2	2					
000	1.175	0.000	5						
000	1.175	0.000	3						
000	1.154	0.000	3						
181	1.157	1.156	2	2					
532	1.125	1.126	6	5					
062	1.112	1.112	6	5					
262	1.087	1.087	1	1					
000	1.041	0.000	17						
000	1.041	0.000	9						
000	1.034	0.000	2						
000	1.032	0.000	2						
462	1.019	1.019	2	1					
581	1.009	1.009	3	3					

x=0.5 at 1200°C

h k l	D-obs.	D-calc.	I-obs.	I-calc.	h k l	D-obs.	D-calc.	I-obs.	I-calc.
0 0 0	7.695	0.000	8		1 8 1	1.156	1.156	2	2
1 1 0	7.179	7.162	22	33	5 3 2	1.126	1.126	4	1
0 0 0	6.401	0.000	4		0 6 2	1.112	1.112	4	5
0 2 0	5.074	5.064	36	36	0 6 2	1.112	1.112	1	2
0 0 0	4.493	0.000	3		2 6 2	1.087	1.086	1	1
0 0 0	3.892	0.000	7		9 3 0	1.068	1.068	1	1
0 0 0	3.690	0.000	4		0 0 0	1.042	0.000	8	
2 2 0	3.582	3.581	9	6	0 0 0	1.042	0.000	5	
1 3 0	3.204	3.203	62	62	1 7 2	1.029	1.029	2	2
0 0 0	3.051	0.000	7		4 6 2	1.018	1.018	1	1
0 0 0	2.984	0.000	7		5 8 1	1.009	1.009	2	3
0 0 0	2.965	0.000	6		0 0 0	1.007	0.000	2	
0 0 0	2.797	0.000	5		3 7 2	0.989	0.989	2	3
0 0 0	2.757	0.000	100		1 2 3	0.963	0.963	1	2
0 0 0	2.701	0.000	4		4 10 0	0.941	0.940	1	1
0 0 0	2.579	0.000	1		6 6 2	0.929	0.929	1	2
0 4 0	2.533	2.532	9	9	5 7 2	0.921	0.921	1	1
1 2 1	2.477	2.476	31	40	0 0 0	0.919	0.000	5	
3 3 0	2.392	2.387	1	3	1 9 2	0.892	0.892	2	3
2 4 0	2.266	2.265	8	7	7 9 0	0.888	0.888	1	2
0 0 0	2.250	0.000	17		0 0 0	0.886	0.000	1	
0 3 1	2.226	2.225	20	23	2 5 3	0.873	0.873	4	4
0 0 0	2.100	0.000	5		0 0 0	0.872	0.000	3	
0 0 0	2.078	0.000	3		2 11 1	0.866	0.866	6	6
3 2 1	2.037	2.037	1	3	2 11 1	0.866	0.866	3	3
5 1 0	1.987	1.986	3	5	4 5 3	0.836	0.837	3	5
0 0 0	1.951	0.000	33		11 4 1	0.830	0.831	4	5
0 0 0	1.900	0.000	6		11 4 1	0.830	0.831	2	2
4 1 1	1.890	1.890	16	17					
4 4 0	1.790	1.790	1	1					
0 0 0	1.745	0.000	3						
0 6 0	1.690	1.688	13	14					
0 5 1	1.672	1.671	4	2					
0 0 0	1.593	0.000	27						
2 5 1	1.588	1.587	41	27					
0 0 0	1.531	0.000	2						
0 0 2	1.479	1.479	5	7					
0 0 2	1.478	1.479	3	3					
1 6 1	1.449	1.451	2	1					
1 7 0	1.431	1.432	1	2					
0 2 2	1.420	1.419	2	1					
4 6 0	1.403	1.405	2	1					
5 4 1	1.395	1.395	16	17					
0 0 0	1.378	0.000	13						
0 0 0	1.377	0.000	8						
1 3 2	1.342	1.342	3	5					
7 3 0	1.330	1.330	3	4					
7 3 0	1.329	1.330	2	2					
3 3 2	1.259	1.257	1	1					
2 7 1	1.259	1.259	1	1					
0 0 0	1.233	0.000	8						
0 0 0	1.233	0.000	6						
6 6 0	1.193	1.194	2	2					
7 5 0	1.176	1.177	3	1					

x=0.5 at 1100°C

hkl	D-obs.	D-calc.	I-obs.	I-calc.	hkl	D-obs.	D-calc.	I-obs.	I-calc.
000	7.695	0.000	32		332	1.258	1.257	1	2
110	7.158	7.155	26	37	271	1.258	1.258	1	2
000	6.403	0.000	23		000	1.234	0.000	8	
020	5.065	5.060	37	41	660	1.193	1.193	3	2
000	4.494	0.000	4		750	1.176	1.176	4	1
000	3.894	0.000	18		181	1.155	1.155	3	4
000	3.771	0.000	3		442	1.138	1.140	1	1
000	3.688	0.000	9		532	1.127	1.126	4	1
220	3.579	3.578	7	6	062	1.112	1.112	3	6
130	3.200	3.200	78	78	000	1.044	0.000	7	
000	3.052	0.000	27		000	1.040	0.000	7	
000	2.984	0.000	28		172	1.028	1.028	2	4
000	2.963	0.000	24		561	1.008	1.008	2	3
000	2.908	0.000	3		372	0.989	0.988	1	3
000	2.794	0.000	13		941	0.970	0.971	1	1
000	2.760	0.000	100		123	0.963	0.963	1	2
000	2.701	0.000	22		662	0.929	0.928	1	2
000	2.649	0.000	4		572	0.920	0.921	5	
000	2.582	0.000	8		143	0.915	0.915	3	2
040	2.530	2.530	8	11	000	0.896	0.000	2	
121	2.476	2.476	40	49	192	0.892	0.892	2	3
330	2.386	2.385	2	3	253	0.873	0.873	5	5
000	2.254	0.000	19		2111	0.865	0.865	7	8
031	2.225	2.224	18	28	000	0.863	0.000	5	
000	2.099	0.000	17		1141	0.830	0.830	2	6
000	2.080	0.000	19						
321	2.037	2.036	3	3					
510	1.987	1.985	7	6					
000	1.946	0.000	28						
000	1.901	0.000	19						
411	1.888	1.889	16	28					
000	1.847	0.000	1						
000	1.818	0.000	2						
530	1.739	1.735	4	1					
060	1.688	1.687	15	17					
051	1.666	1.670	6	3					
000	1.596	0.000	23						
251	1.587	1.586	45	31					
000	1.570	0.000	3						
000	1.554	0.000	5						
000	1.531	0.000	6						
000	1.496	0.000	5						
002	1.479	1.479	7	8					
161	1.448	1.450	2	3					
000	1.409	0.000	7						
640	1.402	1.403	7	2					
541	1.394	1.394	16	21					
000	1.381	0.000	10						
000	1.377	0.000	8						
132	1.342	1.342	2	7					
730	1.329	1.329	3	5					
000	1.313	0.000	1						
701	1.295	1.299	2	1					
042	1.276	1.277	1	2					

x=0.75

at 1300°C				at 1200°C		at 1100°C			
D-obs.	I-obs.	D-obs.	I-obs.	D-obs.	I-obs.	D-obs.	I-obs.	D-obs.	I-obs.
7.675	8	0.974	2	7.705	10	7.705	24	1.067	1
7.156	5	0.918	8	7.179	7	6.408	15	1.042	7
6.394	5	0.918	5	6.412	6	5.071	3	1.039	6
5.062	7	0.894	2	5.072	8	4.496	3	0.975	1
3.892	6	0.871	6	4.505	1	3.894	11	0.940	1
3.684	3	0.871	3	3.900	6	3.777	2	0.919	4
3.580	1	0.831	5	3.689	5	3.690	8	0.918	3
3.246	12	0.831	2	3.204	17	3.492	1	0.872	3
3.198	20			3.052	9	3.204	6	0.869	3
3.049	7			2.985	9	3.053	22	0.864	1
2.978	6			2.966	8	2.985	21	0.831	2
2.960	4			2.799	4	2.965	17		
2.796	3			2.758	100	2.911	2		
2.754	100			2.702	6	2.800	8		
2.697	4			2.653	1	2.757	100		
2.642	1			2.584	3	2.702	13		
2.580	2			2.534	2	2.654	3		
2.530	2			2.477	5	2.583	6		
2.479	7			2.251	16	2.477	2		
2.248	21			2.226	2	2.252	20		
2.223	3			2.100	6	2.100	10		
2.186	1			2.081	5	2.081	13		
2.098	4			1.952	31	2.037	1		
2.078	5			1.901	6	2.002	1		
2.053	3			1.757	2	1.951	27		
1.949	40			1.742	2	1.901	14		
1.899	3			1.689	3	1.885	3		
1.891	5			1.667	2	1.854	2		
1.742	2			1.592	28	1.819	3		
1.689	6			1.587	21	1.758	4		
1.665	2			1.531	2	1.740	3		
1.590	34			1.497	2	1.689	2		
1.589	18			1.409	2	1.666	5		
1.568	1			1.402	3	1.602	6		
1.552	1			1.395	4	1.593	26		
1.530	4			1.378	14	1.588	19		
1.452	3			1.378	9	1.569	2		
1.401	2			1.299	1	1.556	5		
1.394	4			1.233	10	1.531	5		
1.377	17			1.233	5	1.497	3		
1.377	10			1.176	4	1.425	1		
1.359	2			1.175	2	1.409	5		
1.342	1			1.126	3	1.402	6		
1.296	1			1.125	2	1.379	10		
1.232	12			1.042	9	1.375	9		
1.232	6			1.042	5	1.353	1		
1.175	3			0.975	2	1.316	1		
1.125	5			0.919	5	1.299	1		
1.125	3			0.919	4	1.233	8		
1.083	1			0.872	4	1.230	7		
1.041	13			0.871	3	1.176	4		
1.041	6			0.831	3	1.140	1		
1.027	1			0.831	2	1.125	3		

x=1.00

at 1300°C at 1200°C at 1100°C

D-obs.	I-obs.	D-obs.	I-obs.	D-obs.	I-obs.
7.662	13	7.688	8	7.692	12
6.380	6	6.401	5	6.408	8
3.889	4	3.895	5	4.489	2
3.770	2	3.685	3	4.200	9
3.682	2	3.051	8	3.905	4
3.046	7	2.983	8	3.685	4
2.975	6	2.963	6	3.392	1
2.960	7	2.757	100	3.218	10
2.794	3	2.700	5	3.169	5
2.753	100	2.647	1	3.113	3
2.697	5	2.567	2	3.050	10
2.576	3	2.250	19	2.991	20
2.247	21	2.100	4	2.963	10
2.099	5	2.079	5	2.910	2
2.077	8	1.952	40	2.761	100
1.948	40	1.900	4	2.701	8
1.898	3	1.743	2	2.677	3
1.743	3	1.601	3	2.649	2
1.665	2	1.592	35	2.583	4
1.590	33	1.591	17	2.254	24
1.589	17	1.380	18	2.132	2
1.530	2	1.380	10	2.101	9
1.495	1	1.299	2	2.081	6
1.406	1	1.230	12	2.001	1
1.377	21	1.230	5	1.953	33
1.298	1	1.176	5	1.924	1
1.232	12	1.175	2	1.900	6
1.175	4	1.126	5	1.886	4
1.124	6	1.126	2	1.772	1
1.124	3	1.042	13	1.757	3
1.041	14	1.042	7	1.746	2
1.041	7	0.975	2	1.666	4
0.974	2	0.946	1	1.640	1
0.974	1	0.946	1	1.596	25
0.918	8	0.919	7	1.572	2
0.918	4	0.919	3	1.556	1
0.894	2	0.894	2	1.532	2
0.894	1	0.894	1	1.497	2
0.871	7	0.872	5	1.428	1
0.871	3	0.872	3	1.409	2
0.850	1	0.831	3	1.382	13
0.831	4	0.831	2	1.235	8
0.831	2			1.235	6
				1.191	1
				1.175	3
				1.128	3
				1.044	6
				1.035	1
				0.976	1
				0.921	5
				0.873	3
				0.833	2

IMAGE EVALUATION TEST TARGET (QA-3)

150mm

6"

APPLIED IMAGE, Inc
1653 East Main Street
Rochester, NY 14609 USA
Phone: 716/482-0300
Fax: 716/288-5989